

**β - γ phase-amplitude coupling derived from non-invasive
electroencephalogram - insight into the pathophysiology of
Parkinson's disease**

Dissertation
zur Erlangung des akademischen Grades
Dr. rer. nat.

an der Medizinischen Fakultät
der Universität Leipzig

eingereicht von: M.Sc. Ruxue Gong

Geburtsdatum / Geburtsort: 09.11.1993/ Hubei, China

angefertigt an / in: Klinik und Poliklinik für Neurologie, Universitätsklinikum Leipzig
Max - Planck - Institut für Kognitions- und Neurowissenschaften

Betreuer: Prof. Dr. Joseph Claßen
Prof. Dr. Thomas R. Knösche

Beschluss über die Verleihung des Doktorgrades vom: den 06.07.2022

Table of Contents

List of abbreviations	iii
-----------------------------	-----

I	General Introduction	1
----------	-----------------------------	----------

1	General introduction	3
----------	-----------------------------------	----------

1.1	Background of Parkinson's disease (PD)	3
-----	--	---

1.2	Clinical features of PD	3
-----	-------------------------------	---

1.3	The role of basal ganglia-thalamocortical (BGTC) circuits in the pathophysiology of PD	4
-----	--	---

1.4	Target BGTC circuits for the treatment of PD	9
-----	--	---

1.5	Oscillatory nature of pathological BGTC circuits	11
-----	--	----

2	Task definition.....	19
----------	-----------------------------	-----------

2.1	Research questions.....	19
-----	-------------------------	----

2.2	Outline of the thesis	20
-----	-----------------------------	----

II	General Methodology	23
-----------	----------------------------	-----------

3	General methodology.....	25
----------	---------------------------------	-----------

3.1	Participants.....	25
-----	-------------------	----

3.2	Experimental movement paradigm	27
-----	--------------------------------------	----

3.3	EEG recording	33
-----	---------------------	----

3.4	EEG signal preprocessing	34
-----	--------------------------------	----

3.5	EEG source analysis	35
-----	---------------------------	----

3.6	Methods for computing PAC	39
-----	---------------------------------	----

3.7	Statistical methods	43
-----	---------------------------	----

III	Experimental Results	45
------------	-----------------------------	-----------

4	Enhanced phase-amplitude coupling in the resting state of patients with Parkinson's disease	47
----------	--	-----------

4.1	Introduction.....	47
-----	-------------------	----

4.2	Methods.....	48
-----	--------------	----

4.3	Results.....	51
-----	--------------	----

4.4	Summary	57
5	Neural circuits contributing to abnormal phase-amplitude coupling of Parkinson's disease	59
5.1	Introduction.....	59
5.2	Methods.....	60
5.3	Results.....	64
5.4	Summary	71
6	Abnormal repetitive finger tapping of patients with Parkinson's disease.....	73
6.1	Introduction.....	73
6.2	Methods.....	74
6.3	Results.....	76
6.4	Summary	82
7	Phase-amplitude coupling in repetitive movements of patients with Parkinson's disease.....	83
7.1	Introduction.....	83
7.2	Methods.....	84
7.3	Results.....	89
7.4	Summary	97
IV	Discussion	99
8	General summary and discussion.....	101
8.1	General summary	101
8.2	Discussion	103
8.3	Limitations and outlook	112
8.4	Conclusion	114
	Summary.....	117
	Zusammenfassung.....	123
	Bibliography	129
Attachment		
	Erklärung über die eigenständige Abfassung der Arbeit.....	I
	Publications	II
	Acknowledgement.....	III

List of abbreviations

Abbreviations	Full name
ANOVA	Analysis of variance
BA	Broadman area
BEM	Boundary element modelling
CFC	Cross-frequency coupling
CSD	Current source density
DBS	Deep brain stimulation
DLPFC	dorsolateral prefrontal cortex
BGTC	Basal ganglia-thalamocortical circuits
ECoG	Electrocorticography
EEG	Electroencephalography(-gram)
EMG	Electromyography
GPe/GPi	Globus pallidus externa/interna
ICA	Independent component analysis
KL-MI	Kullback–Leibler Modulation index
LCMV	Linearly constrained minimum variance
LFP	Local field potential
M1	Primary motor cortex
MDS-UPDRS III	Movement Disorders Society Unified Parkinson’s Disease Rating Scale
MEG	Magnetoencephalography
MRI	Magnetic resonance imaging
MSNs	Medium spiny neurons
MVL	Mean vector length
NIBS	Non-invasive brain stimulation
PD	Parkinson’s disease
PAC	Phase-amplitude coupling
PCA	Principle component analysis
PLA	Phase-locked amplitude
PSD	Power spectrum density
PMC	Premotor cortex

Abbreviations	Full name
ROI	Region of interest
SNc/SNr	Substantia nigra pars compacta/pars reticulata
SS	Somatosensory cortex
STN	Subthalamic nucleus
tDCS	Transcranial direct current stimulation
tES	Transcranial electrical stimulation
TMS	Transcranial magnetic stimulation

*** When the term first appears in each chapter, the corresponding abbreviation is introduced to facilitate the reader's reading of each chapter separately.**

Part I

General Introduction

Chapter 1

Introduction

1.1 Background of Parkinson's disease (PD)

PD is one of the most common neurodegenerative diseases in the world. The primary neuropathology of PD is characterized by the loss of dopaminergic neurons in the *substantia nigra* and the formation of intra-neuronal protein inclusions, called Lewy bodies [1, 2]. The prevalence of PD is conservatively estimated to be about 0.3% of the general population and as high as 3% in people over 80 years of age [2]. About 6 million people around the world currently have PD. Moreover, the incidence of PD increases 5-10 times after the age of 60. As the world's population ages, the number of PD patients is expected to be twice as large in 2030 as it was in 2005, increasing the medical and economic burden on families and society [2]. The prevalence and causes of PD are still unclear and complex, a phenomenon that may be due to a combination of genetic and environmental factors [1-3]. In current studies, researchers have found that the prevalence and incidence of PD are related to gender [3, 4], race [3], certain genetic factors [5], and certain environments (such as chronic exposure to pesticides or certain chemicals, or a history of traumatic brain injury) [6]. As with other neurodegenerative diseases, there is currently no cure for PD. Therefore, modifying disease progression and further attenuating the disability caused by the disease is a critical need in current and future research efforts.

1.2 Clinical features of PD

The main clinical manifestation of PD is the presence of motor impairments. The most common motor symptoms are rest tremor, abnormal muscle tone ('rigidity'), slowness of movement ('bradykinesia'), and postural instability [1, 7]. Other motor features include postural abnormalities, gait disturbances and freezing, micrographia, disorganized speech, and impairment of facial expression [1, 8]. Typically, motor symptoms are asymmetrically

expressed [9]. The manifestation of these symptoms varies markedly from patient to patient and may progress differently depending on the predominant symptoms [10]. In addition, there is a growing recognition that PD is not just a disorder of the motor system but a complex disease in which non-motor symptoms occur in addition to the major motor symptoms. The non-motor symptoms include a large variety of cognitive impairments, mood disorders, affect disorders, and pain [11, 12]. Among these, hyposmia, depression, constipation, and rapid eye movement sleep behaviour disorder are the most common symptoms [1, 11, 12]. The non-motor symptoms can even arise earlier than the emergence of motor symptoms [13]. However, so far, the main clinical criterion for diagnosing PD is the presence of the cardinal symptoms of bradykinesia, rigidity and tremor. The degree of motor impairment is frequently scored by using the Movement Disorder Society Unified Parkinson's Disease Rating Scale (MDS-UPDRS) [14]. The improvement in motor symptoms in response to levodopa is also a supportive feature in diagnosing PD [15].

1.3 The role of basal ganglia-thalamocortical (BGTC) circuits in the pathophysiology of PD

Discoveries in the anatomy and function of BGTC networks have improved the characterization of neuropathological abnormalities in PD, and studies of genetic and experimental forms of Parkinson's syndrome have advanced this tremendous progress.

1.3.1 Organization of BGTC circuits

The anatomic components of the basal ganglia, in the strictest sense, contain the striatum and the *globus pallidus* (GP, *internus*: GPi; *externus*: GPe), whereas the related nuclei consist of the *substantia nigra* (SN, *pars compacta*: SNc; *pars reticulata*: SNr), and the subthalamic nucleus (STN), as shown in Fig. 1.1 [16, 17]. The striatum is the main input structure of the basal ganglia, which converges the cortical projections and receives inputs from the SNc [18]. The thalamus then receives the projections from the striatum through the pathways containing the GP, STN, and SNr and project back to cortical areas [18]. Several groups of anatomically parallel and segregated loops in BGTC circuits are also functionally different. The main BGTC circuits have been grouped as motor, associative, limbic, and oculomotor (not shown in Fig. 1.1); they originated from and projected back to functionally and spatially distinct cortical regions through specific locations of the basal ganglia nuclei and thalamus, respectively [19].

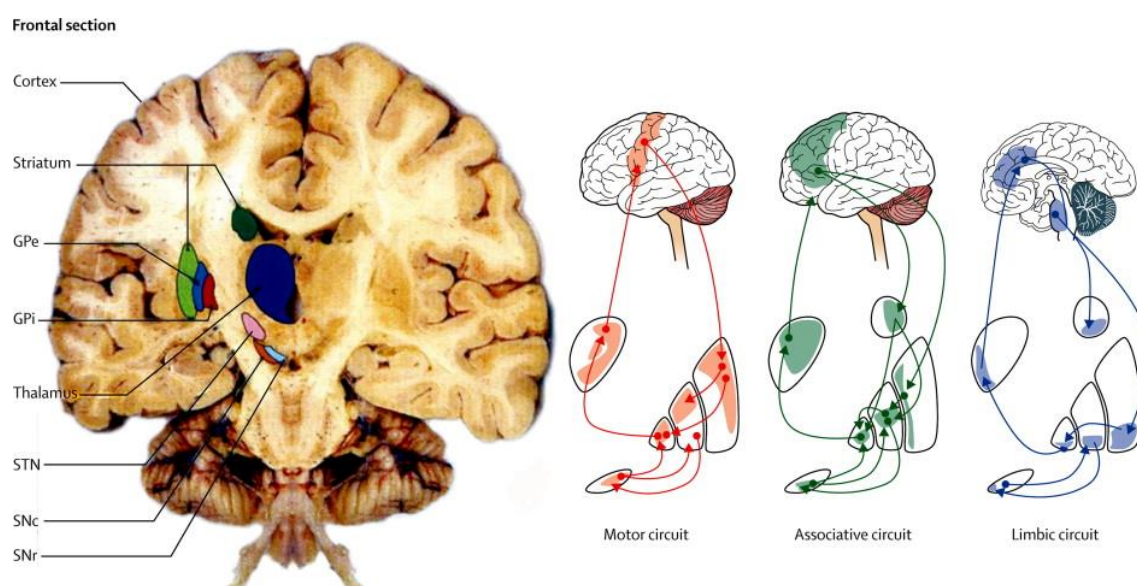


Figure 1.1 The schematic diagram of the anatomical and functional organization of BGTC circuits. Left: The main components and their anatomical locations of BGTC circuits. Right: The BGTC circuits can be functionally segregated into several parallel circuits. For example, this figure displays the motor circuit, associative circuit, and limbic circuit. Functionally distinct circuits also correspond to spatially distinct cortical regions to spatially distinct sub-areas in the basal ganglia nuclei. The figure is reproduced from “The expanding universe of disorders of the basal ganglia”, Obeso et al., 2014, *Lancet*. Copyright 2014 by Elsevier Ltd. Reproduced with permission in the thesis.

The motor BGTC circuit is studied predominantly because of its direct relevance to the pathophysiology of movement disorders. The most frequently applied model of BGTC motor circuits consists of three pathways (Fig. 1.2, left), termed the ‘direct’ pathway, the ‘indirect’ pathway, and the ‘hyperdirect’ pathway [20]. The first two pathways mainly involve the functions of the striatum, which receive excitatory (glutamatergic) projections from the cortex through medium spiny neurons (MSNs) [21]. MSNs express dopaminergic receptors receiving ascending input from dopaminergic projections arising from SNc. The ‘direct’ pathway is defined as direct inhibition (by GABAergic neurotransmitters) of the SNr/GPi by MSNs expressing D1 receptors, whereas in the ‘indirect’ pathway, signalling from the striatum to the GPi requires modulation through the GPe-STN loop [22, 23]. That is, GPe neurons receive inhibitory (GABAergic) projections from MSNs expressing D2 receptors, which then affect the activity of GPi neurons directly and indirectly via the STN [23]. Finally, GPi and SNr GABAergic neurons exert inhibitory influences on the thalamus, which in turn produces excitatory effects on the cortex, resulting in the closure of the BGTC loop. It has been demonstrated that the activation of the ‘direct’ pathway facilitates the movement while the activation of ‘indirect’ pathway suppresses the movement [24, 25]. In addition, a ‘hyperdirect’ pathway through a monosynaptic projection directly from the cortex to the STN acts in parallel

to the ‘direct’ and ‘indirect’ pathways, but it is thought to conduct much faster [26, 27]. The activity of the STN, another prominent input nucleus from the cortex to the basal ganglia – and also regulated by the GPe-STN loop – is now commonly used as an important target to treat Parkinson's motor symptoms [18].

In the normal state, the balance of the three BGTC pathways is regulated by the dopamine level in the brain. According to one hypothesis about the role of the three pathways in BGTC circuits for motor movement [27, 28], the information arriving at the GPi/SNr can initiate a dynamic process of ‘enhancement-inhibition-enhancement’ of neuronal activity, because motor information is transmitted in the three pathways at different speeds. Because the GPi/SNr is connected to the thalamus via inhibitory GABAergic nerve fibres, dynamic modulation of the GPi/SNr neuronal activity can lead to a corresponding ‘inhibition-activation-inhibition’ process in cortical neuronal activities. Although it still represents a gross simplification of the functions of the BGTC circuits, this dynamic model provides a means to explain the precise initiation and cessation of movement.

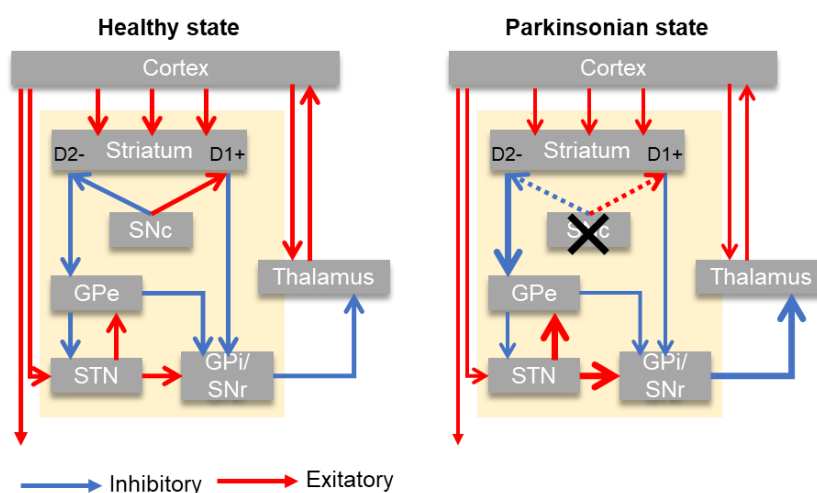


Figure 1.2 The classical model of BGTC circuits in the healthy state (left) and Parkinsonian state (right). The blue and red lines represent the inhibitory and excitatory projections, respectively. The thickness of the lines in the Parkinsonian state represents the increase or decrease in activations of the associated connections compared to that in the healthy state. The dashed lines represent the loss of related connections in the Parkinsonian state.

Nevertheless, there is no doubt that the functional organization of BGTC circuits is far more complex than what is presented in the model consisting of three classical pathways. For example, it was reported that the STN could not only receive inputs from the GPe or cortex, but also that it could be directly modulated by the SNc through dopaminergic receptors [29]. Besides, there is evidence in rats for a direct projection from the STN to the cortex, indicating

that the connection between the STN and the cortex may not be unidirectional [30]. The systematic functional connectivity and mechanisms underlying behavioural processing of the BGTC circuits still needs to be explored further.

1.3.2 Pathophysiology of PD

1.3.2.1 The role of the basal ganglia

The best known neuropathologic feature of PD is the loss of dopaminergic neurons in the SNc-striatum pathway and the widely progressive accumulation and aggregation of intracellular protein (α -synuclein), which eventually irreversibly disrupt both the structure and function of neurons. The loss of dopamine mainly leads to the symptom of bradykinesia in PD patients. Related studies have shown that the loss of dopaminergic neurons in the SNc largely affects the normal functions of BGTC circuits. The classical pathophysiological model of BGTC circuits is illustrated in Fig. 1.2, right, based on the imbalance of the ‘direct’ and ‘indirect’ pathways [31, 32]. Specifically, reducing dopamine leads to a decrease in excitation of MSNs in the ‘direct’ pathway and a decrease in inhibition of MSNs in the ‘indirect’ pathway. The decreased inhibition of GPi and SNr neural activity caused by the excessive activity in the STN through the ‘indirect’ pathway and less inhibition through the ‘direct’ pathway leads to enhanced inhibitory input to the thalamus, thus resulting in the motor impairment of PD due to reduced thalamocortical excitation. This classical model has been developed through the experimental studies of the firing rate in the basal ganglia showing the reduced firing rate of GPe neurons and enhanced firing rate of STN and GPi neurons in Parkinson-like states [33-35].

However, this model has significant limitations because it oversimplifies the complexity of the BGTC organization [36]. For example, it is still unclear how the dysfunction of the ‘hyperdirect’ pathway in the Parkinsonian state would influence STN activity [37]. Besides, the effects of dopamine loss from extrastriatal nuclei in the generation of PD impairments are not considered in the classical model [38]. Moreover, the significance of firing rate changes for the pathophysiology of movement disorders is being challenged due to inconsistent experimental results regarding the functional organizations of striatal neurons [39, 40]. Modern models that consider more elements, such as brain oscillatory or non-oscillatory activities, newly discovered anatomical loci, and synaptic plasticity related to the pathophysiology of PD, need to be investigated for a better understanding of the pathophysiological mechanisms of PD [41].

1.3.2.2 The role of the cerebral cortex

The cerebral cortex is the main input and output of the BGTC circuits. It also processes and combines information from both outside brain stimuli and other subcortical and cortical brain regions. The activities of cortical neurons are also influenced by the interaction with and within local microcircuits. The functional organization of the primary motor cortex (M1) is shown in Fig. 1.3, which displays the layer-specific inputs and outputs of this region [42]. The inputs and outputs of different layers on the motor cortex not only process the signals from the basal ganglia, but also connect with other cortical areas. Besides, D1 and D2 receptors are distributed differently among layers. Therefore, the activities in the cortex in the Parkinsonian state are likely to differ from those in the basal ganglia [43, 44].

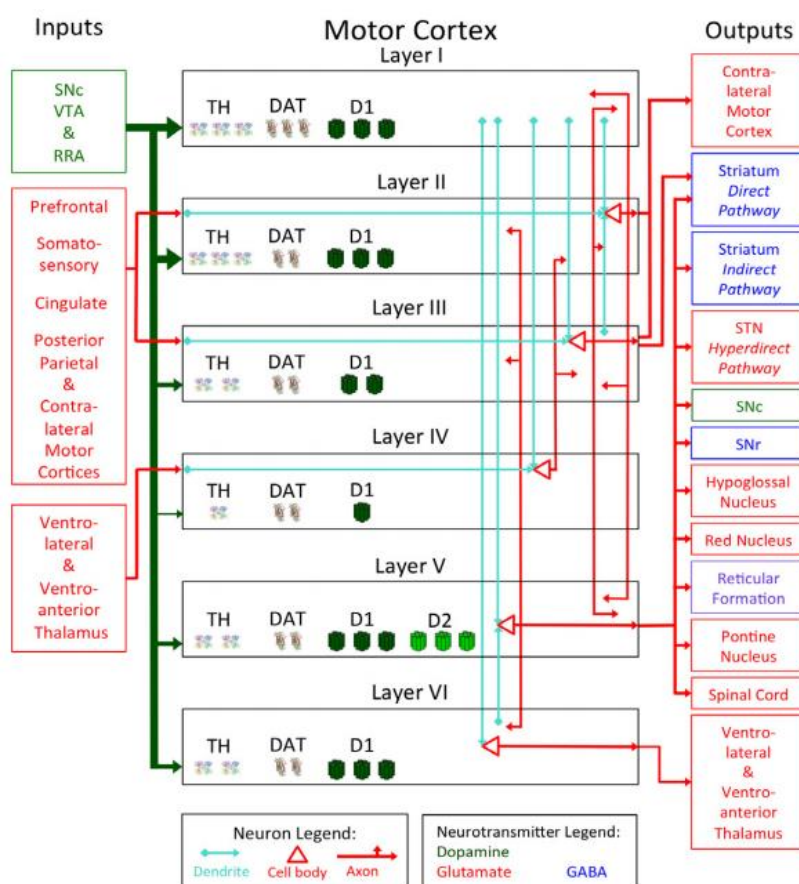


Figure 1.3 Schematic diagram of layer-specific inputs and outputs of the motor cortex. (DAT: dopamine transporter; RRA: retrorubral area; TH: *tyrosine hydroxylase*; VTA: ventral tegmental area). The figure is reproduced from “Critical involvement of the motor cortex in the pathophysiology and treatment of Parkinson’s disease”, Lindenbach & Bishop, 2016, Neuroscience and Biobehavioural Reviews. Copyright 2013 by Elsevier Ltd. Reproduced with permission in the thesis.

Studies in Parkinsonian animal models suggest that the loss of dopamine increases the burst-like firing pattern in M1 pyramidal tract neurons [45], while it decreases the magnitude and the temporal pattern of neuronal activities during movement [46]. Dopamine depletion can also

lead to plasticity changes in M1, as demonstrated by the reduced number of dendritic spines in pyramidal tract neurons located in layer 5b [47]. Although the underlying mechanism is still unclear, the motor cortex has been suggested to play a vital role in the generation of bradykinesia of PD [48, 49], a fact that indicates the motor impairment of PD patients may not be alleviated by changing basal ganglia physiology alone, but also by altering the brain activities in motor cortex.

1.4 Target BGTC circuits for the treatment of PD

Therapies for PD are currently symptom-specific, primarily through modulation of the BGTC dopamine pathways [50]. There are two major categories of therapies used in clinical practice for PD, namely pharmacotherapy and deep brain stimulation (DBS).

1.4.1 Pharmacotherapy

Levodopa is currently the most widely used drug for the treatment of PD [50]. Levodopa is a direct precursor of the neurotransmitter dopamine. It crosses the blood-cerebrospinal fluid barrier, enters the central nervous system, and is converted into dopamine by the action of dopamine decarboxylase to replenish low dopamine levels [51]. Compensatory dopamine could restore the normal function of the BGTC circuits and improve the motor symptoms such as tremor and bradykinesia [51]. The effect of this drug is notable and can also be used to support the diagnosis of PD [15]. However, long-term use of levodopa can have side effects [52]; the major ones, also known as levodopa-induced dyskinesia and motor fluctuations, are characterized by involuntary movements of the head, hands, feet, limbs, and trunk [53]. Levodopa-induced dyskinesia and motor fluctuations occur primarily due to unstable dopamine concentrations in the brain [54]. Unlike a continuous supply of dopamine under normal conditions, the use of levodopa causes phasic stimulation of dopaminergic neurons [54].

1.4.2 DBS therapy and its development

DBS therapy in PD was first proposed in the late 1980s [55]. In the late 1990s and early 2000s, it was adopted in Europe, Canada, Australia, and the United States to treat severe PD. DBS of the thalamus, STN, and GPi have been developed to treat the motor symptoms of PD [56]. DBS is utilized particularly when motor fluctuations occur and for the treatment of tremor that is resistant to pharmacotherapy [57]. Exactly how DBS improves Parkinsonian motor symptoms has not yet been fully established. However, several lines of evidence have been demonstrated that DBS could ‘wash out’ or override the target nuclei’s abnormal electrical activities [56]. The current, most preferred target for DBS treatment is the STN [58]. DBS of the STN can

mainly improve the symptoms of bradykinesia and rigidity. Besides, STN DBS has been reported to reduce medication use by more than 50% [59]. DBS of the GPi can also be applied to improve bradykinesia but cannot reduce medication use during the treatment [58, 59]. Thalamic DBS could also be considered to treat patients when resting tremor is the predominant symptom [58, 59]. In recent decades, researchers have been seeking more effective and individualized DBS treatment protocols. Adaptive DBS and closed-loop DBS have been proposed as promising directions for the development of future DBS therapies [60]. In adaptive DBS, the stimulation is guided by the ongoing electrical activities recorded from the target nuclei or related nuclei to treat the pathological features of PD more effectively [61, 62]. Therefore, identifying and verifying characteristic abnormal electrophysiological signs in the BGTC circuits for PD has been considered a main focus of neuroscientists in recent years, and this endeavour will continue. Besides, DBS therapy still presents limitations. The main limitation is that DBS treatment is not suitable for all PD patients. Because of the invasive surgical risks associated with implanting a DBS system, DBS implantation should, in principle, only be considered in PD patients who present with motor fluctuations or dyskinesias that are not adequately controlled by optimal medical therapy or who develop medicine-refractory tremor [57]. Surgical risk and risk of stimulation-induced side effects are higher in patients with aged over 70-75 years [57]. In addition, patients can also experience high treatment cost from DBS therapy [57, 63].

1.4.3 Potential non-invasive brain stimulation (NIBS) treatment for PD

NIBS therapy, taking advantage of the absence of invasive surgical risk, high safety, easy adjustability, and low cost, has been considered an alternative adjuvant therapy for PD (for review, please refer to Biagioni et al. [64]). NIBS can be sub-grouped as transcranial magnetic stimulation (TMS) and transcranial electric stimulation (tES, which can mainly be subdivided into transcranial direct current stimulation [tDCS] and transcranial alternating current stimulation). In TMS, secondary currents at the cortical surface generated by transient changes in the magnetic field trigger neuronal action potentials. In tES, an electrical current is applied directly to modulate neural membrane potentials but not trigger action potentials. It has the potential to normalize the BGTC circuits via the cortical-STN ‘hyperdirect’ pathway or corticostriatal pathway. Evidence has also been provided that high-frequency repetitive TMS (rTMS) could increase dopamine release in the striatum [65, 66].

NIBS therapies have been studied and shown to have effects on several neural diseases, such as TMS for depression [67], and tDCS for stroke [68]. However, the effectiveness of NIBS in

PD is still at the stage of academic clinical trials. Kim and co-workers – reviewing the studies related to the effects of NIBS on freezing of gait of PD patients – made a positive conclusion that the freezing of gait could be improved after NIBS [69]. Most of the studies reviewed rTMS on the motor cortex and prefrontal cortex, while the effect size when targeting the motor cortex is larger than targeting the prefrontal cortex [69]. It has also been reported that tDCS can benefit bradykinesia of PD that the effects last for longer than 3 months [70]. Besides, another advantage of NIBS therapy over DBS is that NIBS is expected to improve non-motor symptoms in PD patients [71]. However, the effects of NIBS on PD are not always consistent. Several research groups have reported negative findings when applying rTMS over the motor cortex to treat dyskinesia [72]. In addition, even though positive effects of rTMS have been reported, the long-term sustainability of this modality is uncertain [73]. One reason for the variability in the effects of NIBS in PD patients may be that stimulation is applied without taking into account the variability in intrinsic brain states of patients.

1.5 Oscillatory nature of pathological BGTC circuits

As a summary from the section 1.4, neurostimulation for PD is widely accepted as a partial alternative and adjunctive treatment option to pharmacotherapy under current conditions. It urges physicians and neuroscientists to explore optimal stimulation parameters and protocols, either for the development of adaptive DBS or NIBS therapies, to achieve significant improvement in symptoms with fewer side effects and improved safety for PD patients. Besides, stimulation treatment can also play a role in studying systematically the functional mechanisms that operate in pathological BGTC circuits. Electrophysiological biomarkers of PD are of great importance, not only because they may provide necessary targets guiding and informing stimulation interventions, but also because they shed light on the pathophysiological mechanisms of PD. In the following sections, the abnormal oscillatory activities in BGTC circuits in the Parkinsonian state are reviewed. If they can be recorded simultaneously during the stimulation treatment, it may be possible to adjust stimulation in real time. They may also be interesting as surrogate endpoint for NIBS interventions, if they are tightly coupled to motor behaviour.

1.5.1 Neural oscillations

Neural oscillations are rhythmic neural activities generated throughout the central neural system, which have been investigated from the microscopic to the macroscopic levels [74]. Oscillations at the microscopic level can be detected as a sequence of spiking trains or from the fluctuations of membrane potentials that do not reach the threshold producing action

potentials [75]. The synchronization among firing rates in neural populations at the mesoscopic level can also lead to oscillatory activities [75]. In addition, at the macroscopic level, the recurrent network between different brain regions can also give rise to oscillations [76]. Neural oscillations can be recorded invasively as local field potentials (LFP) using implanted electrodes in the subcortical regions or electrocorticography (ECoG) on the surface of the cortex. It can also be recorded non-invasively through electroencephalography (EEG) or magnetoencephalography (MEG). Although the recording approaches can be different, all recordings are thought to reflect similar underlying oscillations of neural activity [77, 78]. Commonly, brain oscillations can be subdivided based on the features of frequency, such as δ (1-4 Hz), θ (4-8 Hz), α (8-12 Hz), β (12-30 Hz), and γ (> 30 Hz). Oscillations in different frequency bands not only reflect the neural processing under different temporal resolution but also relate to functions at different spatial resolution [76]. The characteristics and dynamic modulations of neural oscillations have been related to brain functions and behaviours from many aspects, such as perception, memory, sleep, consciousness, and motor coordination [79-81]. More importantly, evidence from animal and human recordings suggest that the features of neural oscillations play a crucial role in both the physiological and pathophysiological BGTC circuits, making them potential biomarkers for Parkinson's pathology [82, 83]. Recordings from a Parkinsonian animal model showed that the magnitude of oscillations was dramatically increased in the basal ganglia in the Parkinsonian state [82].

1.5.2 Neural oscillations in the Parkinsonian state

So far, three leading frequency bands of oscillations generated from BGTC circuits have been found to be associated with PD, namely the θ/α frequency band (4-10 Hz), the β frequency (12-30 Hz), and the γ frequency band (>60 Hz) [83]. Alternations in these oscillations are thought to reflect distinct mechanisms underlying the generation of PD abnormalities.

1.5.2.1 Oscillations in the θ/α frequency band

Increasing the oscillations in the θ/α frequency range is considered to associate with the resting tremor of PD. In studies of 1-methyl-4-phenyl-1,2,3,6-tetrahydropyridine (MPTP) treated monkeys, the percentage of neurons that showed oscillatory bursting at around 3-10 Hz was dramatically increased in the STN, GPe, GPi, and thalamus, along with the development of Parkinsonian symptoms with tremor at a similar frequency range (4-11 Hz) [84]. The observations have also been confirmed by studies that applied microelectrodes to record signals in the basal ganglia of PD patients and with limb tremor [85, 86]. Although the dopamine depletion could cause the presence of resting tremor, its severity was reported to have no direct

correlation with the reduction of dopamine in striatum [87]. Besides, not all human PD patients or MPTP-affected monkeys develop the resting tremor, in contrast to bradykinesia and rigidity [88]. Because MPTP is recognized as a neurotoxin that destroys the dopaminergic neurons in SNc, these findings may indicate that resting tremor is not entirely related to the pathological dopaminergic pathways of PD [89]. Moreover, the tremor-related oscillations can also be found in cerebellothalamocortical circuits and more extended cortical areas, which suggests that other non-dopaminergic pathways may also play a role in the generation of resting tremor [90]. Therefore, tremor-related oscillations are not always considered as a main biomarker of PD.

1.5.2.2 Oscillations in the β band

The characteristics of β oscillations have been primarily studied in PD. β oscillations are commonly known to be associated with the initiation and maintenance of voluntary movement [91-93], and they are hypothesized as a critical hallmark in pathophysiological BGTC circuits [94]. Abnormal synchronized β oscillatory activity has been found at multiple levels in the basal ganglia in Parkinsonian animal models such as MPTP-treated monkeys [95] and 6-hydroxydopamine-lesioned rodents [96], as well as in PD patients [82, 97]. Besides, it has been reported that the enhanced β power in the STN and GPi of PD patients is more related to the severity of bradykinesia and rigidity rather than tremor [98], and the suppression of β power under levodopa treatment in the basal ganglia is only correlated with the alleviation of bradykinesia and rigidity [99]. These findings indicate that the generation of pathological β activities in the basal ganglia is closely related to the pathology of dopaminergic pathways in BGTC circuits. Levodopa treatment and STN DBS treatment could effectively reduce β synchronization [99, 100]. Several studies in the Parkinsonian rodent model have detected that hyperactivity of MSNs in the striatum in a state of chronic dopamine depletion could lead to an increase in activities of the β frequency range; these activities are then propagated to the STN and GP, suggesting that the striatum is an important source for generating abnormal β oscillations in the Parkinsonian state [101, 102]. Besides, the coherence of the activities at the β frequency range between different basal ganglia nuclei, or between the basal ganglia and cortex, has been found to be increased abnormally [103-105]. In addition, considering that physiological β activity is not elevated continuously but comprises short-lived phasic burst, recent studies have also found another biomarker of PD in the STN, which is the longer maintenance duration of the β bursts [106, 107]. Based on the above findings, researchers have proposed a more efficient way to treat PD by closed-loop DBS, which uses the amplitude and phase of β activity in the STN as the neural target [108, 109]. However, as all information about oscillations in the basal ganglia in humans has been derived from patients with movement

disorders, our understanding of the normal basal ganglia network functions is still limited.

Although the motor cortex is tightly connected with the basal ganglia, it remains uncertain how the activities in BGTC circuits are reflected in electrical activity recorded from the motor cortex. Only around 20% of the variance in the cortical activities in the β band is reported to be explained by basal ganglia activities in PD patients [110, 111]. The findings regarding overactive β activities on the cortical level are not consistent. ECoG recordings from Parkinsonian animal models and recordings from PD patients have revealed abnormally enhanced β activities in the cortex [112-116], while others have reported no differences between patients and controls [117, 118]. Therefore, detecting a more reliable electrophysiological neural signature of PD at the cortical level remains an important scientific goal.

1.5.2.3 Oscillations in the γ band

Compared with numerous studies on β activities, little is known about the role of γ activities in the function of BGTC circuits. The relatively most studied γ oscillations are the activities around 60-90 Hz. It has been reported that the γ activities recorded by LFP in the thalamus and STN increased in the awake state, during movement, and after levodopa treatment [119, 120]. Besides, Litvak et al. reported that the power of γ activities (60-90 Hz) in M1 and high-frequency activities (200-300 Hz) in the STN, and the coherence between M1 and STN at 60-90 Hz in PD patients, could also be increased with movement and levodopa treatment. These findings suggest that the synchronization in BGTC circuits at 60-90 Hz reflects a prokinetic state [121]. By contrast, it has also been reported that broadband γ activities recorded by ECoG are increased in PD patients in the off-medication state over the sensorimotor area [117]. Finally, γ activities are also enhanced during the hyperkinetic state of patients [120, 122]. Therefore, broadband γ activities on the cortex and narrowband γ oscillations at 60-90 Hz in the basal ganglia are likely to reflect distinct neural mechanisms. However, because the findings are inconsistent and no actual relationship between the γ activities and the motor severity of PD has been found, it is still unknown whether the γ power itself has a pathological role in PD.

1.5.3 Phase-amplitude coupling (PAC) as a new oscillatory sign for PD

Overall, the oscillatory features of pathological BGTC circuits of PD have been widely investigated. However, the pathophysiology of PD has been suggested to be more complicated and may involve multiple functional modalities [123]. Evidence of inconsistent findings of increased β synchronization in Parkinsonian animal model and PD patients indicates that only

activities in the β frequency range insufficiently capture the pathophysiological mechanism in PD [41, 124]. Therefore, the fact has prompted the investigation of interactions in Parkinson's-related oscillations at different temporal and spatial dimensions throughout the BGTC network.

1.5.3.1 Cross-frequency coupling (CFC)

As discussed above, the neural oscillations in different frequency bands play a crucial functional role at different temporal and spatial scales in the brain. More importantly, the rhythms in distinct frequencies can also interact with each other, enabling brain functions such as the local-to-global or long-range communication across brain regions. Those interactions can also be called CFC, and mainly include phase-phase coupling, amplitude-amplitude coupling, phase-frequency coupling, and PAC, as shown in Fig. 1.4 [125]. Because the parameters characterizing neural oscillations (frequency, phase, and amplitude) represent different patterns of information transmission, the different types of CFCs may characterize different implications of brain activities [125, 126], and may be associated with a variety of neurological disorders [127-129]. The synaptic and electrical coupling between subpopulations of interneurons has been suggested as a potential mechanism underlying CFC [129, 130].

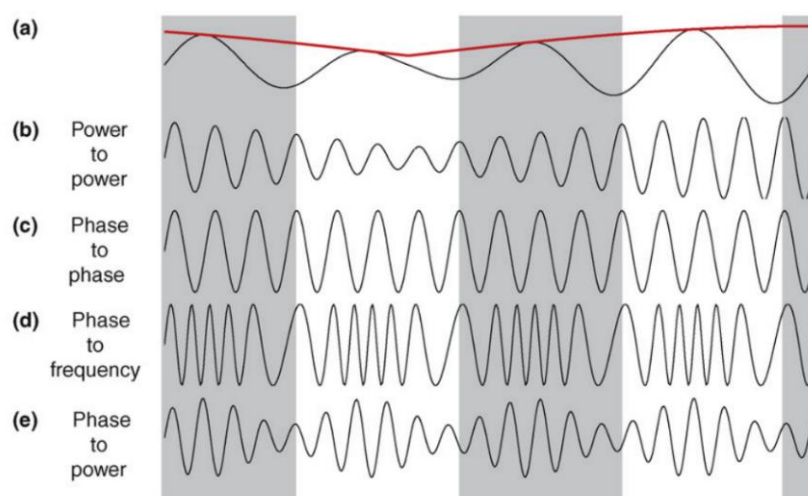


Figure 1.4 Schematic diagram for different types of CFC. (a) The rhythm of low-frequency oscillations. (b) High-frequency oscillations whose amplitude is coupled to the amplitude of low-frequency oscillations. (c) High-frequency oscillations whose phase is coupled to the phase of low-frequency oscillations. (d) High-frequency oscillations whose frequency is coupled to the phase of low-frequency oscillations. (e) High-frequency oscillations whose amplitude is coupled to the phase of low-frequency oscillations. The figure is reproduced from “Cross-frequency coupling between neuronal oscillations”, Jensen et al., 2007, Trends in Cognitive Science. Copyright 2007 by Elsevier Ltd. Reproduced with permission in the thesis.

Specifically, PAC – as a class of CFC, referring to the modulation of amplitudes of high-frequency oscillations by phase from activities at relatively low frequencies – is considered a

fundamental mechanism behind cognitive processing [131, 132] and motor processing [133]. In recent decades, researchers have identified that exaggerated PAC between the phase of β activities and amplitudes of broadband γ activities holds promise as a new biomarker at both the subcortical and cortical levels [108].

1.5.3.2 Abnormal PAC in the Parkinsonian state

The exaggerated coupling between the phase of β (13-30 Hz) oscillations and the amplitude of high-frequency oscillations (~250-350 Hz) had first been reported in the STN LFP recordings of PD patients [134-136]. The abnormal coupling in the STN was found to be correlated with the clinical severity of PD patients [134]. More intriguingly, using the combination of DBS electrode and ECoG electrode recordings on motor areas, de Hemptinne and co-workers [118] demonstrated enhanced coupling between the β phase of the STN and the γ amplitude of the premotor cortex (PMC)/M1, as well as enhanced coupling between the phase of M1 β activities and PMC/M1 γ activities (~50-200 Hz) in PD patients. This finding indicates that depletion of dopamine not only changes the coupling pattern in the basal ganglia, but extends across the BGTC pathways. Several studies using EEG/MEG sensor recording demonstrated that abnormal cortical PAC could even be detected non-invasively [137-139], which may motivate the potential use of exaggerated cortical PAC as a Parkinsonian target for NIBS treatment. Although no direct relationship has been found between clinical severity and the abnormal cortical coupling, researchers have demonstrated that the exaggerated coupling can be reduced by levodopa treatment and DBS therapy of the STN and GPe [138-140]. The reduction in abnormal PAC by levodopa has been correlated with the alleviation of bradykinesia and rigidity [139, 140], supporting the hypothesis that abnormal cortical PAC may be involved in the pathophysiological mechanisms of these motor symptoms characteristic of PD. All these findings highlight the possibilities to establish the abnormal cortical PAC as a surface biomarker for PD.

Nevertheless, the mechanisms underlying abnormal cortical PAC need to be explored further. Regarding the generation of PAC in the Parkinsonian state, several hypotheses have been proposed. One hypothesis states that it is generated as the local neuronal spiking activities in the motor cortex that is entrained by β activity synchronized in the basal ganglia and propagated through BGTC circuits [118]. This hypothesis is supported by the existence of abnormal STN-M1 β - γ PAC [118]. On the other hand, several studies have detected non-sinusoidal waveforms of β activities highly correlated with the strength of PAC, indicating that the cortical PAC may arise from synchronized synaptic input to the motor cortex [115, 141]. In fact, PAC measured

through electrophysiological signals can simultaneously exhibit both entrained and synchronized modes [142]. Therefore, investigating the origin of abnormal cortical PAC would help researchers to understand the pathophysiology of PD. Furthermore, the characteristics of PAC in the Parkinsonian state have not been investigated fully, especially the dynamics of PAC during movement in the presence of bradykinesia and rigidity, which is essential to help researchers understand the causal relationship between the manifestation of PAC and motor impairment of PD.

Chapter 2

Task definition

Researchers have studied a large number of biomarkers classified as clinical, biochemical, genetic, and neuroimaging biomarkers for the diagnosis and treatment of Parkinson's disease (PD) [143]. Among these, electrophysiological biomarkers stand out because they are directly related to the pathological operation of basal ganglia-thalamocortical (BGTC) circuits. Electrophysiological biomarkers not only shed light on pathological mechanisms of PD, but may also have value for neurophysiological interventions through electrical stimulation to improve the motor impairment of PD patients. The neuro-pathophysiology of PD seems to involve interactions between distinct neuronal activities across the BGTC system. In the past decade, a specific oscillatory pattern, termed phase-amplitude coupling (PAC) between the phase of β activities and the amplitude of γ activities, has been proposed as a biomarker for the pathological network of PD [144, 145] that is more selective than the enhancement of spectral power in the β -frequency band. The exaggerated coupling in the resting state has been found in the subthalamic nucleus (STN), motor cortex, and the interaction between the two regions [118, 136]. The enhanced cortical PAC in the resting state has also been considered a promising non-invasive biomarker of PD [137, 139]. However, the characteristics of cortical PAC and its underlying mechanisms remain unclear, limiting its utility in treating PD. Therefore, it is essential to have a more comprehensive understanding of the features and functional role of cortical PAC in the Parkinsonian state, as well as the related pathophysiological mechanisms underlying PD.

2.1 Research questions

In this thesis, I aim to understand the pathophysiological role of enhanced cortical PAC both in the resting state and during voluntary movement derived by non-invasive scalp electroencephalography (EEG) recordings. Specifically, I am interested in the following research questions:

- 1) What is the spatial organization of abnormally enhanced β -broadband γ PAC in the cortex of PD patients?
- 2) What is the mechanism generating the exaggerated cortical PAC in PD at rest?
- 3) How is PAC during voluntary movement directly related to Parkinsonian motor symptoms?

By answering the above questions, we will advance our comprehension of the mechanism underlying abnormal PAC, as well as gain further insight into pathophysiological mechanism of PD. Such fundamental knowledge will help researchers better understand the functional role of the abnormal PAC as a non-invasive biomarker for PD, and may ultimately improve the development of non-invasive stimulation treatment for the disease.

2.2 Outline of the thesis

In **Chapter 3**, we provide detailed information about the characteristics of subjects, the experimental design, and the main methodology we applied to investigate the research questions in the thesis. The specific methods that were used for specific findings are also described in detail in the corresponding chapters of the results.

The following four chapters aim to give readers a comprehensive view of the experimental findings of the thesis. In order to answer the first research question, in **Chapter 4**, we set out to investigate spatiotemporal features of the cortical PAC of PD patients in the resting state, focusing on the anatomical spatial distribution of abnormal cortical PAC. The anatomical spatial distribution of the pathological signal is of great importance because the anatomy of the cortex also relates to the information of specific brain functions. Therefore, examining anatomical spatial distribution may shed light on the relationship between the neuronal nature and symptoms of the disease.

In the subsequent study, reported in **Chapter 5**, we go a step further to investigate the potential mechanisms of abnormal PAC. We aim to investigate the mesoscopic organizations of abnormal PAC of PD patients in the resting state, which may indicate the origin of PAC-involved β and γ activities. Specifically, we investigate the phase relationship between the PAC-involved β and γ activities, as well as their spatial source distributions at a local region.

Although we have a better understanding of abnormally enhanced PAC in the resting state of PD patients from the Chapter 4 and 5, it is still unclear how the abnormal coupling is related directly to the behavioural abnormalities of PD patients. Therefore, the remaining two chapters

(**Chapter 6 and 7**) of the experimental findings help us to solve the third research question.

Before investigating the features of movement-related PAC of PD, we need first to understand the motor behaviour that is related to the motor impairment of PD. In the clinic, bradykinesia is evident by using finger tapping tests [146]. Thus, in **Chapter 6**, we test several types of repetitive voluntary finger movements and comprehensively characterize the behavioural normality and abnormality in PD patients.

Subsequently, in **Chapter 7**, the dynamics of PAC is estimated during transients of movements in those brain regions related to motor control, that showed an abnormal pattern at rest. We investigate the absolute strength of PAC in different movement tasks, its modulation during the change in movement states, as well as the differences of both between PD patients and healthy subjects. We expect this study to reveal insight into the functional role of PAC in the execution of repetitive movements and its possible association with the pathophysiology of PD.

Finally, **Chapter 8** provides a general summary and detailed discussion of all the findings of this thesis, as well as the future directions and expectations. Through this thesis, I hope that the reader will gain a more comprehensive understanding of the functional role of cortical β -broadband γ PAC in PD, its underlying physiological and pathophysiological mechanisms, and its potential application as a non-invasive surface biomarker for PD patients.

Part II

General Methodology

Chapter 3

General methodology

This chapter is intended to introduce the reader to the methodology regarding the core research questions of this thesis. In this chapter, we describe the recruitment of subjects, the experimental design of the protocol, the equipment and techniques used for electrical signal recording, and the main analytical methods used to address the main research questions of this thesis. Thereby, we aim to provide the reader with a deeper understanding of the thesis's core technical approaches and facilitate the reproduction of the results.

3.1 Participants

The study protocol was approved by the local Ethics Committee at the Medical Faculty of Leipzig University (Reference number: 147/18-ek). All participants were right-handed, as confirmed by the Edinburgh Handedness Inventory [147]. Written informed consent was obtained from all study participants.

We recruited 21 patients with Parkinson's disease (PD) according to the current diagnostic criteria [148] from the outpatient clinic of the Department of Neurology, University of Leipzig Medical Center. Motor function of all patients was assessed before the experiments, using part III of the Movement Disorders Society Unified Parkinson's Disease Rating Scale (MDS-UPDRS III) [149]. A neurologist confirmed that patients were in a practically defined "off-medication" state after overnight withdrawal (at least 12 h) of Parkinsonian medication. The exclusion criteria for PD patients were: severe tremor (resting tremor score > 2), presence of a neurological disorder other than PD, presence of deep brain stimulation (DBS) electrodes or other cranial implants, and refusal or inability to participate in magnetic resonance imaging (MRI) scanning. Two patients were excluded from the cohort. One was excluded because of serious tremor activity interfering with the electroencephalogram (EEG), and the other was excluded from MRI scanning because of uncertificated metal implant. Therefore, 19 patients were included in the subsequent analysis. The structural MRI images for all patients were

acquired at the Max Planck Institute for Human Cognitive and Brain Sciences (MPI CBS), except for one patient whose MRI image was acquired at University of Leipzig Medical Center. The detailed characteristics of patients are presented in Table 3.1. On average, patients had been diagnosed with PD 5.3 ± 4.5 years before the current investigation.

Table 3.1 Characteristics of PD patients

ID	Sex	Age, years	Disease Duration, years	Clinically more affected body side	Total MDS-UPDRS III (medication off)	L-Dopa equivalent dose mg/day
01	Male	57	4	Right	15	310
02	Female	46	1	Left	6	210
03	Male	54	1	Left	22	400
04	Female	65	3	Left	10	152
05	Male	55	1	Left	12	500
06	Male	49	4	Right	30	735
07	Male	67	12	Right	20	682.5
08	Female	74	11	Left	24	400
09	Male	75	3	Left	30	525
10	Male	76	2	Right	12	100
11	Female	78	4	Left	32	300
12	Female	58	6	Left	19	955
13	Male	71	12	Left	35	1395
14	Male	56	2	Right	11	355
15	Female	57	3	Left	26	930
16	Male	63	6	Right	20	400
17	Male	61	17	Right	29	1185
18	Male	38	2	Right	21	520
19	Male	57	6	Right	14	930

MDS-UPDRS III: part III of the Movement Disorders Society Unified Parkinson's Disease Rating Scale; L-Dopa: levodopa

Twenty-three age- and sex-matched healthy controls were recruited through various media. One healthy subject was excluded from the analysis due to an abnormal finding on the MRI. Exclusion criteria for healthy controls included the presence of any neurological disorder and the use of psychotropic medication. The structural MRI images for all healthy controls were available in the database of MPI CBS. The parameter settings of the MRI images of healthy controls were the same for the patients. MRI images represent 3-Tesla, T1-weighted images scanned by an MPRAGE sequence with the dimensions in $240 \times 256 \times 176$ and the voxel sizes in $1 \times 1 \times 1 \text{ mm}^3$.

In the following signal preprocessing procedures (please refer to section 3.4), two healthy controls were excluded from the later analysis because of poor data quality. In the end, the results presented in this thesis are based on the recordings from 19 patients (6 females, age \pm

standard deviation [SD]: 60.89 ± 10.80 years) and 20 controls (8 females, age \pm SD: 62.55 ± 7.85 years). There was not a significant age difference between patients and controls ($p = 0.527$).

3.2 Experimental movement paradigm

3.2.1 Movement recording

Pressing and tapping tasks (please refer to section 3.2.2) were recorded by using a custom-made device consisting of a force transducer and two photoelectric beam sensors (Fig. 3.1A). The digital signal from the force transducer served to determine the real time movement onset and offset of the pressing task. During the pressing task, the onset of pressing was defined as the moment when the force transducer passed a threshold of 1.3 N. This threshold was determined based on the pilot measurements. The maximum force that the transducer could detect was 4.4 N.

The lower photoelectric sensor was placed at a height just above the finger when it was placed on the pressure sensing board, and the higher photoelectric sensor was placed at the height of the extended index finger in a position parallel to the table. During the tapping tasks, the real time movement onset of index finger extension was defined as the time when the light beam of the lower photoelectric sensor was interrupted by the extended index finger. The signal from the upper photoelectric sensor was used as a criterion regarding the height of the extended index finger during tapping. In a tapping movement, an omission was recorded if the index finger was not fully extended to the height of the upper photoelectric sensor. Fig. 3.1B illustrates how information of movement events was determined during the pressing and tapping tasks. The mechanical onsets recorded online were verified visually afterwards for mechanical or performance errors.

3.2.2 Movement tasks

Participants were asked to perform three different voluntary movement tasks involving repetitive index finger actions: pressing, and tapping at a slow and fast speed. We tested the performance of the patients on the hand side most prominently affected by the disease as indicated by the bradykinesia MDS-UPDRS III hemi-body scores (10 patients on the left and 9 patients on the right). In healthy controls, the side for performing the movement tasks was chosen pseudorandomly to match the respective sub-sample sizes of patients (10 controls on the left and 10 controls on the right). Before the start of each trial, the subjects were asked to place their arm on an armrest and place their index finger on the pressure sensing board. The

participants were asked to start the index finger movements as soon as a white cross appeared at the centre of the computer screen.

The experimental protocol is illustrated in Fig. 3.1C. In the pressing task, the subjects were asked to perform a self-initiated pressing and releasing movement using their index finger at a comfortable rate (2 trials of 3 min each). In the slow tapping tasks, subjects were asked to perform a self-paced tapping at a relatively slow but comfortable tapping rate (6 trials of 30 s each) with the instruction ‘tap at self-determined speed’ given before each trial. In the fast tapping tasks, subjects were asked to tap as fast as possible in each trial (10 trials of 12 s or 15 s each, two blocks [9 patients and 11 controls tapped for 12 s per trial in the second block of fast tapping tasks]) with the instruction ‘tap as fast as possible’ given before each trial. Between trials and tasks, subjects were allowed sufficient time to rest in order to minimize fatigue. During both tapping tasks, subjects were asked to tap using their maximal index finger extension. Two conditions were designed for each tapping task (Fig. 3.1D). The conditions differed in the absence or presence of feedback on whether the extension of the index finger had met the upper height criterion as detected by the upper photoelectric light beam. In the first condition, subjects were asked to perform repetitive tapping at the instructed tapping rate without receiving feedback about the tapping amplitude (Fig. 3.1D, left). In the second condition, they received continuous colour feedback indicating whether the index finger extension had reached the upper height criterion reported by the upper photoelectric sensor (Fig. 3.1D, right). In the feedback conditions, subjects were instructed to increase their index finger height according to the feedback if necessary. The feedback was updated after every single tapping movement. Therefore, the motor tasks consisted of five conditions: repeated pressing at a slow rate, slow tapping without feedback, slow tapping with feedback, fast tapping without feedback, and fast tapping with feedback.

The quantitative performance measurement includes the estimation of movement rate, tapping variability, completion ratio, and decrement of tapping amplitude. The precise procedures for the estimation of performances and related results are described in detail in **Chapter 6**, which illustrates the performance characteristics of PD patients.

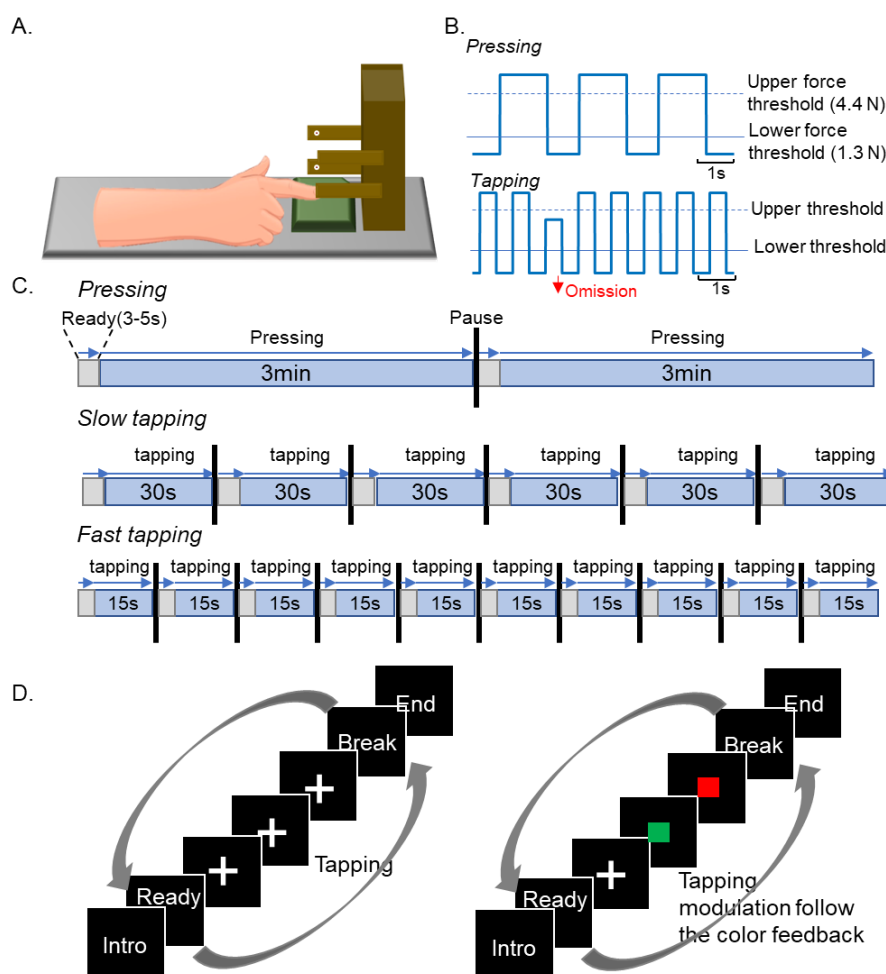


Figure 3.1 Experimental design. (A) Schematic diagram of the repetitive movement device, comprising a force transducer (green plate) and two photoelectric sensors (light barriers; white). (B) Schematic representation of the force and amplitude trajectories during pressing (upper curve) and slow tapping (lower curve), respectively. In pressing, movement onset was defined as the moment when the force signal exceeded the lower force threshold (1.3 N). No force signals were resolved above the upper threshold of 4.4 N. In tapping, movement onset was defined as the moment when the index finger was extended above the light beam of the lower photoelectric sensor. An omission was recorded if the index finger was not extended high enough to reach or cross the light beam of the upper sensor. (C) Experimental protocol for movement tasks. (D) Experimental design of the tapping tasks. There are two conditions for each tapping task. Left: In the first condition, subjects perform repetitive tapping when looking at the cross all the time. Right: In the second condition, subjects start tapping when looking at a cross but then receive continuous colour feedback indicating the tapping magnitude. Green indicates that subjects perform appropriately when the maximum tapping magnitude is beyond the higher beam light sensor. Red indicates that the subjects tapped too low to reach the higher light sensor. Subjects were asked to adjust their tapping when receiving red feedback.

3.2.3 The definition of four trigger points indicating movement transitions

3.2.3.1 The definition of mechanical trigger points

To investigate the dynamics of brain activities during transitions between movement states, we

first determined in each subject when movement transitions occurred between different movement phases. Therefore, we first separated the movement into five periods by four trigger points derived from the digital kinetic (pressing) or kinematic (tapping) signals recorded in real time during the movement for each individual. Trigger points were established individually for each movement cycle. Because the movement transient is too quick during the fast tapping task to be segmented, this part of the analysis included the pressing and slow tapping tasks exclusively.

For the pressing task, the four mechanical trigger points were defined as 1) the movement onset – the real-time mechanical onset (force level exceeding 1.3 N); 2) the end of the pressing build up – the detected end of the pressing build-up that was defined as the moment when the pressing force exceeded the maximally detectable force of the device (4.4 N) or – if the maximally attained force level was below 4.4 N – the sign of the slope changed from at least two consecutive positive signs to 0 or negative; 3) the start of releasing – the detected start of releasing that was defined as the moment when the force fell below 4.4 N or – if the maximally attained force level was below 4.4N – the sign of the slope changed from 0 or positive to at least two consecutive negative signs; and 4) and the movement offset – the real-time mechanical offset (force level falling below 1.3 N).

For the tapping task, the four mechanical trigger points were defined based on the lower and upper photoelectric sensors as 1) movement onset – the time when the index finger had reached the height of the lower photoelectric sensor; 2) the end of finger extension – the time when the index finger had been extended up to the height of the upper photoelectric sensor; 3) the start of finger flexion – the time when the index finger had been lowered below the upper photoelectric sensor; and 4) the movement offset – the time when the index finger had been lowered below the lower photoelectric sensor.

3.2.3.2 The definition of adjusted trigger points at the level of the cortex

Importantly, to estimate the timing of the transition times at the cortical level with the best possible accuracy, we adjusted the trigger points by considering the influence of general delay (including general mechanical and electromechanical delays, as well as the corticomuscular conduction time) from mechanical trigger points (defined in section 3.2.3.1) across subjects in pressing and tapping events. The electromechanical delay is the time delay between the onset of muscle activation and the measurable movement – reflecting both electrochemical and mechanical processes – had previously been demonstrated to be around 50 ms [150]. The corticomuscular conduction time was defined as the time lag from the activation of the motor

cortex to the activation of muscle, which was measured as 20 ms in general, as demonstrated by the transcranial magnetic stimulation (TMS) experiment [151].

It is then important to estimate the mechanical delay. For practical purposes, movement onset and offset were defined by the time of passing the lower force threshold for pressing tasks or the activation of the lower light beam sensor for tapping tasks. The mechanical delay was defined as the delay from the actual movement onset/offset to the practically defined real-time mechanical events as determined by the force threshold or photoelectric sensor signal.

We used kinetic signals recorded from the force transducer in both pressing tasks and slow tapping tasks to objectively assess the actual movement onset and offset. For each subject, the digital signals derived from the force transducer were first segmented into 3 s epochs (-1 s before the real-time mechanical onset/offset and 2 s after the real-time mechanical onset/offset). The values representing signals of the four light beam sensors were set to NaN. Then the signals were interpolated to bring the sampling rate to the same value (2 kHz). An averaged digital signal across epochs was calculated for each subject. Because the frequency of the movements for pressing and slow tapping tasks was considerably lower than 5 Hz for our cohort, the signals were smoothed through a second-order low-pass Butterworth filter at 10 Hz to avoid interference from high-frequency activities.

We determined the actual movement onset for pressing movements when pressure acceleration reached the maximum and the movement offset as the time when pressure acceleration reached the minimum. To this end, we calculated the second derivative of the digital signals in every 10 ms window with a 5 ms time step. The movement onset was then determined at the location of the peak (local maximum) close to the real-time mechanical onset, or the location of the valley (local minimum) close to the real-time mechanical offset, as shown in Fig. 3.2A&B (left panel), respectively. The mechanical delay for each subject on the movement onset/offset is given by the time differences between the actual onset/offset to the real-time detected mechanical onset/offset. The general mechanical delay was then calculated as the averaged mechanical delay across subjects. In this way, the general mechanical delay at the movement onset was 43 ms (Fig. 3.2A, right panel), while the general mechanical delay at movement offset was 9.8 ms (Fig. 3.2B, right panel).

For slow tapping movements, we determined the actual movement onset when the pressure rate reached the minimum, which indicated that the finger had left the pressure plate (one subject was excluded from the analysis because of the loss of the online records of the force transducer).

Therefore, we calculated the first derivative of the digital signals in every 10 ms window with a 5 ms time step. The movement onset was then determined on the valley (local minimum) close to the real-time mechanical onset, as shown in Fig. 3.2C (left panel). Therefore, the general mechanical delay across subjects at the movement onset was calculated to be 60 ms (Fig. 3.2C, right panel). Regarding the movement offset, we checked when the finger started to touch the pressure plate. We found a quick (< 10 ms) deflection of the force signal right after the finger flexion had crossed the lower light beam sensor (Fig. 3.2D). We neglected this delay at the movement offset because of its brevity.

Overall, in the pressing task, the general delay in total from the adjusted movement onset at the cortical level to the real-time mechanical onset of pressing was estimated as 113 ms (20 ms + 50 ms + 43 ms). The general delay from the adjusted movement offset to the real-time mechanical offset of pressing was estimated as 60 ms (20 ms + 50 ms - 10 ms). Besides, due to the force saturation (the maximum force that can be detected is 4.4 N) during the pressing in most cases, the realistic ending of pressing and start of releasing cannot be acquired, the general delays for the two trigger points between the movement onset and offset only included the general electromechanical delay and the corticomuscular conduction time, which are 70 ms.

In the slow tapping task, the general delay in total from the adjusted movement onset at the cortical level to the real-time mechanical onset of tapping was estimated as 130 ms (20 ms + 50 ms + 60 ms). The general delay from the adjusted movement offset to the real-time offset of tapping only contains the general electromechanical delay and the corticomuscular conduction time, which in total was 70 ms. Moreover, because the device did not record the entire trace of the finger tapping when the finger left the pressing board, the general delays for the two trigger points between the movement onset and offset only included the general electromechanical delay and the corticomuscular conduction time, which are 70 ms.

We further applied the adjusted trigger points at the cortical level to investigate in detail the EEG oscillatory activities during movement transitions in **Chapter 7**.

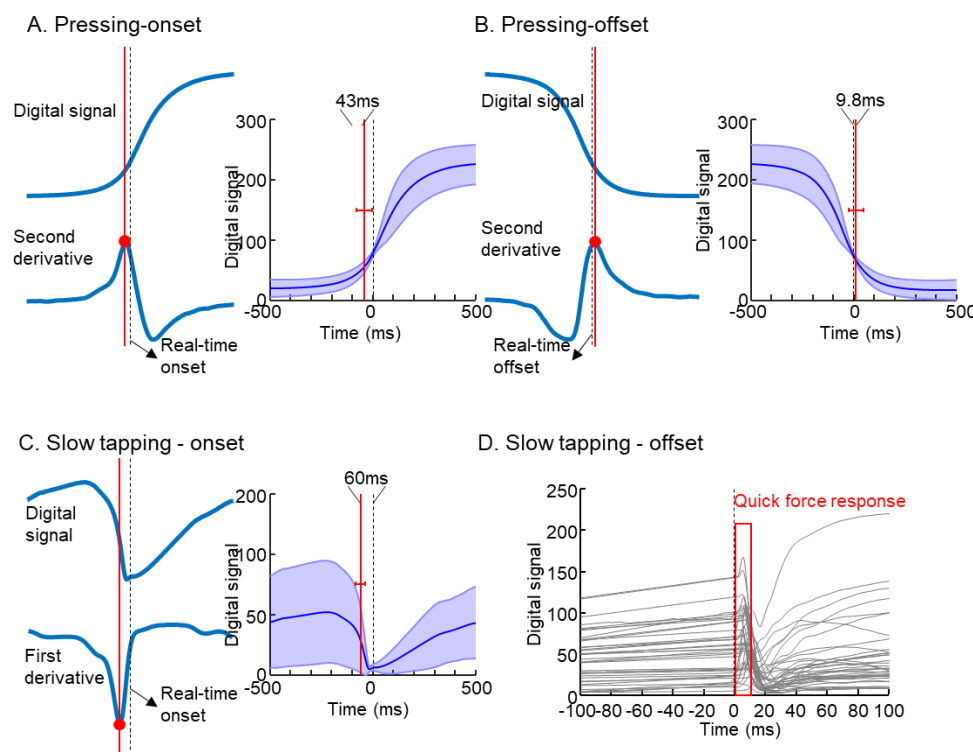


Figure 3.2 Estimation of mechanical delays in pressing and slow tapping tasks via digital signals from force transducer. (A) Mechanical delay at the movement onset of pressing task. Left: the adjusted movement onset was determined at the local maximum of the second derivative of the digital signals from the force transducer for each subject. Right: the general mechanical delay was estimated by the time difference between the real-time mechanical onset (0 ms point) and the averaged moments for adjusted movement onset across subjects. (B) Mechanical delay at the movement offset of pressing task. Left: the adjusted movement onset was determined at the local maximum of the second derivative of the digital signals from the force transducer for each subject. Right: the general mechanical delay was estimated by the time difference between the real-time mechanical offset (0 ms point) and the averaged movements for adjusted movement offset across subjects. (C) Mechanical delay at the movement onset of slow tapping task. Left: the adjusted movement onset was determined at the local minimum of the first derivative of the digital signals from the force transducer for each subject. Right: the general mechanical delay was estimated by the time difference between the real-time mechanical onset (0 ms point) and the averaged moments for adjusted movement onset across subjects. (D) Mechanical delay at the movement offset of the slow tapping task. The line plot showed interpolated digital signals of all subjects. Most subjects showed a quick and large force response right after the finger flexion interrupted the lower light sensor (real-time mechanical offset, 0 ms point). The period from real-time mechanical offset to the deflection of the force transducer was neglected because of its brevity.

3.3 EEG recording

In the present thesis, the brain signals of each subject were recorded using a 64-channel EEG system (eegoTMmylab, ANT Neuro, the Netherlands) with 24-bit resolution and sampled at 2000 Hz. Vertical electrooculography and bipolar electromyography (EMG) of the first dorsal interosseous (FDI) muscle were also recorded. The EMG signals were recorded from the hand

performing the movement tasks (refer to section 3.2.2, left hand: 10 patients and 10 controls; right hand: 9 patients and 10 controls).

Before the start of the EEG recordings, the positions of the EEG electrodes were recorded using a three-dimensional optical digitization system (EEG Pinpoint, Localite, Germany). To allow better and more accurate offline co-registration between an individual's electrode positions and head models created from structural MRI images, we also acquired another three fiducial markers (nasion, left pre-auricular and right pre-auricular) and 30 face markers (markers on the nasal and brow bones).

Regarding the EEG recording, we first recorded 5 min of the signal under resting conditions. Subjects were asked to relax and to fixate on a white cross displayed at the centre of a black computer screen 80 cm in front of them during the recordings. Then, signals were recorded under the movement tasks described above. The experimental recording protocol is presented in Fig. 3.3.



Figure 3.3 the experimental paradigm for EEG recording. The 6 conditions were recorded for all subjects in the same chronological order (FB-: without colour feedback, FB+: with colour feedback).

3.4 EEG signal preprocessing

EEG signals were first preprocessed using the EEGLAB toolbox [152] (<https://sccn.ucsd.edu/eeglab/index.php>) and custom MATLAB scripts. The basic preprocessing procedures were the same for each subject under each recording session using a standard pipeline. Signals were first detrended and then high-pass filtered at 0.5 Hz (eegfilt.m in EEGLAB with a finite impulse response filter default settings). Channels with poor data quality were excluded either based on visually detected artefacts (long-term large spiking-like activities) or if their power spectra failed to follow the canonical 1/f pattern [153]. Independent component analysis (ICA) was applied to remove the components that contained eye movement artifacts, channel noise, line noise, heart beats, or major muscle artifacts. Before removing ICA components, artifacts from transitory muscle activities were detected visually and marked in the continuous raw data. The data of two healthy controls were excluded from later analysis through preprocessing, because more than 50% of the data in the resting state recordings were contaminated by noise. Afterwards, all data were re-referenced to the average

of all electrodes.

3.5 EEG source analysis

Although the EEG technique allows non-invasive investigations of brain activities, the traditional analysis based on sensor signals suffers from spatial mixing due to the volume conductor properties of the head. Therefore, spatial demixing methods are important for separating the source signals and assigning them to specific locations in the brain.

3.5.1 Surface Laplacian

One common method to improve the spatial specificity at the sensor level is the calculation of current source density (CSD), also known as a surface Laplacian. It is a second spatial derivative operator that increases spatial specificity by attenuating the broad spatial features of the signals [154]. These broad spatial features can be volume conducted potentials or contaminating muscle activities that affect the electric potentials on the entire (or large parts of the) head surface. In contrast to source imaging (see section 3.5.2), it does not require any volume conductor model of the head. Here, we computed the surface Laplacian using spherical spline interpolations as introduced by Perrin et al. [155] and implemented in the CSD toolbox (<https://psychophysiology.cpmc.columbia.edu/Software/CSDtoolbox>) in the MATLAB environment.

3.5.2 EEG source imaging

Although CSD helped us isolate the local functional brain activities from broadly distributed signals, the spatial information we obtained is still limited to the topography of the EEG sensors. As a result, we still lacked information on the correspondence between the signals at the electrodes and the signals at the realistic anatomical cortical sites. Over the past two decades, researchers have developed approaches that convert EEG electrode signals into a true neuroimaging modality by combining structural MRI images containing realistic anatomical information with EEG signals containing information with a high temporal resolution. This is referred to as EEG source imaging or source reconstruction. Two main vital concepts in source analysis are the forward solution and the inverse problem. The forward solution is to compute the possible relationship between given source configurations in the brain and the potentials of the given EEG electrode, while solving the inverse problem is to estimate the feature of the sources based on the observed EEG. In this thesis, we used EEG source imaging to differentiate the fine spatial structure of cortical oscillators within a local region.

The main procedures for EEG source estimation in the present thesis are displayed in Fig.3.4.

The method mainly comprises four main steps: 1) creating a realistic head model using individual MRI image; 2) solving the inverse problem by applying a beamformer filter; 3) defining the functionally related brain regions according to the cortical anatomy; and 4) deriving spatiotemporal source components. In the following sections, I introduce the procedures step by step.

3.5.2.1 Forward solution

To improve source localization accuracy, the computation of a forward solution in the thesis requires information about the location of possible sources, the position of electrodes, and a volume conduction model based on individual MRI images and individual EEG electrode positions. The volume conduction model describes how the currents flow through the tissue, which needs the realistic geometrical description of the head (a realistic forward head model) and a description of the conductivity of tissues. We implemented Freesurfer [156] (<https://surfer.nmr.mgh.harvard.edu/>) and Fieldtrip toolbox (<https://www.fieldtriptoolbox.org/>) [157] in the thesis to address the forward solution. First, we co-registered the recorded electrode positions to the MRI using the fiducial markers. Then, we applied the Freesurfer toolbox to the individual MRI images to construct triangulated surfaces describing the outer boundary of the head, the inner and outer boundaries of the skull, and the surface of the cortex. The first three surfaces (each surface subsampled to 5120 vertices) were used to construct a realistic head model by applying the boundary element method (BEM) for the description of volume conduction properties of the head [158]. The BEM approximates the volume conduction properties by treating the realistic compartments of the head as isotropic and homogeneous conductivities. It is more accurate than the simplified spherical symmetry model which does not consider the true shape of the head components [159]. Moreover, the BEM has the advantage of using only surface meshes instead of volume meshes, resulting in a more efficient calculation compared with the finite element method [160]. Specifically, we generated a BEM model by applying the linear collocation method with an isolated skull approach (named ‘dipoli’ in Fieldtrip toolbox) [161] with optimized volume conductivity (0.33 S/m for the scalp and brain compartments, 0.33/40 S/m for the skull) [162]. In addition, the cortical surface was used to construct source space that describes a set of positions and orientations of equivalent current dipoles (subsampled to 8196 dipoles) distributed on the realistic surface. Finally, using the volume conduction model, the information of source space, and the information of co-registered electrode positions, we computed the lead-field matrix, which describes the output of a particular electrode (matrix row) due to a particular dipole source (matrix column). The dipole orientations were chosen perpendicular to the surface because EEG is mainly generated

by the apical dendrites of pyramidal cells [163].

3.5.2.2 Inverse problem

The inverse problem of EEG source analysis is not unique, which means that any EEG pattern at the sensors could be traced back to many possible source configurations [154]. Beamforming is one of the most common adaptive distributed source imaging approaches [164, 165] and offers optimal spatial resolution [166, 167]. Beamforming in EEG source analysis acts as a spatial filter calculating the linear combinations of signals measured at different sensors, retaining the signal components from the desired direction or location while suppressing interference from other directions or locations [168]. In this thesis, because we aimed to project the time-domain signals from the sensor level to source space, a spatial filter was constructed by using a linearly constrained minimum variance (LCMV) beamformer [169] on the covariance matrix of artifacts-removed EEG signals (C) and the lead-field matrix (L). Then for each dipole location r , the spatial filter W was calculated as:

$$W^T = (L^T(r)C^{-1}L(r))^{-1}L^T(r)C^{-1}.$$

We used the equation that has been implemented in the Fieldtrip toolbox (beamformer_lcmv.m).

3.5.2.3 Selecting the region of interest (ROI)

With the two procedures described in sections 3.5.2.1 and 3.5.2.2, we constructed the signals of 8196 source dipoles throughout the constructed cortical surface from the EEG sensor signals. Source signals were then selected and grouped corresponding to particular cortical ROIs associated with specific brain functions. In our study, the ROIs were defined by the Human Connectome Project atlas based on multi-modal parcellation of the cortex [170]. In the atlas, 180 cortical areas are defined. One of our main focuses in the thesis is the spatial organization of abnormal cortical phase-amplitude coupling (PAC) of PD. Because the abnormal PAC of PD has been reported in recordings from C3 and C4 EEG electrodes [137, 139] – which only broadly reflect neuronal activity originating from sensorimotor brain regions – we aimed at the further spatial specification of PAC, mainly focusing on the regions involved in motor control. Thus, we kept a fine resolution in the regions ‘Somatosensory and Motor Cortex’ and ‘Paracentral Lobular and Mid Cingulate Cortex’. Specifically, as described in the supplement of the work by Glasser et al. [171], the region ‘Somatosensory and Motor Cortex’ contains three (sub)regions, namely the primary motor cortex, the primary somatosensory cortex, and the primary somatosensory complex, and the region ‘Paracentral Lobular and Mid Cingulate

Cortex' contains three (sub)regions, namely the cingulate motor area, the supplementary motor area, and area 5. For all other parts of the brain, we retained the coarser resolution of 20 regions as defined by Glasser et al. (2016) to avoid statistical power issues. As a result, 26 ROIs were defined covering the whole brain at variable resolution.

3.5.2.4 Source-space ICA

From the method in section 3.3.2.3, the signals of sources from a local brain region extracted by the defined parcellation are likely to share similar information. However, the large regions might still contain smaller networks of neural loops that can be differentiated by the EEG data and may interact with each other locally. These subnetworks can be further delineated according to their activation time course (or oscillation patterns) and spatial distribution. In signal processing, ICA was introduced as a computational method for separating a multivariate signal into statistically independent subcomponents. It has been widely used on EEG sensor signals to create scalp maps with mutually independent activation time courses (also applied in section 3.4) [172]. Here, we used the source-space ICA method developed by Jonmohamadi et al. [173] to segregate the local subnetworks in the source signals of a specific brain region. Specifically, principal component analysis (PCA) was first applied to reduce the noise by keeping the main components explaining 95% of the data variance. Then, to detect statistically independent stationary sources, we employed ICA to evaluate the PCA-truncated source signals separately for each ROI. PCA and ICA were computed by `runica.m` in EEGLAB with the rank of 95% data variance.

In the thesis, considering the analysis of PAC described in section 3.6, we applied the beamformer weights and PCA-ICA weights to the artefact-marked signals to generate continuous, breakpoint-free data (artefacts should be finally removed after applying bandpass filters to signals for PAC calculation). Therefore, we applied the above steps to all the data sets covered in this thesis. However, there are still some differences in the number and characteristics of the acquired source ICA signals due to the different data sets we investigated and discussed in the different chapters. I describe the details of methods in **Chapter 4 and 7**.

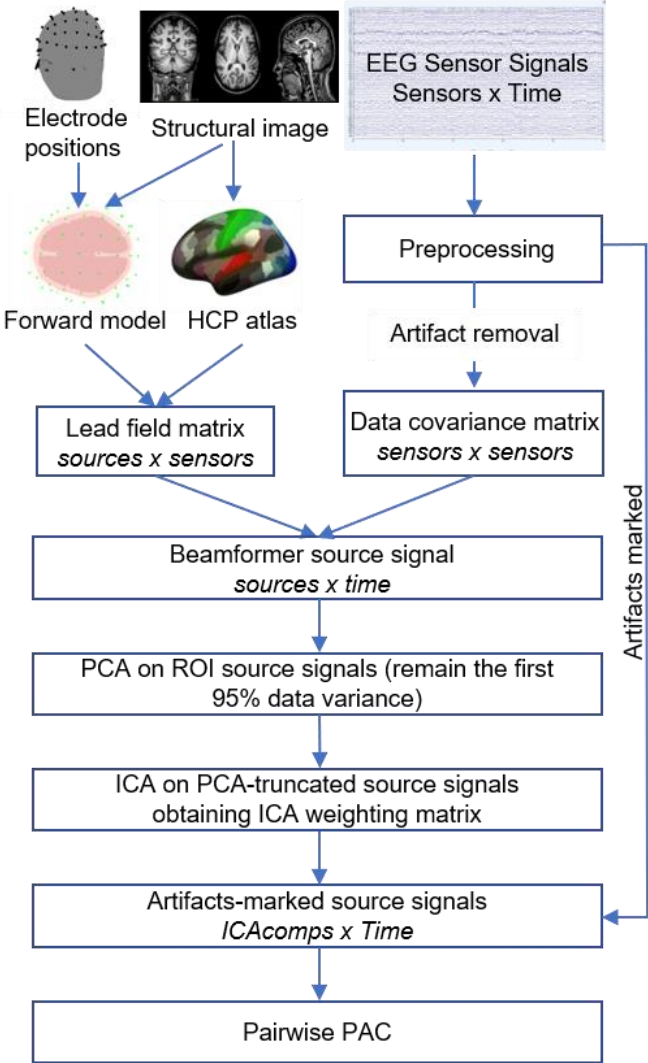


Figure 3.4 Workflow of ROI-based EEG source analysis. We first used individual MRI images and electrode positions to create forward models. The model is displayed as a brain outline (the head model in light pink and the source model in dark pink) with sensors (green dots) on the top left of the figure. Using the HCP atlas information, we created the ROI lead-field matrix. After preprocessing of EEG sensor signals, artefacts-removed and artefacts-marked EEG datasets were prepared for further analysis. A data covariance matrix was computed using artefacts-removed EEG signals. Next, we applied beamformer techniques to project artefacts-removed EEG signals from the sensor to source space. PCA-ICA was then applied on artefacts-removed source signals of each ROI to obtain the ICA weighting matrices. We then applied PCA-ICA weighting matrices to artefacts-marked EEG signals to obtain artefact-marked time series of the ICA source components.

3.6 Methods for computing PAC

In order to assess quantitatively the degree of coupling between the phase of low-frequency activity and the amplitude of high-frequency activity, we first have to extract their corresponding phase and amplitude information. One of the most common ways to extract time-resolved phase and amplitude information for the calculation of PAC is the Hilbert

transformation [174]. It calculates the analytical representation for a real-valued signal. The analytical signal is formulated in a polar coordinate as:

$$S_a(t) = A(t)e^{j\phi(t)},$$

where the analytical representation is $S_a(t)$, $A(t)$ represents the instantaneous amplitude or envelope, and $\phi(t)$ represents the instantaneous phase. Note that to obtain a reliable estimation of the instantaneous phase, the data should first be bandpass filtered.

There are several methods to evaluate PAC, but none has been chosen as the gold standard for detecting the phenomenon. In general, there are three most widely used methods to measure the strength of PAC; the phase-locking value (PLV) [175], the mean vector length (MVL) [176], and the Kullback–Leibler modulation index (KL-MI) [177]. The disadvantage of PLV in the calculation of PAC is that, in contrast to the other two methods, PLV needs additional transformation to extract phases from the envelopes of high-frequency activities while the actual amplitude information is not used. Therefore, in the present thesis, we used KL-MI and MVL exclusively to calculate the PAC under different considerations.

3.6.1 KL-MI method

The MI was calculated by comparing statistically the distance between the phase-amplitude distribution from real signals to the uniform distribution. First, we created phase-amplitude distributions as shown in Fig. 3.5. The phases (from -180 to 180 degrees) extracted from the low-frequency signal were sorted into a certain number of bins (in the thesis, we used 18 bins), and the amplitudes of the high-frequency signal were averaged accordingly for each bin. A uniform phase-amplitude distribution would represent an identical amplitude at each phase bin, while a non-uniform distribution would reflect the presence of PAC. The state of the distribution is assessed quantitatively by Shannon entropy, a measure representing the amount of information inherent in a variable:

$$H(p) = - \sum_{i=1}^N p(i) \log(p(i)),$$

where p is the vector of normalized averaged amplitudes per phase bin and N is the total number of bins. The maximum Shannon entropy is obtained for a uniform phase-amplitude distribution. MI is defined by a distribution that significantly deviates from the uniform distribution, calculated by means of the Kullback–Leibler divergence:

$$MI = \frac{\log(N) - H(p)}{\log(N)}$$

In this equation, $\log(N) - H(p)$ represents the Kullback–Leibler divergence and $\log(N)$ indicates the uniform distribution.

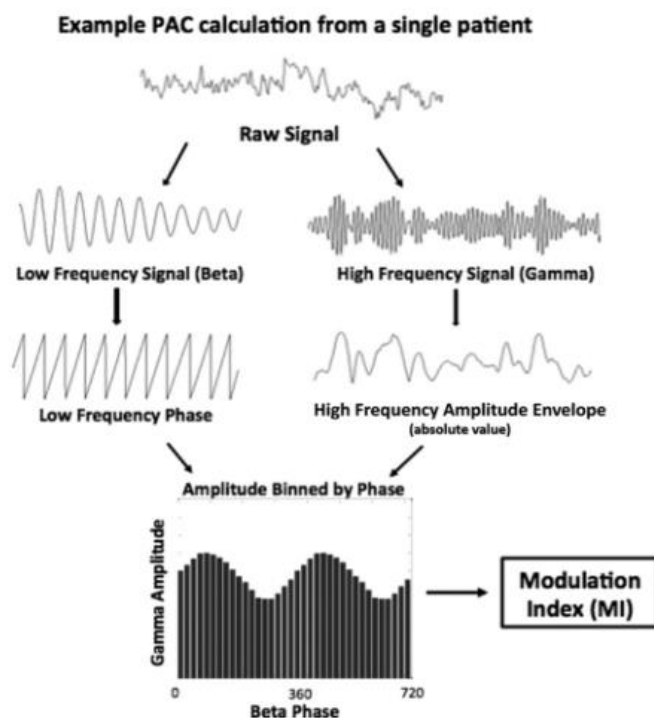


Figure 3.5 The procedure for calculating PAC using the KL-MI method. The raw signal was first bandpass filtered to obtain low-frequency and high-frequency signals. Then the phase of low-frequency signals and the amplitude of high-frequency signal were extracted using the Hilbert transform. The modulation index was calculated according to the phase-amplitude distributions. The figure is reproduced from “Effect of levodopa on electroencephalographic biomarkers of the parkinsonian state”, Miller, AM., et al., 2019, *Journal of neurophysiology*. Copyright 2019 by American Physiological Society. Reproduced with permission in the thesis.

3.6.2 MVL method

The MVL would assess PAC differently. We also first obtained the phase information from low-frequency oscillations and the amplitude information from high-frequency oscillations by bandpass filters and Hilbert transform. Importantly, in this method, the phase information from low-frequency oscillations and amplitude information from high-frequency oscillations is recombined as a new complex value in each data point, yielding a surrogate analytical time series. The complex values of that time series can be presented as vectors in a polar plane. If the amplitude is not coupled to a certain phase, the directions and the amplitudes would be distributed randomly and uniformly across the polar plane and would cancel each other out

when geometrically averaged. If there is coupling, different phase angles will be associated with different amplitudes, and averaging will result in a non-zero vector length. The MVL was calculated according to the following formula:

$$MVL = \frac{\left| \int_0^T a(t)e^{i\theta t} dt \right|}{\sqrt{\frac{1}{T} \int_0^T a^2(t) dt}},$$

where a is the amplitude of high-frequency activities and θ is the phase of low-frequency activities. The complex value was normalized by the root mean square of the amplitudes to avoid the effect of high-frequency amplitudes itself [178].

The reliability of PAC measurement could be affected by the data length and the signal-to-noise ratio [179]. If a signal is a perfect coupled signal without any noise component, one complete cycle of the low-frequency rhythm would be enough of the PAC measurement. However, because the real signal recorded from the brain contains significant noise, enough cycles would be counted to average out the effects of noise. Tort and co-workers [179] estimated θ - γ PAC from local field potential signals and suggested that computing the KL-MI from the data more than 30 s (or more than 200 cycles in theta rhythm) could provide a reliable measurement. They also reported that both the KL-MI and MVL methods perform well in long-term datasets, which has also been demonstrated by other researchers [180]. Because the KL-MI has been reported to be the most conservative method with less sensitivity to noise [181-183], it has been chosen as the preferred method for PAC measurement in many studies with long-term electrocorticography or EEG recordings [118, 137, 139, 140].

By contrast, when dealing with the issues that PAC has to be measured on a small time scale (several cycles of low-frequency rhythms), the MVL has been reported to perform better than the KL-MI for calculating PAC in very short epochs [178, 184]. Moreover, researchers have suggested performing surrogate control analysis to avoid the artificial coupling caused by random fluctuations in a short epoch [179, 185]. The control analysis could generate a chance distribution of PAC values from surrogate time series that share statistical properties with the PAC value from the original data [185]. The surrogate time series can be created by shuffling the amplitudes of high-frequency time series. Then we could measure the distance of the original PAC to the surrogate PAC distribution by computing the z-score of PAC:

$$zPAC = \frac{PAC_{ori} - \text{mean}(PAC_{surr})}{\text{std}(PAC_{surr})},$$

where $zPAC$ refers to z-score transformed PAC, PAC_{ori} refers to the original PAC value, $mean(PAC_{surr})$ refers to the average of the surrogate PAC distribution, and $std(PAC_{surr})$ refers to the standard deviation of the surrogate PAC distribution. A $zPAC$ value greater than 1.96 (95% confidence interval) indicates that the original PAC is unlikely to be detected by chance.

Based on all the above considerations, in this thesis, we applied the KL-MI method to calculate PAC with long-term datasets (i.e., long-term resting-state recording in **Chapter 4**) and the MVL method with surrogate control analysis to calculate the PAC in short epochs to investigate movement-related PAC (in **Chapter 7**). Therefore, while the general algorithms for calculating PAC that are applied in the thesis have been described above, the precise procedures for their particular application are described in the methodological sections of the corresponding chapters (**Chapters 4 and 7**).

3.7 Statistical methods

Due to the limitation of the number of subjects and the fact that not all results are normally distributed, we applied non-parametric statistical tests. In particular, we applied the two-tailed Wilcoxon rank-sum test (MATLAB rank-sum function) to compare between groups and the two-tailed Wilcoxon signed-rank test (MATLAB signed-rank function) to compare within groups. Moreover, to investigate the main and interaction effects of multiple factors (such as group, ROIs, and conditions), we used the ARTool package in the R environment (an introduction can be found at <https://depts.washington.edu/accelab/proj/art/index.html>), which implements a non-parametric factorial analysis of variance (ANOVA) [186]. ARTool, also referred to as aligned rank transform, first aligns the responses for each measurement of main and interaction effects and transforms the aligned data into ranks. Then, the transformed data are examined in a factorial ANOVA. The details of factor settings are further explained in the corresponding chapters (**Chapters 6 and 7**). Moreover, we applied false discovery rate (FDR) correction to the p-values (FDR $p < 0.05$) to deal with multiple comparisons.

Part III

Experimental Results

Chapter 4

Enhanced phase-amplitude coupling in the resting state of patients with Parkinson's disease

Based on:

Spatiotemporal features of β - γ phase-amplitude coupling in Parkinson's disease derived from scalp EEG

Ruxue Gong^{1,2}, Mirko Wegscheider¹, Christoph Mühlberg¹, Richard Gast², Christopher Fricke¹, Jost-Julian Rumpf¹, Vadim Nikulin³, Thomas R. Knösche^{*2}, Joseph Classen^{*1}

(*) co-corresponding authors

1. Department of Neurology, Leipzig University Medical Center, Leipzig, Germany

2. Method and Development Group Brain Networks, Max Planck Institute for Human Cognitive and Brain Sciences, Leipzig, Germany

3. Research Group Neural Interactions and Dynamics, Department of Neurology, Max Planck Institute for Human Cognitive and Brain Sciences, Leipzig, Germany

Published in *Brain*, Volume 144, Issue 2, February 2021, Pages 487–503, <https://doi.org/10.1093/brain/awaa400>

4.1 Introduction

Exaggerated phase-amplitude coupling (PAC) between β and broadband- γ activities has been detected in the subthalamic nucleus (STN), motor cortex, and interactions between the two regions of patients with Parkinson's disease (PD) via electrocorticography (ECoG) and local field potential (LFP) recordings [118, 187]. It has also been shown that enhanced PAC, as well as Parkinsonian bradykinesia, can be reduced by dopaminergic therapy [139] or through deep brain stimulation (DBS) in STN [134, 138, 140], suggesting that abnormally enhanced PAC might represent a neural circuit abnormality that is close to the causative pathophysiological mechanism underlying Parkinsonian bradykinesia. Recently, two electroencephalography (EEG) studies have shown that even non-invasive techniques can be used to differentiate patients from healthy individuals and that the state of drug-induced improvement of mobility

in PD patients can be differentiated from the akinetic state by means of PAC [137, 139].

However, one main issue related to the abnormal PAC of PD has not been satisfactorily addressed, which restricts its further investigation and application as a non-invasive biomarker. This issue is that the spatial localization of the brain regions from where the pathological coupling originates has been incompletely explored. EEG sensor signals show a poor spatial correspondence to the brain areas generating the underlying neuronal activity, because each signal represents a mixture of differently weighted contributions from numerous brain areas due to the volume conduction effects. In addition, the electrode positions on the scalp are determined by the precision of the operation of wearing the electrode cap and the layout of the cap, a fact that may lead to differences in the signal obtained from the same electrode in different subjects. This issue is vital because the spatial distribution of abnormal PAC informs about its possible origin within anatomically segregated loops of the basal ganglia-thalamocortical (BGTC) system, which may relate to the distinct motor and non-motor functions [188]. Fortunately, the recent development of EEG source analysis provides means to solve this problem partially. Therefore, in this chapter, we applied advanced EEG source analysis to investigate the spatial distribution of the exaggerated PAC of PD patients.

4.2 Methods

4.2.1 Data recording

The characteristics of the participants and experimental procedures have been described in Chapter 3 (Section 3.1). Since this chapter aims to characterize the anatomical spatial origin of the enhanced PAC in the resting state of PD patients, as reported in previous studies [118, 137], the data from the 5 min resting state recordings of 19 PD patients and 20 age and sex-matched healthy controls were analysed.

4.2.2 Data processing

The pre-processing procedures and the procedures for source reconstruction of the EEG signals have been described in Chapter 3 (Section 3.4 & 3.5.2). In brief, after the standard procedures to prepare the EEG sensor signals, we obtained EEG source signals by projecting EEG sensor signals recorded in the resting state to the individual cortical surface using a linear constrained minimum variance (LCMV) beamformer filter [169]. Furthermore, source-space independent component analysis (ICA) was applied to separate independent spatiotemporal components from the source signals in each of the 26 region of interests (ROIs) that have been introduced in Chapter 3 (Section 3.5.2.4). Table 4.1 presents the sizes of 26 ROIs as indexed by the average

numbers of dipoles across subjects, and the average number of ICA components derived under the current analysis for patients and controls in all 26 ROIs. None of the 26 ROIs showed significant differences in the number of ICA components between patients and controls (two-tailed Wilcoxon rank-sum test, $p > 0.05$).

Table 4.1 Information on 26 ROIs (mean \pm standard deviation)

ROI	Number of dipoles	Number of ICA components (patients)	Number of ICA components (controls)
Primary motor cortex	96.3 \pm 8.0	10.7 \pm 0.5	10.6 \pm 0.5
Primary somatosensory cortex	119.8 \pm 9.9	10.8 \pm 0.6	10.9 \pm 0.5
Primary somatosensory complex	132.3 \pm 10.0	11.0 \pm 0.5	10.9 \pm 0.6
Premotor cortex	135.2 \pm 11.4	10.7 \pm 0.6	10.8 \pm 0.5
Cingulate motor areas	43.3 \pm 4.7	6.7 \pm 0.5	6.6 \pm 0.5
Supplementary motor cortex	80.0 \pm 11.3	8.4 \pm 0.6	8.3 \pm 0.5
Area 5	55.2 \pm 5.2	7.6 \pm 0.6	7.5 \pm 0.5
Early auditory cortex	77.1 \pm 7.4	7.0 \pm 0.4	7.0 \pm 0.5
Auditory association cortex	140.5 \pm 8.1	7.5 \pm 0.5	7.6 \pm 0.6
Primary visual cortex	90.5 \pm 14.9	8.8 \pm 0.7	8.7 \pm 0.8
Early visual cortex	170.5 \pm 19.2	10.5 \pm 0.9	10.7 \pm 1.0
Dorsal stream visual cortex	77.5 \pm 6.3	8.2 \pm 0.7	8.1 \pm 0.5
Ventral stream visual cortex	87.4 \pm 8.6	7.6 \pm 0.6	7.6 \pm 0.6
MT + Complex and Neighboring visual cortex	90.4 \pm 10.0	7.9 \pm 0.8	7.8 \pm 0.8
Posterior opercular cortex	98.9 \pm 8.9	7.2 \pm 0.3	7.2 \pm 0.5
Insular and frontal opercular cortex	132.1 \pm 8.4	8.6 \pm 0.7	8.6 \pm 0.9
Medial temporal cortex	140.2 \pm 9.8	6.6 \pm 0.5	6.7 \pm 0.4
Lateral temporal cortex	263.1 \pm 15.3	8.4 \pm 0.7	8.6 \pm 0.6
Temporo-Parieto-Occipital Junction	113.9 \pm 11.7	8.0 \pm 0.7	8.1 \pm 0.7
Superior parietal cortex	181.0 \pm 18.4	11.4 \pm 0.7	11.3 \pm 0.8
Inferior parietal cortex	339.7 \pm 29.4	12.4 \pm 0.7	12.6 \pm 0.8
Posterior cingulate cortex	248.7 \pm 13.8	12.0 \pm 1.0	12.0 \pm 0.8
Anterior cingulate and medial frontal cortex	185.2 \pm 11.5	10.3 \pm 1.7	10.8 \pm 1.0
Orbital and polar frontal cortex	195.1 \pm 10.2	7.9 \pm 0.9	8.1 \pm 0.7
Inferior frontal cortex	125.9 \pm 9.8	8.0 \pm 0.8	8.0 \pm 0.7
Dorsolateral prefrontal cortex	282.9 \pm 22.0	12.1 \pm 0.9	12.5 \pm 1.1

ROI: Region of interest; ICA: Independent component analysis

4.2.3 PAC calculation

We calculated PAC values on sensor and source signals through the Kullback-Leibler

modulation index (KL-MI) as described in Chapter 3 (Section 3.6.1). We computed KL-MI values in phase-amplitude signal pairs in which the frequencies of phase signals range from 4 to 40Hz in 2Hz steps and that of amplitude signals from 32 to 200 Hz in 4 Hz steps. First, we filtered the signals for phase and amplitude estimation. For the phase estimation, we applied a set of narrow-band bandpass filters to the original signal, ranging from 4 to 40 Hz in 2 Hz steps with 2 Hz bandwidth. For the amplitude estimation, we applied bandpass filters from 32 to 200 Hz in 4 Hz steps with 40 Hz bandwidth. The reason for applying 40 Hz bandwidth for the amplitude estimation is because it is recommended to set the bandwidth of the filter at least the same as the frequency for the phase estimation so that the modulation frequencies can be covered [189]. Thus, for each sensor or component pair (explained in the next paragraph), we gained 18*42 phase-amplitude pairs. Marked artefacts were removed from the signals only after filtering to avoid pseudo γ oscillations produced by filtering sharp edges. Hilbert transform was applied to the filtered signals to extract instantaneous phase and amplitude separately. Only the phase-amplitude pairs whose phase frequency was lower than the lower cutoff frequency of amplitude signals were considered for calculating KL-MI values.

In sensor space, we calculated KL-MI values for each sensor signal separately. To enhance the spatial specificity of the sensor signals, we applied the surface Laplacian (as described in Chapter 3, Section 3.5.1) before computing PAC. At the source level, we calculated KL-MI values in ICA component pairs within each ROI. That is, we not only calculated the KL-MI values for each component separately, but also investigated the coupling between different components within the same ROI.

Next, a single KL-MI value was computed for each sensor or component pair by averaging the KL-MI values over the a priori defined phase-frequency range of 13-30 Hz, and the a priori defined amplitude-frequency range of 50-150 Hz [137]. This yielded, for a ROI with n ICA components at the source level, $n \times n$ KL-MI values were calculated.

Finally, we computed a single PAC value for each ROI of each subject for comparison between groups. This was obtained by weighted averaging across the $n \times n$ KL-MI values. Considering the different contributions of the ICA components to the original source signals, they were weighted by the percent of variance (pvar) for each component pair before averaging. The pvar reflects to what percentage the specific ICA component pair can explain the variance of the original data. The pvar for each ICA component can be computed as (refer to 'pvarf' function in EEGLAB):

$$pvar = 100 - 100 * \frac{\text{mean}(\text{var}(\text{dat}_{ori} - \text{dat}_{backproj}))}{\text{mean}(\text{var}(\text{dat}_{ori}))}$$

Here, dat_{ori} represents the original source signals, $\text{dat}_{backproj}$ represents the signals projected back from ICA components signals to source signals after removing the specific ICA component. In our study, considering that every two components in a pair would both have impacts on the PAC calculation, the pvar of each component pair is calculated as the geometric mean of the pvar values of the corresponding two components.

4.2.4 Power spectral density (PSD)

For calculating PSD, we applied Welch's method implemented in MATLAB (function 'pwelch') [190], which is one of the most popular methods for PSD estimation. The window was set to Hamming window in 2000 ms with 50% overlap. We then computed the normalized log PSD values for each ICA component. The normalization was done by subtracting the mean log PSD across frequencies (excluding 50 Hz and its harmonics) to reduce the inter-subject variability.

4.2.5 Statistical analysis

We defined the 'contralateral' hemisphere for patients as the hemisphere contralateral to the clinically more affected hemi-body (also the selected hand side for electromyography [EMG] recording), and controls as the hemisphere contralateral to the selected hand side for EMG recording (details in Chapter 3, section 3.3). For statistical comparison, we applied nonparametric statistical tests. Specifically, the two-tailed Wilcoxon 'rank-sum' test was used for comparisons between groups and the two-tailed Wilcoxon 'signed-rank' test for comparisons within subjects. We applied false discovery rate correction to the p-values (FDR $p < 0.05$) to deal with multiple comparisons.

4.3 Result

4.3.1 Exaggerated PAC in multiple cortical sources

β -broadband γ PAC as computed by the KL-MI method in 26 brain regions showed a markedly inhomogeneous distribution across the brain, which was similar between patients and controls. However, comparison between patients and controls revealed specific regional differences as illustrated in Fig. 4.1. First, we analyzed the differences in PAC by pooling the homologous regions of both hemispheres (Fig. 4.1A). In patients, β - γ PAC was enhanced, relative to controls, in 6 ROIs comprising the inferior frontal cortex (IFC, FDR corrected, $p=0.034$,

Z=2.80), the dorsolateral prefrontal cortex (DLPFC, FDR corrected, $p=0.034$, $Z=2.88$), the premotor cortex (PMC, FDR corrected, $p=0.023$, $Z=3.33$), the primary motor cortex (M1, FDR corrected, $p=0.037$, $Z=2.63$), the primary somatosensory cortex (SS-Broadman area 3 [BA3], FDR corrected, $p=0.037$, $Z=2.68$), and the primary somatosensory complex (SS-Broadman area 1&2 [BA1&2], FDR corrected, $p=0.034$, $Z=2.80$). Z-statistic was highest for PMC. Because of the asymmetry in clinical Parkinsonian motor symptoms, we also separately considered the hemispheres located contralaterally and ipsilaterally to the clinically more affected hemi-body. In the contralateral hemisphere of patients, 5 ROIs including DLPFC (FDR corrected, $p=0.035$, $Z=2.99$), PMC (FDR corrected, $p=0.035$, $Z=3.25$), M1 (FDR corrected, $p=0.035$, $Z=2.80$), BA3 (FDR corrected, $p=0.035$, $Z=2.77$), and BA1&2 (FDR corrected, $p=0.035$, $Z=2.74$) showed higher PAC than in controls (Fig. 4.1B). The comodulograms of the median KL-MI values in all five regions also clearly shows enhanced PAC in patients (Fig. 4.1C). However, the differences did not reach statistical significance in the ipsilateral hemisphere (Fig. 4.1B) although we found the similar tendency that patients have relatively higher PAC value than controls (uncorrected DLPFC: $p=0.062$, PMC: $p=0.062$, M1: $p=0.070$, BA3: $p=0.084$, BA1&2: $p=0.16$). We also did not explicitly find significant differences of PAC between contralateral and ipsilateral hemispheres in either patients or controls (uncorrected $p > 0.1$). PAC from temporal ROIs (i.e., the lateral temporal cortex, FDR corrected, $p=0.172$, $Z=1.62$, the medial temporal cortex, FDR corrected, $p=0.412$, $Z=0.96$) did not differ between patients and controls, suggesting that the enhanced PAC in patients was unlikely to be driven by muscle artifacts from pericranial muscles. Since we did not find any differences in the number of ICA components between patients and controls in any of the 26 ROIs, the PAC differences between patients and controls are unlikely to be caused by differences in the number of components. Moreover, we applied a Pearson correlation test to estimate the correlation in each ROI between the number of components and PAC values for 39 subjects. It showed no significant correlation in any of the 26 ROIs (FDR $p>0.2$).

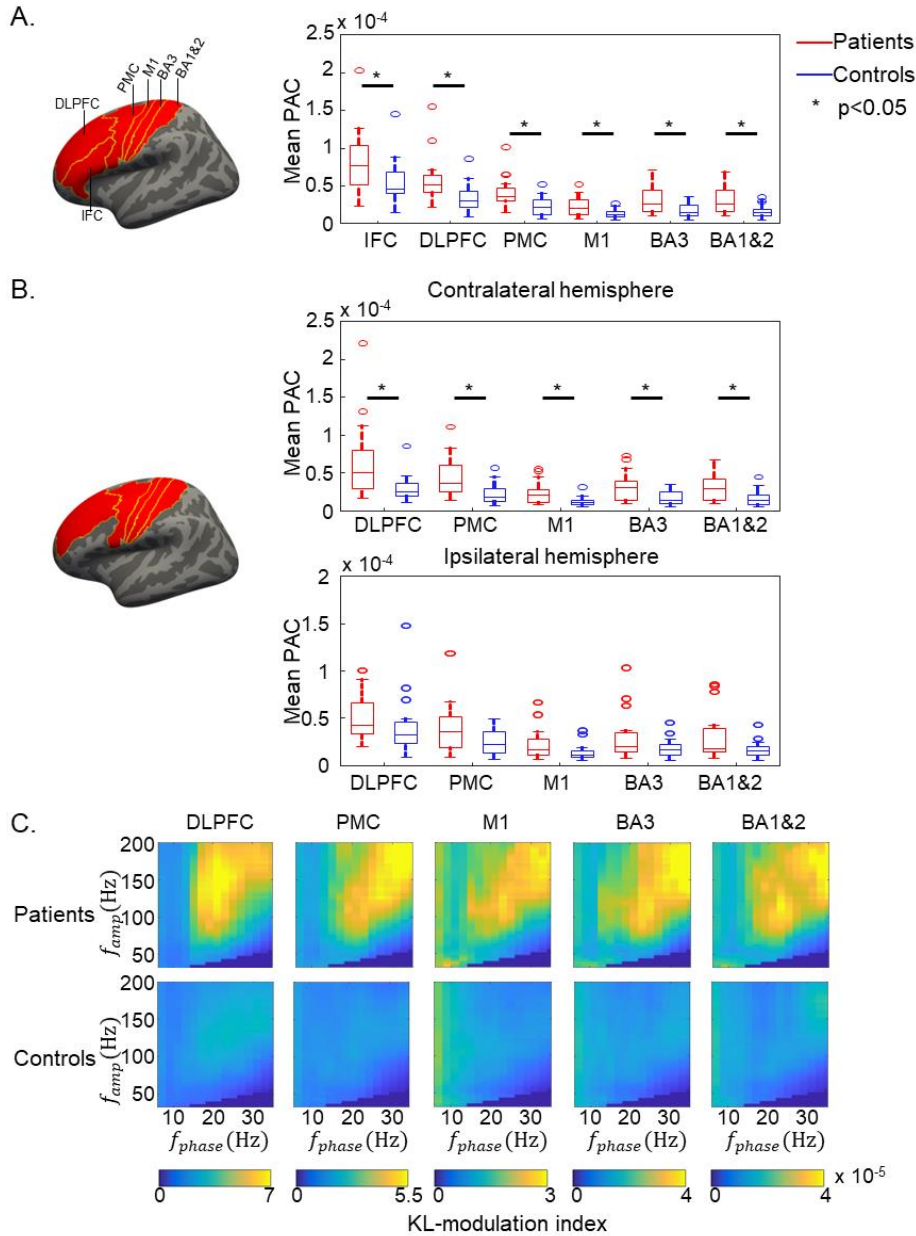


Figure 4.1 PAC observed at the source level. (A) Analysis of PAC distribution across 26 ROIs of the whole brain anatomy when averaging PAC from two hemispheres. Left: Regions marked as red showed significant differences between patients and controls after FDR correction. Right: Boxplot showing the PAC of the 6 ROIs, which presents significant differences between patients and controls (marked by asterisks). (B) Analysis of PAC distribution across 26 ROIs of the whole brain anatomy by considering contralateral and ipsilateral hemisphere separately. Left: The five regions marked in red show significant differences between patients and controls in the contralateral hemisphere after FDR correction. Right: Boxplots presenting that PAC of the 5 ROIs shows a significant difference in the contralateral hemisphere between patients and controls (upper right), and in the ipsilateral hemisphere (bottom right) the differences between groups do not reach the significance but follow the same tendency as in the contralateral hemisphere. (C) Group comodulograms showing the median of single KL-MI across subjects on the contralateral hemisphere in each group in the 5 ROIs.

In addition, to further prove that the selection of methods for the calculation of PAC would not primarily affect the result, we also tested the measurement of PAC in M1 using the mean vector length (MVL) algorithm (as described in Chapter 3, Section 3.6.2) in replacement of KL-MI algorithm. The Pearson correlation analysis showed a highly linear correlation between the two measurements ($p < 0.001$, $R = 0.93$).

4.3.2 Non-significant differences between patients and controls on sensor level

Previous studies reported enhanced PAC of PD patients when PAC was directly computed from signals of C3 and C4 electrodes [191] located over motor regions. However, in our study, patients and controls did not differ when the analysis was performed on signals recorded by C3 or C4 electrode, roughly located above the contralateral or ipsilateral motor areas, respectively (contralateral hemisphere: $p = 0.126$; ipsilateral hemisphere: $p = 0.267$). Besides, we did not find any significant difference between groups in signals from other electrodes, including the F3/F4 (FDR corrected, contralateral: $p = 0.438$; ipsilateral: $p = 0.693$), the FC3/FC4 (FDR corrected, contralateral: $p = 0.178$; ipsilateral: $p = 0.747$), and the CP3/CP4 (FDR corrected, contralateral: $p = 0.178$; ipsilateral: $p = 0.693$), which are related to the frontal and sensorimotor areas (Fig. 4.2). No difference was present between patients and controls even when sensors from both hemispheres were collectively considered (FDR, F3&4 $p = 0.553$, FC3&4 $p = 0.177$, C3&4 $p = 0.177$, CP3&4 $p = 0.177$).

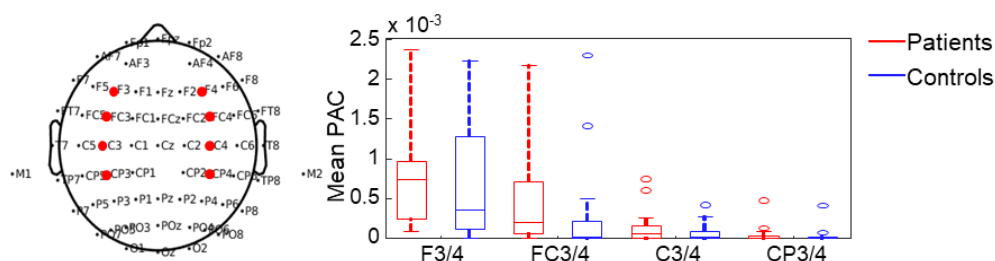


Figure 4.2 Analysis of PAC on sensor level. Left: F3&F4, FC3&FC4, C3&C4, CP3&CP4, which are related to frontal and motor-sensory areas, were selected for comparison to the results on the source level. Right: Boxplot showing the PAC extracted from the 4 pairs of electrodes on the contralateral hemisphere of both patients and controls. None of the differences reached statistical significance. To refer collectively to the electrodes relating to the most affected hemispheres of patients, we used notation with a slash ‘/’ (e.g., F3/4), because the most affected hemispheres varied between patients. For instance, the F3/4 refers either to F3 or F4, depending on the patient’s dominantly affected side.

4.3.3 The relationship between exaggerated PAC and the severity of motor impairment

To explore the relationship between source located PAC and the severity of motor impairment of PD patients, we computed the correlation between PAC values of contralateral and

ipsilateral hemispheres with the total Movement Disorders Society Unified Parkinson's Disease Rating Scale III (MDS-UPDRS III) hemi-body scores. The correlations between PAC and clinical scores in all 5 ROIs are shown in Fig. 4.3. We found the overall PAC to be significantly correlated with MDS-UPDRS III hemi-body scores in M1, but not in the other 4 ROIs.

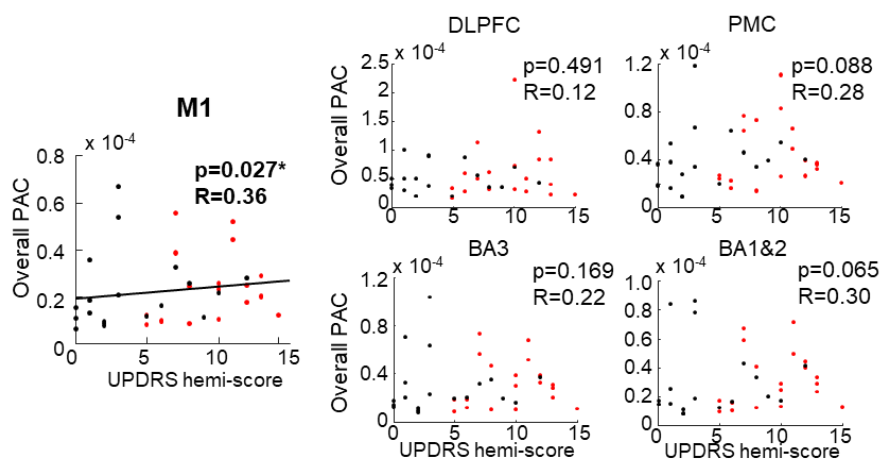


Figure 4.3 Relationship between PAC and clinical severity of the 5 ROIs. We found only significant correlation between mean PAC with MDS-UPDRS III hemi-body scores in M1 but not in the other 4 ROIs (black lines designate statistically significant correlations).

4.3.4 PAC is not solely driven by power

We examined the possibility that enhanced PAC may be driven by altered spectral power in either the β or γ band in patients. In M1 (Fig. 4.4A), β power differed significantly between patients and controls in both the contralateral hemisphere (FDR, $p = 0.040$), and the ipsilateral hemisphere (FDR, $p = 0.019$). Furthermore, γ power differed significantly in the contralateral hemisphere (FDR, $p = 0.011$), but not in the ipsilateral hemisphere (FDR, $p = 0.093$). The other 4 ROIs showed similar results.

We calculated the Spearman correlation between PAC and β or γ power for each ROI (Table 4.2). We found no relationship between β power and PAC in any of the 5 ROIs. While γ power was not significantly correlated with PAC in either DLPFC, PMC, or M1, both metrics were correlated in BA3 and BA1&2. Since power was not correlated with PAC in any of the three regions exhibiting the largest PAC difference between patients and controls (DLPFC, PMC or M1), the enhancement of power is unlikely to underlie the enhancement of PAC in patients. Moreover, we compared the frequencies at which the largest PAC value was noted with the frequencies where the largest β or γ power was detected. A correlation test applied on each signal pair in M1 showed no correlation between the peak PAC frequency and the power peak

frequency in either the β or γ band (Fig. 4.4B). Similar results were obtained in the other 4 ROIs (data not shown). Three examples from the dataset of patients are displayed in Fig. 4.4C. Together, the above findings indicate that the detected PAC enhancement in patients was unlikely to be driven by differences in spectral power.

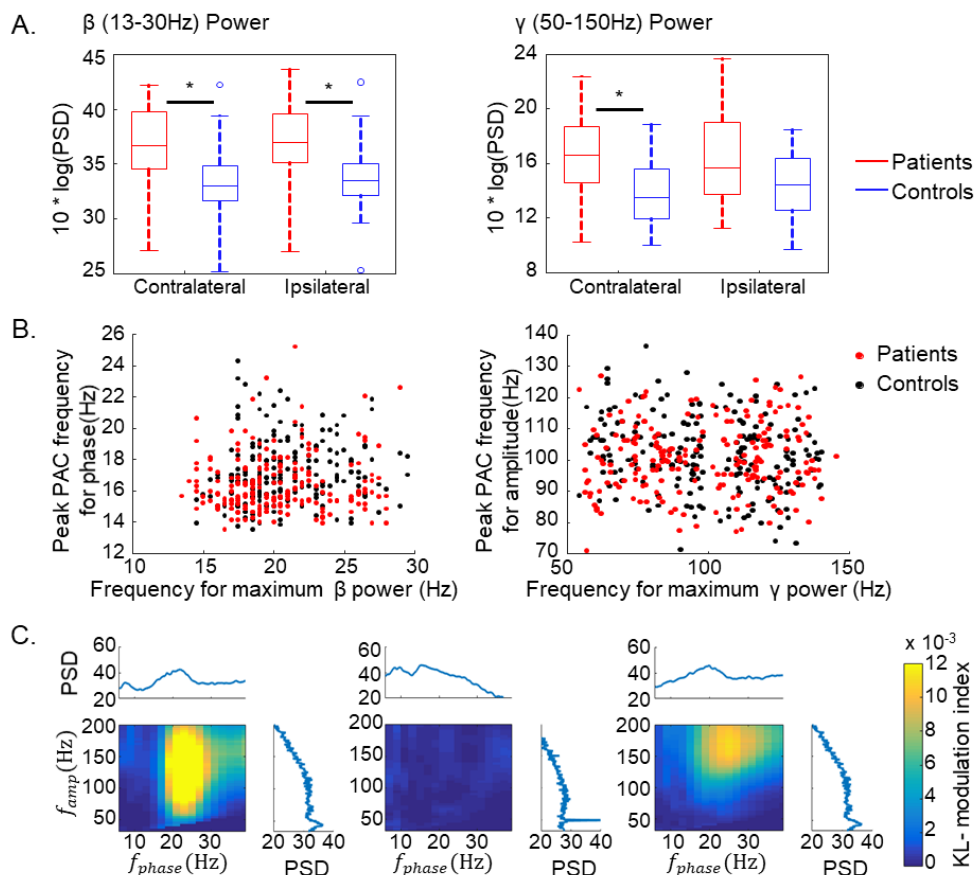


Figure 4.4 Relationship between PSD and PAC in M1. (A) Boxplots of PSD in the β frequency range (right), and in the γ frequency range (left) in patients and controls. Significant differences between groups are marked by asterisks. (B) Left: Non-significant correlation between power peak frequency at β range and peak PAC frequency for phase. Right: Non-significant correlation between power peak frequency at γ range and peak PAC frequency for amplitude. (C) Examples of comodulograms of PAC and the related β and γ power from patients. Left: Phase- and amplitude-frequency of the largest PAC are related to the β and γ power peak. Middle: Lack of PAC even when there is a clearly discernible β power peak. Right: The phase frequency and the amplitude-frequency of the largest PAC are not related to the β and γ power peaks.

Table 4.2 Correlation between PAC and PSD

ROI	β power vs. PAC				γ power vs. PAC			
	Contralateral side		Ipsilateral side		Contralateral side		Ipsilateral side	
	Patient	Control	Patient	Control	Patient	Control	Patient	Control
DLPFC	p=0.322, R=0.31	p=0.248, R=0.39	p=0.248, R=-0.41	p=0.937, R=0.04	p=0.322, R=0.314	p=0.248, R=0.47	p=0.417, R=-0.24	p=0.937, R=0.020
PMC	p=0.763, R=-0.10	p=0.316, R=0.33	p=0.587, R=-0.19	p=0.763, R=0.07	p=0.080, R=0.55	p=0.080, R=0.52	p=0.472, R=0.25	p=0.272, R=0.38
M1	p=0.423, R=-0.24	p=0.326, R=0.30	p=0.804, R=-0.06	p=0.470, R=0.19	p=0.060, R=0.59	p=0.075, R=0.51	p=0.075, R=0.52	p=0.125, R=0.43
BA3	p=0.585, R=-0.15	p=0.208, R=0.35	p=0.585, R=0.13	p=0.500, R=0.209	p=0.003, R=0.75	p=0.003, R=0.71	p=0.208, R=0.39	p=0.147, R=0.44
BA1&2	p=0.547, R=-0.20	p=0.110, R=0.43	p=0.605, R=0.13	p=0.563, R=0.17	p=0.016, R=0.64	p=0.003, R=0.74	p=0.110, R=0.43	p=0.019, R=0.59

ROI: Region of interest; PAC; phase-amplitude coupling; DLPFC: Dorsolateral prefrontal cortex; PMC: Premotor cortex; M1: Primary motor cortex; BA3: Broadman area 3; BA1&2: Broadman area 1&2. p values were corrected (for each ROI); significant p values (FDR $p < 0.05$) are marked in bold.

4.4 Summary

This chapter aims to demonstrate the spatial distribution of exaggerated β -broadband γ PAC on the cortex of PD patients from non-invasive EEG recordings at rest. By applying an advanced source localization algorithm, the present study has localized abnormal PAC in DLPFC, PMC, M1 and SS (including BA3, BA1&2) contralateral to clinically more affected body side of PD patients compared with healthy controls. The present findings appear to be the first to provide non-invasive evidence of abnormal PAC located in DLPFC and SS. This finding may indicate the role of DLPFC and SS in the pathophysiology of BGTC circuits of PD. Besides, we also found a relationship between the exaggerated PAC in M1 and the clinical severity as indicated by UPDRS III hemi-body scores, highlighting the significance of the abnormal coupling in the motor impairment of PD. However, we did not detect the enhanced PAC of PD patients at the EEG sensor level. This may suggest that source reconstruction helps to increase the signal-to-noise ratio and thereby enhances the chance for non-invasive detection of this biomarker. Furthermore, we found no consistent relationship between enhanced power and exaggerated PAC, which indicates that the exaggerated PAC in patients was not solely driven by spectral power.

Chapter 5

Neural circuits contributing to abnormal phase-amplitude coupling of Parkinson's disease

Based on:

Spatiotemporal features of β - γ phase-amplitude coupling in Parkinson's disease derived from scalp EEG

Ruxue Gong^{1,2}, Mirko Wegscheider¹, Christoph Mühlberg¹, Richard Gast², Christopher Fricke¹, Jost-Julian Rumpf¹, Vadim Nikulin³, Thomas R. Knösche^{*2}, Joseph Classen^{*1}

(*) co-corresponding authors

1. Department of Neurology, Leipzig University Medical Center, Leipzig, Germany

2. Method and Development Group Brain Networks, Max Planck Institute for Human Cognitive and Brain Sciences, Leipzig, Germany

3. Research Group Neural Interactions and Dynamics, Department of Neurology, Max Planck Institute for Human Cognitive and Brain Sciences, Leipzig, Germany

Published in *Brain*, Volume 144, Issue 2, February 2021, Pages 487–503, <https://doi.org/10.1093/brain/awaa400>

5.1 Introduction

In Chapter 4, we addressed the anatomical spatial distribution of abnormal β (13-30 Hz)-broadband γ (50-150 Hz) phase-amplitude coupling (PAC) of patients with Parkinson's disease (PD) in the resting state. This chapter continues to investigate the mechanisms of enhanced resting PAC in PD on a mesoscopic scale. We seek to elucidate the spatial relationship between PAC-involved β and γ activities and its relationship to the Parkinsonian motor impairment.

Three main scenarios could underlie PAC between β and γ oscillations. First, the manifestation of the β - γ PAC could originate from a single non-sinusoidal oscillator of β rhythm, in which the fast activities are simply harmonic components of non-sinusoidal slow oscillations from Fourier transformation [192]. In the second scenario, both slow and fast activities are nested

and originate from a single oscillator, in which slow and fast rhythms are tightly phase coupled [193]. Furthermore, slow and fast activities may originate from relatively independent neural circuits co-located in the same brain region, in which β and γ networks are only weakly coupled. In this scenario, the β signal could only modulate the gain of the γ network, resulting in PAC without phase-phase coupling [131]. All of these scenarios may have important implications for the mechanisms of PAC and its pathophysiological significance. Previous research has demonstrated the role of non-sinusoidal β oscillations in the generation of exaggerated PAC [141]. However, it is still unknown whether non-phase-phase coupled activities could also cause exaggerated PAC in PD. Moreover, the three scenarios may be linked to distinct spatial patterns of the coupled activities. In the first two scenarios, the β and γ activities would be generated in the same network or two highly dependent networks (which then would essentially form a single network). In the latter scenario, the spatial distributions of these two oscillators could be different and, in principle, distinguishable via their dynamics. However, it is not a priori clear that they can be distinguished within the methodological limits of scalp electroencephalography (EEG). With the help of independent spatiotemporal components derived from the EEG source signals by source-space independent component analysis (ICA) in a local region, we aim to gain a more comprehensive understanding of the mechanism generating exaggerated PAC in PD at rest.

5.2 Methods

In Chapter 4, we have demonstrated exaggerated β -broadband γ PAC in the resting state of PD patients compared with healthy controls. The enhanced PAC was located in the dorsolateral prefrontal cortex (DLPFC), the premotor cortex (PMC), the primary motor cortex (M1), and the somatosensory cortex (SS, including primary somatosensory cortex [Brodmann area 3, BA3] and primary somatosensory complex [Brodmann area 1&2-BA1&2]), contralateral to the clinically more affected body side. Therefore, in this chapter, we focused on the spatiotemporal characteristics of the 5 brain regions.

5.2.1 PAC calculation

The detailed procedure for calculating PAC at the source level has been described in Chapter 3 and 4. In general, we obtained source signals of components derived by source-space ICA in a local region of interest (ROI), the method that was described in Chapter 3, section 3.5.2. Then, for n ICA components in a ROI, we computed a single PAC value (averaged Kullback–Leibler modulation indexes [KL-MI] in the phase-frequency range from 13-30 Hz and amplitude-frequency range from 50-150 Hz) for each component pair in order to create a $n \times n$ pairwise

PAC matrix among all component pairs (Chapter 4, section 4.2.3). The $n \times n$ pairwise PAC matrix of a ROI is shown in Fig. 5.1A. In Chapter 4, we obtained weighted average PAC value across the overall $n \times n$ pairs for each subject and performed the group comparison between patients and controls. In this chapter, to further investigate the function of subnetworks to the enhanced PAC, we segregated the PAC values in which the β and γ activities stem from different components or the same components. Then, for each subject in a specific region, we computed weighted averages of PAC values between different components as inter-component coupling (PAC_{inter}), and of PAC values from identical components as intra-component coupling (PAC_{iden}).

5.2.2 Waveform analysis

When estimating the strength of phase-phase coupling between β and γ activities, the common method is computing the n:m phase-locking value in which the β and γ phases and the ratio between the phases are directly defined [194, 195]. However, a direct phase definition is not feasible for broadband- γ activity since it is composed of many different frequencies. Thus, in order to test whether some of the γ -phases are indeed locked to the β -phase, we defined the phase-phase coupling between β and broadband- γ activities as the correlation of the γ signal with β -phase across β -cycles. For this, we applied the method of waveform analysis.

To examine whether the PAC-involved γ activities were also phase-phase coupled to β activities, we generated averaged waveforms for γ activities (50-150 Hz, z-score normalized) time-locked to the β -phase (13-30 Hz, z-score normalized, then Hilbert transformed) zero crossings. We also averaged the envelopes of γ activities (from Hilbert transformation), time-locked to the β -phase. For calculating the averaged waveforms, we extracted epochs of 160ms (a period of around 2 cycles at 13 Hz) from both signals centered at the β -peaks. To avoid overlapping, we used only every second epoch for averaging. The maximum amplitudes of the averaged waveforms in a β -cycle were identified as the phase-locked amplitude (PLA) to the β -phase. The mean PLA of component pairs represented PLA for each subject. The PLAs of γ oscillations were defined as PLA_{osci} , while those of γ envelopes were defined as PLA_{amp} . By comparing PLA_{osci} and PLA_{amp} within subjects, and between groups, we examined to which degree abnormal PAC in PD is accompanied by phase-phase coupling.

5.2.3 The contributions of ICA components to PAC

For each PAC value of a component pair, one ICA component provides the β -phase, and another (or the same) component provides the γ -amplitude. The overall contribution of a particular component to the β -phase information or γ -amplitude information in PAC of an ROI

can then be quantified by summing all PAC values that involve that component as a β -contributor or as a γ -contributor, respectively. For each ROI, the values can be arranged in a matrix, as illustrated in Fig. 5.1A. In that matrix, the sum of each column represents the cumulative contribution of β -phases by the respective component, while the sum of each row represents the cumulative contribution of γ -amplitudes by the respective component. In order to obtain the relative contributions of a component to the β -phases and γ -amplitudes, respectively, these values were normalized to the sum of the entire PAC matrix of the ROI.

Finally, to estimate the inequality of the relative contributions of ICA components to β -phases and γ -amplitudes of the observed PAC in an ROI, a Gini coefficient [196] was calculated in each case. As shown in Fig. 5.1B, the Gini coefficient is usually defined mathematically based on the Lorenz curve, which plots the proportion of the cumulative proportion of values in the y-axis obtained by the cumulative share of populations in the x-axis. Thus, the line at 45 degrees represents perfect equal distributions, while the extreme line at 90 degrees to the x-axis represents perfect inequality (Fig. 5.1B). The Gini coefficient can then be calculated as the ratio of the area between the line of equality and the Lorenz curve (Area A in Fig. 5.1B) over the total area under the line of equality (Area A and B in the Fig. 5.1B).

Therefore, in our study, a high Gini coefficient indicates that the most contribution to the PAC comes from a few components, while a low Gini coefficient means that there are no such prominent contributors. By comparing the Gini coefficients between two groups, we circumvented the problem that ICA components differ between subjects, and this approach enabled us to investigate whether some subnetworks in the same ROI stand out among others with regard to their contribution to the β -phases and γ -amplitudes involved in the observed PAC of PD patients.

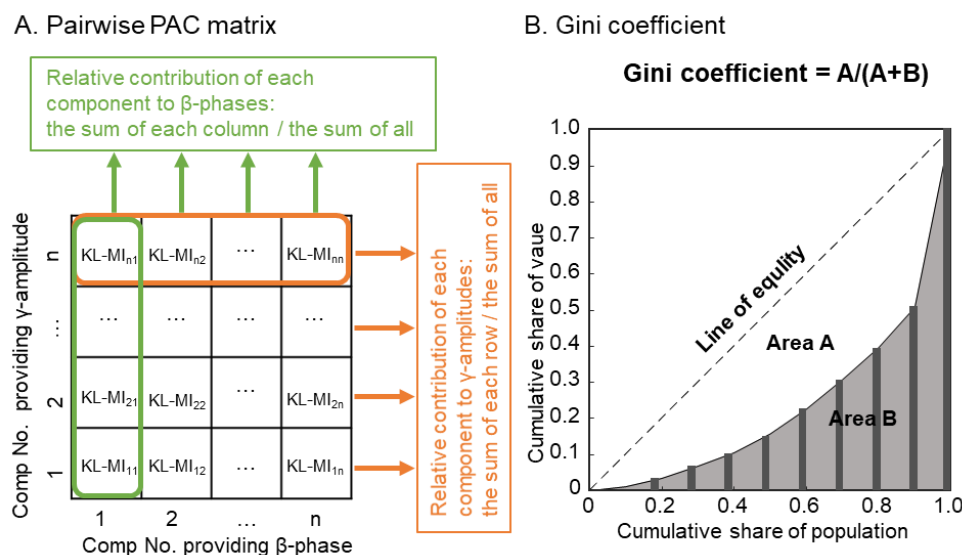


Figure 5.1 Methodology for the estimation of subnetworks contributions. (A) A pairwise PAC matrix across components in a ROI. For each subject, we computed single KL-MI values (average KL-MI values in the phase-frequency range [13-30 Hz] and amplitude-frequency range [50-150 Hz]) for $n \times n$ component pairs to create a pairwise PAC matrix among n ICA components. Each column represents the KL-MI values when the respective component provided the β -phases. Each row represents the KL-MI values when the respective component provided the γ -amplitudes. (B) Diagram for the calculation of Gini coefficients. See text for more explanation.

5.2.4 PAC weighted ICA topography

Each ICA source component defines an independent network with a unique spatiotemporal pattern [197] on the individual cortical surface. For each ICA component, we computed the topography as the spatial distribution of absolute values of the ICA weights. To characterize the topographic distributions of sources contributing to β -phases and coupled γ -amplitudes for each subject, we computed the average ICA topographies (as ‘ β -topography’ and ‘ γ -topography’, respectively) by averaging the topographies of all ICA components after weighting them according to their relative contributions to β -phases and γ -amplitudes, respectively. To compare the ICA topographies of the left or right hemisphere across subjects, they were mapped and morphed to the left hemisphere of a template source model from “fsaverage_sym”. Absolute Spearman correlation coefficients were calculated for each subject to compare the spatial similarity between the β - and γ -topography, and between subjects to estimate the spatial similarity of the topographies across subjects.

5.2.5 Statistical analysis

For statistical comparison, we applied nonparametric statistical tests (also introduced in Chapter 3, section 3.7). Specifically, we applied Wilcoxon non-parametric rank-sum tests for between-group comparisons and signed-rank tests for within-group comparisons. We applied

false discovery rate correction to the p-values (FDR p-values < 0.05) to deal with multiple comparisons. In addition, we applied Spearman correlation to investigate the relationship between PAC values and clinical scores indexed by part III of Movement Disorders Society Unified Parkinson's Disease Rating Scale (MDS-UPDRS III).

5.3 Results

5.3.1 Enhanced PAC-involved oscillations are not solely phase-phase coupled

While PAC indicates a coupling between γ -amplitude and β -phase, its presence does not imply nor exclude the possibility of additional phase-phase coupling. Therefore, we addressed this issue separately. The phase-phase coupling between PAC-involved β and γ activity can be distinguished when γ activity is averaged across epochs centred at a specific β -phase. This idea is illustrated in Fig. 5.2, which shows two cases. In both cases, the amplitude of high-frequency oscillation (HFO) is coupled to the phase of the low-frequency oscillation (LFO), but only in one case, there is additional phase-phase coupling between HFO and LFO. The average waveform of HFO in the non-phase-locked case results in a relatively flat waveform compared with that of the envelope of HFO, while the HFO is retained in the other case. In both cases, the shape of the envelopes is similar to the phase-amplitude distribution which is used for calculating PAC as indicated by KL-MI values. Therefore, the largest amplitude of the averaged waveform can be used for estimating the phase relationship between PAC-involved activities.

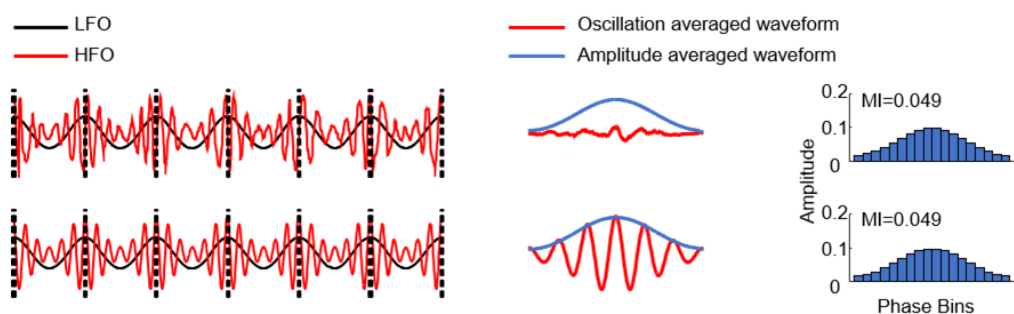


Figure 5.2 Simulation of phase-locked and non-phase-locked conditions on PAC-involved oscillations. Left: Two oscillatory signals in which the amplitude of the high-frequency oscillation (HFO, red) is coupled to the peak of the low-frequency oscillation (LFO, black). In the upper case, the phase relation between both signals varies over time, whereas in the bottom case, the HFO is phase-locked to the LFO. Middle: The varying phase relation (upper case) results in a relatively flat average waveform (red) of the LFO, when compared with the average of the instantaneous envelope of HFO (blue). By contrast, in the bottom part, the HFO is retained when it is phase-locked to the LFO. Right: In both cases, the KL-MI values are identical.

The results in M1 revealed that the PLA_{amp} was larger than PLA_{osci} both in the contralateral (Fig. 5.3A, left) and ipsilateral hemispheres for each subject, which rules out that γ and β activities were completely phase-phase coupled in both patients (FDR $p < 0.001$) and controls (FDR $p < 0.001$). In addition, in the contralateral hemisphere (Fig. 5.3A, left), we found no significant difference of PLA_{osci} between patients and controls (FDR $p = 0.399$), but a significant difference in PLA_{amp} (FDR $p = 0.005$). We found no significant difference between the two groups in either PLA_{osci} (FDR, $p = 0.189$) or PLA_{amp} (FDR, $p = 0.479$) in the ipsilateral hemisphere. Correlation analysis revealed no significant correlation between PAC and the PLA_{osci} (Fig. 5.3A, middle) in patients (FDR $p = 0.278$) and controls (FDR $p = 0.456$) in the contralateral hemisphere, but a significant positive correlation between PAC and the PLA_{amp} (Fig. 5.3A, right), both in patients (FDR $p < 0.001$, $R = 0.80$) and controls (FDR $p = 0.016$, $R = 0.58$).

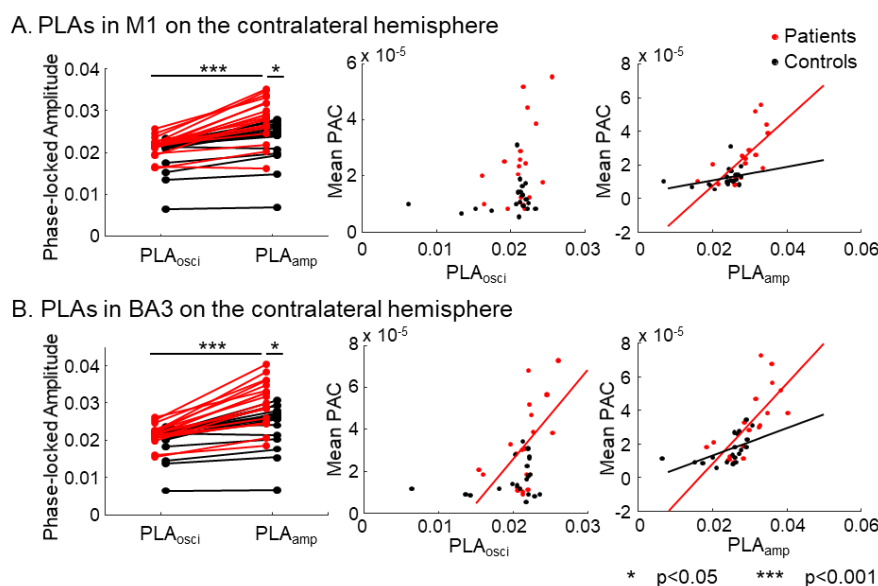


Figure 5.3 Waveform estimation of PLA. (A) Experimental results on PLA in M1 on the contralateral hemisphere. Left: Paired plot showing that PLA_{osci} (PLA of γ oscillations) was always lower than PLA_{amp} (PLA of γ envelopes) within subjects. Furthermore, PLA_{amp} were significantly larger in patients than in controls. Significant differences are marked by asterisks. Middle: No significant correlation of PLA_{osci} vs. mean PAC in patients and controls. Right: Significant correlation of PLA_{amp} vs. mean PAC in patients (red line) and controls (black line). (B) Experimental results on PLA in BA3 on the contralateral hemisphere. Left: Paired plot showing that PLA_{osci} were always lower than PLA_{amp} in patients and controls. Furthermore, PLA_{amp} was significantly larger in patients than in controls. Significant differences between patients and controls are marked by asterisks. Middle: Significant correlation of PLA_{osci} vs. mean PAC in patients (red line) but not in controls. Right: Significant correlation of PLA_{amp} vs. mean PAC in patients (red line) and controls (black line). Lines are only displayed if the correlation was statistically significant.

The results for DLPFC and PMC were highly similar to M1, but slightly different from SS (Fig.

5.3B). In SS, the PAC_{osci} was also correlated with PAC in patients, which indicates that the phase-coupled β and γ activities also contribute to the generation of PAC. However, even in the SS areas, the PLA_{osci} values are still lower than PLA_{amp} values (FDR $p < 0.001$). These findings demonstrate that PAC-involved β and γ activities are not completely phase-phase coupled, and PAC between β and γ activities that are not strictly phase-phase coupled becomes stronger in the pathological state.

5.3.2 Subnetworks contributing to PAC

We further characterized abnormal PAC by investigating whether the enhanced PAC of patients could be caused by β and γ activities from different ICA components. We segregated the KL-MI values of phase-amplitude pairs originating from two different components (PAC_{inter}) and those from the same component (PAC_{iden}). The results are shown in Fig. 5.4. Compared with controls, in the contralateral hemisphere of patients (Fig. 5.4B), significantly enhanced PAC_{iden} was found in DLPFC (FDR $p = 0.018$), PMC (FDR $p = 0.006$), M1 (FDR $p = 0.016$), BA1&2 (FDR $p = 0.026$), and in BA3 (FDR $p = 0.074$), where the difference was marginally significant. In addition, we found a significant difference of PAC_{inter} between patients and controls in all 5 ROIs (FDR corrected, DLPFC: $p = 0.001$, PMC: $p = 0.001$, M1: $p = 0.001$, BA3: $p = 0.001$, BA1&2: $p = 0.001$, Fig. 5.4A). Although KL-MI values were relatively higher when phase-amplitude pairs were from identical components, we also found the couplings between different components to be enhanced in patients compared with controls. This result indicates that the PAC-involved β and γ activities could be generated from different subnetworks, which provides support for our conclusion that abnormally enhanced coupling comprises distinct subnetworks in at least the 5 brain regions of patients.

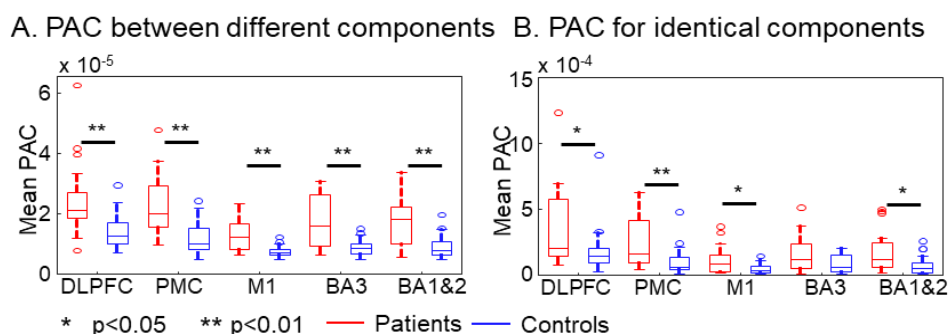


Figure 5.4 PAC computed on identical or different ICA components. (A) PAC differences for all ROIs between patients and controls from interactions between different components. (B) PAC differences for all ROIs between patients and controls from identical ICA components, in the contralateral hemisphere. Significant differences between groups are marked by asterisks.

In Chapter 4, we reported that the overall PAC (no segregation between component pairs within

a given region) is significantly correlated with MDS-UPDRS III hemi-body scores in M1, but not in the other 4 ROIs. In this chapter, we also investigated the relationship between the severity of motor impairment of PD patients and the PAC generated from either identical components or from the interaction between different components, respectively. Therefore, we computed the correlations between clinical scores and PAC_{inter} as well as PAC_{iden} , as displayed in Fig. 5.5. PAC_{inter} showed a significant correlation with UPDRS III hemi-body scores in PMC, M1, BA3, and BA1&2. However, we did not find a significant correlation between clinical scores and PAC_{iden} in any of the 5 ROIs. Moreover, we did not find any significant correlation between PAC values from DLPFC and clinical scores.

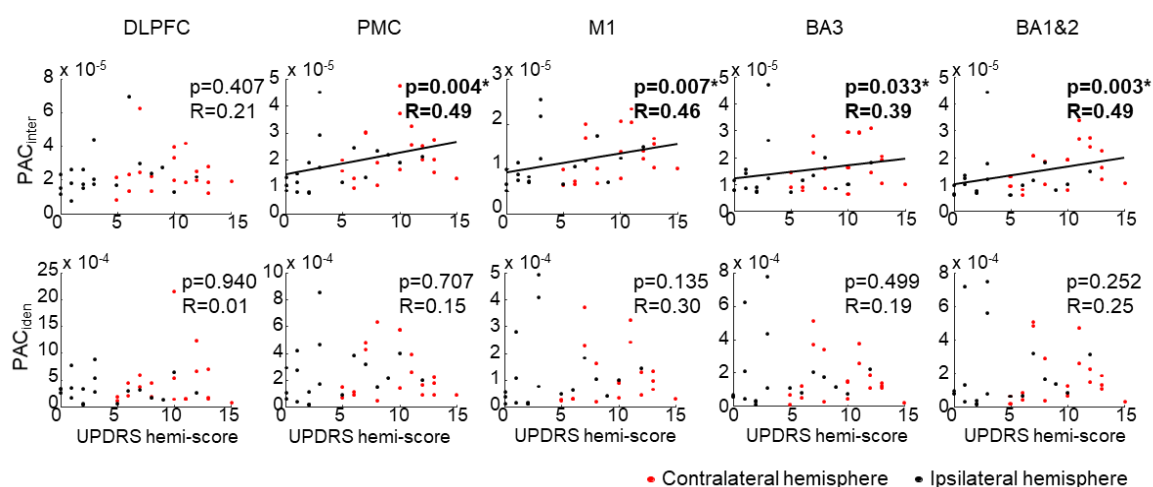


Figure 5.5 Correlation between PAC and clinical scores of the 5 ROIs. Upper: Correlation between mean PAC from the interaction between different components (PAC_{inter}) and MDS-UPDRS III hemi-body scores. Bottom: Correlation between mean PAC from identical components (PAC_{iden}) and MDS-UPDRS III hemi-body scores. Correlation coefficients and the corresponding p-values are also shown. p values were corrected (for each ROI). Significant p values are marked by an asterisk. Black lines designate statistically significant correlations.

5.3.3 The contributions of subnetworks to enhanced PAC

Since PAC_{inter} was correlated with the clinical severity, we asked whether the enhanced PAC_{inter} in patients resulted from the abnormal enhancement of all or just a few dominant components. Since ICA components are generally different across subjects, this question cannot be examined directly. However, the pathological dominance of a subset of components in patients can be inferred indirectly by comparing the distribution of relative contributions of components to PAC between groups. An abnormal contribution of only a subset of components in patients would be likely if the relative contributions of components were more unevenly distributed in patients than in controls. By contrast, if there were no outstanding contributors to the PAC enhancement in patients, the contributions of ICA components to the β -phases or γ -amplitudes

of PAC would be similarly distributed in patients and controls. The evenness/unevenness of the distribution can be estimated by the Gini coefficient, a metric widely used in social statistics (see Methods section 5.2.3). Since the enhanced PAC in patients was more robust in the contralateral hemisphere, this analysis was done on that hemisphere.

As shown in Fig. 5.6, Gini coefficients in the sensorimotor cortex were significantly different between patients and controls, suggesting that the contributions of different ICA components to the β -phases (FDR corrected, M1: $p = 0.005$, BA3: $p = 0.028$, BA1&2: $p = 0.008$) and γ -amplitudes (FDR corrected, M1: $p = 0.044$, BA3: $p = 0.040$, BA1&2: $p = 0.030$) depended on the disease state. DLPFC and PMC showed significant differences between patients and controls in terms of contributions to β -phases (FDR corrected, DLPFC: $p = 0.047$; PMC: $p = 0.017$), although not the contributions to γ -amplitudes (FDR corrected, DLPFC: $p = 0.407$; PMC: $p = 0.089$). This finding indicates that, compared with relatively equivalent contributions of subnetworks to PAC in controls, a relatively small number of subnetworks in the prefrontal and sensorimotor areas of patients contribute β -phases or γ -amplitudes to exaggerated PAC.

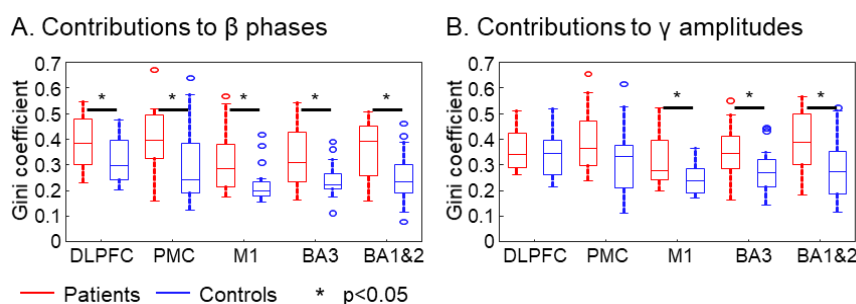


Figure 5.6 Gini coefficients regarding subnetworks contributions to β -phases and γ -amplitudes in DLPFC, PMC, M1, BA3, and BA1&2. (A) Boxplot of Gini coefficients comparing the inequality of contributions of ICA components to β -phases between patients and controls. (B) Boxplot of Gini coefficients comparing the inequality of contributions of ICA components to γ -amplitudes between patients and controls. Significant differences between patients and controls are marked by asterisks.

Besides, the Gini coefficients of both patients and controls in all the five regions also showed significant correlations with the PAC strengths, regardless of the coefficients to β -phases or γ -amplitudes, as shown in Table 5.1. These findings indicate that the enlarged PAC is related to enhanced contributions from a few subnetworks in at least those five regions.

Table 5.1. Correlation between PAC and Gini coefficients

ROI	Gini coefficients of contributions to β -phases vs. PAC		Gini coefficients of contributions to γ -amplitudes vs. PAC	
	Patients	Controls	Patients	Controls
DLPFC	p<0.001, R=0.81	p<0.001, R=0.80	p=0.001*, R=0.71	p=0.053, R=0.44
PMC	p=0.003, R=0.68	p<0.001, R=0.75	p=0.026, R=0.51	p=0.001, R=0.71
M1	p=0.002, R=0.73	p=0.033, R=0.48	p=0.011, R=0.61	p<0.001, R=0.77
BA3	p<0.001, R=0.90	p=0.002, R=0.67	p=0.002, R=0.69	p<0.001 R=0.79
BA1&2	p<0.001, R=0.83	p=0.004, R=0.63	p=0.003, R=0.68	p=0.002 R=0.69

ROI: Region of interest; PAC: Phase-amplitude coupling; DLPFC: Dorsolateral prefrontal cortex; PMC: Premotor cortex; M1: Primary motor cortex; BA3: Broadman area 3; BA1&2: Broadman area 1&2. p values were corrected (for each ROI); significant p values (FDR $p < 0.05$) in marked in bold.

5.3.4 The spatial organization of subnetworks

Finally, we examined how the networks contributing to β -phases and γ -amplitudes involved in PAC_{inter} were spatially organized on a local scale. As introduced in the Methods section, we studied the ‘ β -topography’ and ‘ γ -topography’ for each subject in the contralateral hemisphere. The β -topography and γ -topography in a local region represent the averages of the spatial distributions of the ICA components, after weighting them by their respective contributions to the PAC in terms of β -phases and γ -amplitudes. Fig. 5.7 illustrates examples of β -topographies and related γ -topographies of the 5 ROIs. The example shows a similar but not identical spatial pattern between both topographies within each ROI.

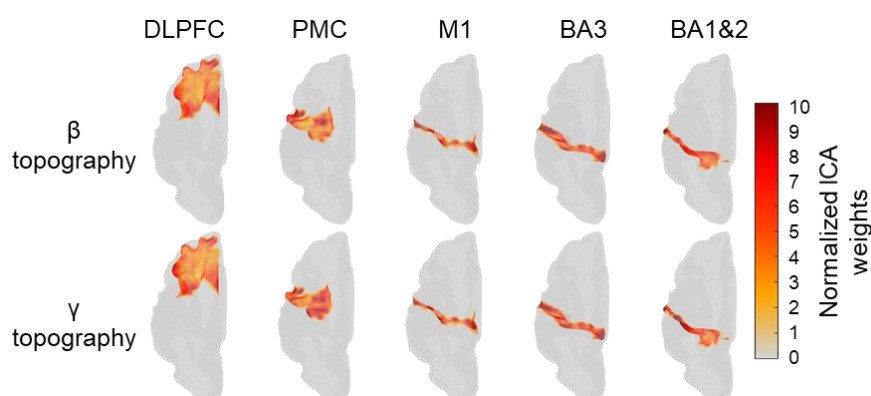


Figure 5.7 Examples of weighted average β -topographies and the corresponding γ -topographies of the 5 ROIs. ICA weights were z-score normalized. Note that the spatial patterns are similar between β - and γ -topographies within the ROIs but not completely identical.

For statistic estimation of the spatial similarity between β - and γ -topographies within each

subject in each of the five brain regions, we computed the spatial similarity for each subject, which is displayed in the histograms (Fig. 5.8). In M1, the results showed that the β - and γ -topographies for each individual were highly spatially correlated, both in patients ($R = 0.96 \pm 0.03$) and in controls ($R = 0.98 \pm 0.02$). The other four regions showed similar results. However, there was a strong tendency for the β - γ topographic similarities of patients to be reduced in M1 compared with controls (Wilcoxon rank-sum test, $p = 0.051$). This observation indicates that abnormally enhanced interactions became more prevalent between a few spatially distinct subnetworks in patients than in controls. The lower spatial similarity within patients was also observed in BA1&2 ($p = 0.026$), but not in the other 3 regions.

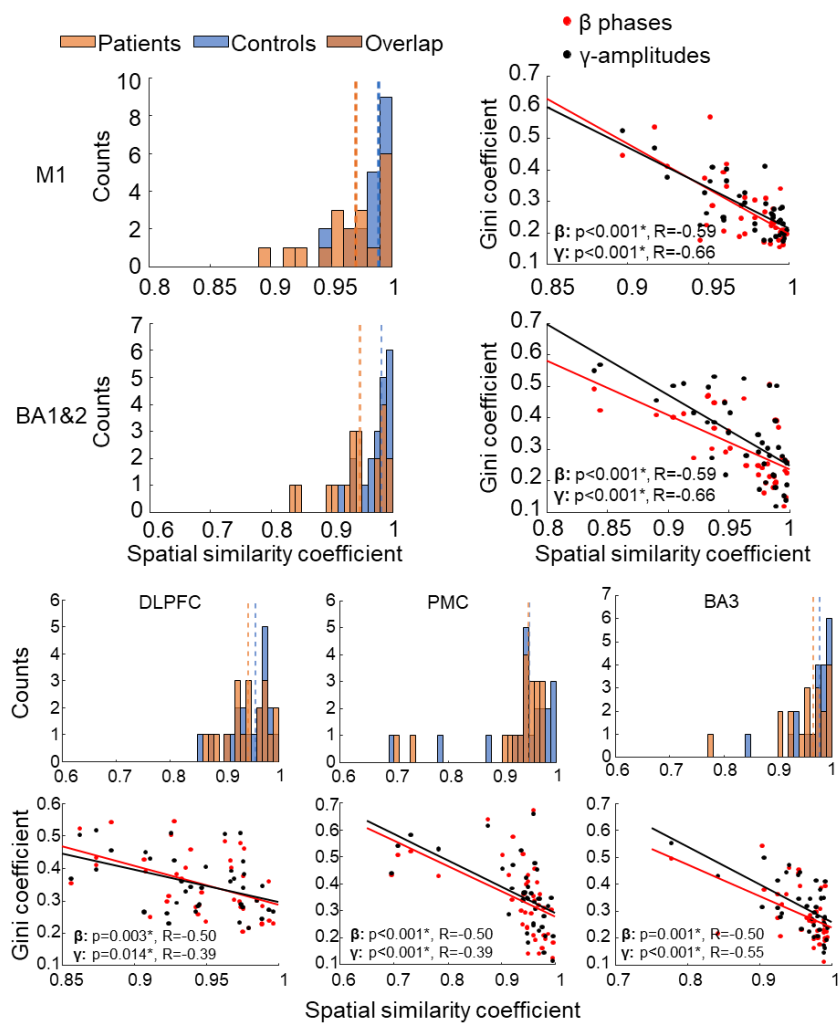


Figure 5.8 The spatial similarity between β - and γ -topographies in 5 ROIs. Histogram of Spearman correlation coefficients of 5 ROIs showing raw correlation values between β - and γ -topographies for patients and controls (the dash lines represent the median value of each group). The spatial similarity between β - and γ -topographies is significantly lower in M1 and BA1&2 of patients than controls, while not in the other 3 ROIs. The scatter plots show significant correlations between β - γ topographic similarity and Gini coefficient of component contributions to β -phases and γ -amplitudes (red and black lines indicate statistically significant correlations) in all 5 ROIs.

However, the β - γ topographic similarities were negatively correlated with the Gini coefficients for component contributions to γ -amplitudes as well as to β -phases in all five regions (Fig. 5.8), which indicates that the more inhomogeneous the contributions of subnetworks to the enhanced PAC, the more pronounced the difference between source distributions providing β -phases and γ -amplitudes.

Furthermore, when estimating the topographic similarity across subjects in M1 (Fig. 5.9), we found that both the similarities of β -topographies among patients (median $R = 0.30$) and controls (median $R = 0.25$) were low, and similar findings were detected in terms of the similarities of γ -topographies among patients (median $R = 0.30$) and controls (median $R = 0.24$). The other 4 ROIs also showed similar results. These findings indicate that there was no consistent spatial pattern of β - γ PAC across subjects.

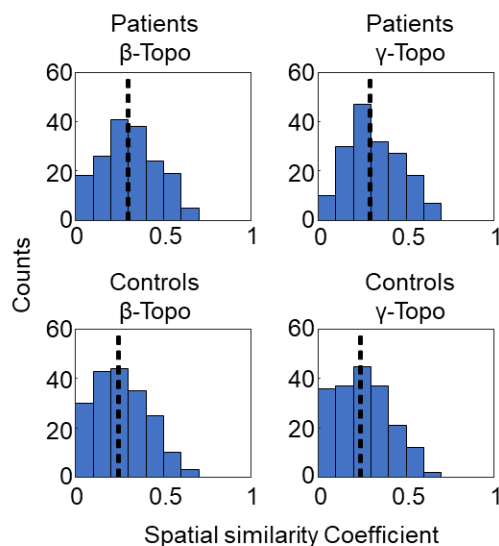


Figure 5.9 Histograms of Spearman correlation coefficients of weighted average topographies in M1 across subjects. Note the large variability of similarities of topographies across subjects. Black dashed lines represent the median coefficient of each distribution and show low similarity among subjects.

5.4 Summary

This chapter goes a step further from macroscopic level to mesoscopic level, investigating the temporal and spatial organization of β and γ activities involved in the generation of exaggerated PAC in the resting state in the 5 ROIs (i.e., DLPFC, PMC, M1, BA3, BA1&2) of PD patients. We demonstrated that the PAC-involved β and γ activities were not strictly phase-phase coupled, which suggests that two different, not rigidly coupled, oscillators producing β and γ activities may play a role in the generation of exaggerated PAC of patients in the resting state.

It was further demonstrated that PAC interactions, involving both identical and spatially distinct components, could distinguish patients from healthy controls in at least the 5 ROIs. In addition, a relationship with the clinical motor severity as indexed by UPDRS III hemi-body scores was only found for the couplings between different components, highlighting the pathophysiological significance of inter-component coupling. Moreover, we only found significant correlations in PMC, M1, BA3, and BA1&2, but not in DLPFC, which may underscore the specificity of the PAC phenomenon to motor control functions. The investigation on the contributions of components to PAC-involved β and γ activities by Gini coefficients showed that only a relatively small number of spatiotemporal components contribute to enhancing the inter-component PAC of patients. Interestingly, the unequal contribution of components to the enhanced PAC was associated with larger discrepancies between the spatial distribution of sources generating PAC-involved β -activities and γ -activities. This finding may suggest that the abnormal enhancement of PAC in PD reflects the abnormal dominance of a relatively small number of coupled subnetworks. Moreover, we did not find a uniform pattern of PAC-weighted topographies across patients or controls – which may be due to physiological heterogeneity – emphasizes the importance of individualized treatment of PD.

Chapter 6

Abnormal repetitive finger tapping of patients with Parkinson's disease

Based on:

Cross-frequency phase-amplitude coupling in repetitive movements in patients with Parkinson's disease

Ruxue Gong^{1,2}, Christoph Mühlberg¹, Mirko Wegscheider¹, Christopher Fricke¹, Jost-Julian Rumpf¹, Thomas R. Knösche^{*2}, Joseph Classen^{*1}

(*) co-corresponding authors

1. Department of Neurology, Leipzig University Medical Center, Leipzig, Germany

2. Method and Development Group Brain Networks, Max Planck Institute for Human Cognitive and Brain Sciences, Leipzig, Germany

Posted on medRxiv: <https://medrxiv.org/cgi/content/short/2021.07.26.21261085v1>

Published in Journal of Neurophysiology, Volume 127, Issue 6, June 2022, Pages 1606-1621, <https://doi.org/10.1152/jn.00541.2021>

6.1 Introduction

In Chapters 4 and 5, we have investigated the features of phase-amplitude coupling (PAC) at rest. However, it is still unclear how abnormal PAC is involved in the pathophysiology of Parkinsonian motor symptoms. In order to understand the functional role of PAC during movement and its direct relationship with motor impairment of patients with Parkinson's disease (PD), it is crucial to have a view about the behavioural abnormalities of PD patients in advance.

The behavioural abnormalities of PD patients have been investigated for decades. Slowing and amplitude decrement in repetitive movements represent cardinal manifestations of bradykinesia of PD patients [146]. Experiments have also confirmed that the reaction time can

be prolonged due to the pre-movement excitability increasing more slowly in patients than in normal subjects [198]. However, not all studies show such a difference in reaction time [187]. Moreover, not all movement parameters are actually abnormal in patients, such as, the tapping rate when asked to tap at the most comfortable pace [199]. Besides, it has also been reported that external sensory inputs may help patients to improve their performance [200, 201]. It seems that voluntary repetitive movements rather than cued movements would be more related to the cardinal motor symptoms of PD.

A unifying pathophysiological mechanism should reflect the behavioural pattern, i.e., it should be abnormal during abnormal motor behaviour and normal during normal motor behaviour. Therefore, in this study, we designed multiple self-paced, repetitive movement tasks involving different movement patterns, movement rates, and the presence of movement-related feedback. We used these tasks to gain a more comprehensive understanding of the status of abnormal and normal movement patterns in our group of PD patients when performing voluntary movements, as well as the relation of their motor performance to their clinical assessment. This study is an essential premise for investigating the characteristics of PAC during the movement of PD patients.

6.2 Methods

The description of the movement tasks has been introduced in Chapter 3, section 3.2. Briefly, we conducted three different types of repetitive voluntary movement tasks, which consist of a pressing task (repetitive press-release actions), slow tapping tasks (repetitive tapping at subjects' comfortable rate), and fast tapping tasks (repetitive tapping at subjects' fastest rate). We designed each of the tapping tasks in two conditions. The conditions differed in the absence or presence of feedback on whether the index finger extension had met the upper height criterion (upper photoelectric sensor). We recorded the digital signals produced by the device for movement measurement as introduced in Chapter 3. The signal acquisition schematic is shown in Fig. 6.1A.

6.2.1 Performance estimation

In each tapping task, motor performance was indexed by tapping rate, tapping variability, and the completion ratio. The mean tapping rate was calculated in each tapping task as the number of all index finger extensions crossing the lower light beam per second. The tapping variability was calculated as the standard deviation of the normalized movement intervals across a trial. A larger standard deviation means a greater inter-tap-variability of the tapping movements. The

movement intervals were obtained as the time intervals between adjacent movement onsets of each trial. Concerning the variation of movement rates between subjects, time intervals were normalized to the maximum interval in a trial. We finally computed the mean tapping variability across trials per task for each subject. The completion ratio was computed as the ratio of index finger extensions reaching the level of the upper photoelectric sensor divided by the total number of index finger extensions in a task.

Based on the completion ratio, we further evaluated the degree of decrement of tapping amplitude in tapping tasks. The decrement of amplitude can be evaluated on two scales: the decrement within and across trials in a task. The decrement within a trial was defined as the decrease of tapping amplitude over one trial. To estimate the decrement, the trials were first divided into 12 time bins in the slow and the fast tapping task (the first 12 s). Decrement was then defined as a decrease of the completion ratios from the first to the twelfth time bin in a trial. We evaluated the decrement by estimating the effect of time bin on the completion ratios in a mixed model (completion ratios \sim time bin + random(1|SubjectID)). To compare the decrements in the slow and fast tapping tasks over identical time spans, we also calculated completion ratios for each 1 s time bin during the first 12 s of slow tapping.

The decrement across trials was defined as the continuous decrease of the averaged completion ratios across trials within a task. In this case, we computed the completion ratio of each trial (6 trials in slow tapping and 10 trials in fast tapping) for each participant. The decrement across trials was also evaluated in a mixed-effect model (Completion ratios \sim Trial No. + random(1|SubjectID)).

6.2.2 Electromyography (EMG) signal processing

The EMG signals were first preprocessed together with the EEG signals in the procedures of demeaning, high pass filtering at 0.5 Hz, and artifacts detection (also refer to Chapter 3). We then applied a broad bandpass filter (5-200 Hz) as well as notch filters (50 Hz and its harmonics) to the EMG signals. The EMG signals were then segmented into 3 s epochs, starting with 1 s before the mechanical movement onset (lower photoelectric sensor) to 2 s after the mechanical movement onset. We obtained the smoothed EMG signals by applying a 5th order Butterworth low pass filter at 5 Hz to the rectified signals. For each subject, the EMG signals were averaged across epochs. Based on the mean EMG signal of each subject, we calculated the EMG slope as the slope between the 25% and 75% percentile of the normalized EMG amplitudes close to the mechanical onset (as shown in Fig. 6.1B). EMG signals were z-score normalized before computing the EMG slope to compensate for individual variability of EMG amplitudes.

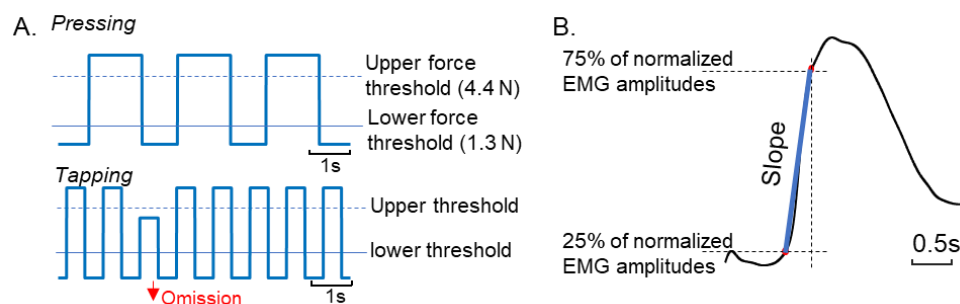


Figure 6.1 Schematic diagram of performance estimation. (A) Example digital signals of the pressing and slow tapping tasks. Top: Example digital signals indicating the force of repetitive pressing. Bottom: Example digital signals indicating the finger extension during rhythmic tapping. Note that the device was not recorded beyond the upper thresholds (either maximum force in pressing task and upper amplitude threshold in tapping task). (B) The estimation of the EMG slope, defined as the slope of the blue line connecting the 25% and 75% percentiles (red dots) of the normalized EMG signal closest to the mechanical onset of tapping.

6.2.3 Statistical analysis

We applied Wilcoxon non-parametric rank-sum tests for between-group comparisons and signed-rank tests for within-group comparisons. To investigate the effects of factors, especially the effects of Group and Feedback on the performance in the tapping tasks, we applied a nonparametric ANOVA as described in Chapter 3 (Section 3.7). We applied Spearman correlation to compute the correlation between performance and clinical scores indexed by part III of Movement Disorders Society Unified Parkinson's Disease Rating Scale (MDS-UPDRS III). False discovery rate correction (FDR, $p < 0.05$) was applied for multiple comparisons.

6.3 Results

6.3.1 Performance in pressing task

We estimated the performance reflected by the mean movement rate and the characteristics of the EMG signals. Patients and controls performed presses and releases at similar rates (patients, 0.33 ± 0.08 /s; controls, 0.31 ± 0.09 /s; $p = 0.633$; Fig. 6.2A). Regarding the characteristics of the EMG signals, we found no differences in EMG maximum amplitudes between patients and controls ($p = 0.684$, Fig. 6.2B). We also estimated the EMG slopes associated with pressing and releasing. In both cases patients could perform as normal as controls (press: $p = 0.527$; release: $p > 0.99$, Fig. 6.2C).

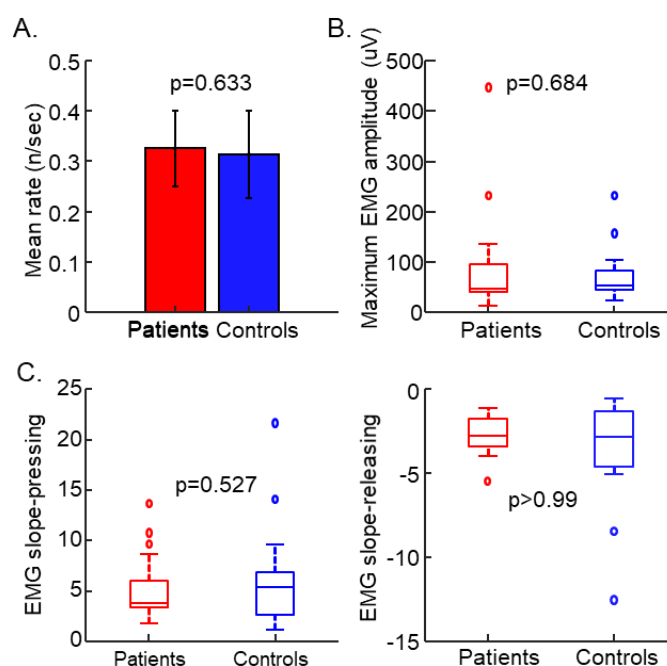


Figure 6.2 Performance estimation in pressing task. (A) Bar plot showing mean movement rates. (B) Boxplot showing maximum EMG amplitudes. (C) Boxplot showing EMG slope during index finger pressing (left) and releasing (right). No differences between patients and controls were found.

6.3.2 Performance in slow tapping tasks

To evaluate performance in the slow tapping tasks, we applied a two-way mixed ANOVA with the factors Group (2 levels, patients and controls) and Feedback (2 levels, with or without feedback) on the three performance parameters (mean tapping rate, tapping variability, and completion ratio). The tapping rate was slightly higher in patients compared with controls (main effect: Group, $F(1,37) = 4.68$, $p = 0.037$, Fig. 6.3A, left). With visual feedback, the tapping rate increased in both groups (main effect: Feedback, $F(1,37) = 14.63$, $p < 0.001$), probably through an effect of pacing by the visual feedback. As for the tapping variability, we did not find any differences between patients and controls (main effect: Group, $F(1,37) = 0.19$, $p = 0.667$, Fig. 6.3A, middle), and the group comparison was not affected by feedback (main effect: Feedback, $F(1,37) = 0.11$, $p = 0.74$). However, in terms of the averaged completion ratio in the slow tapping task, we found a significant interaction effect between Group and Feedback ($F(1,37) = 8.91$, $p = 0.005$, Fig. 6.3A, right). As shown in the right panel of Fig. 6.3A, although post-hoc testing revealed that the completion ratio increased with visual feedback in patients ($p = 0.005$), but not in controls ($p = 0.081$), no significant differences were found between patients and controls in either the without-feedback ($p = 0.115$) or the with-feedback condition ($p = 0.220$).

The decrement of the tapping amplitude within a trial, defined as the decrease of completion

ratio along with the time bins within a trial of each task, was evaluated for tapping without visual feedback. Mixed ANOVA analysis on the completion ratio in the sequence of 12 time bins within a 30 s trial revealed an interaction between Group and Time Bins in the slow tapping task ($F(11,407) = 7.19, p < 0.001$). Subsequently, we evaluated the decrement trend by computing the mixed-effects model 'Completion ratio \sim Time bin + random(Subjects)', separately for patients and controls. Patients showed a significant effect of Time Bin on the completion ratio in slow tapping ($t(226) = -4.69, p < 0.001$, FDR corrected), whereas in controls, the completion ratio increased with time ($t(198) = 3.87, p < 0.001$, FDR corrected). However, when we only considered the first 12s of the tapping for comparison to the fast tapping task, the decrease of the completion ratio during a trial was not present in patients ($t(226) = -1.58, p = 0.115$; Fig. 6.3B, left).

Furthermore, the comparisons between groups revealed significant differences (after FDR correction) in completion ratio in 4 out of the 6 trials (Fig. 6.3B, right). The decrement of tapping amplitude across trials was then evaluated by a mixed-effect model 'Completion ratio \sim Trial No. + random(Subjects)' for patients and controls, respectively. The result showed that for both patients ($t(112) = -1.96, p = 0.106$, FDR corrected) and controls ($t(118) = 0.87, p = 0.383$, FDR corrected), there was no significant effect of trial order in the completion ratios, which suggests that the differences of completion ratios of trials between patients and controls were not caused by the decrement of tapping amplitude over trials in slow tapping tasks.

We also investigated the features of EMG signals in the slow tapping tasks. Patients and controls showed no significant differences in the maximum amplitude ($p=0.922$; Fig. 6.3C, left). However, regarding the EMG slope at the tapping onset (index finger extension), we found a significantly lower EMG slope in patients compared with controls (FDR corrected, $p < 0.001$; Fig. 6.3C, middle). The EMG slope associated with finger flexion did not significantly differ between patients and controls (FDR corrected, $p = 0.133$; Fig. 6.3C, right).

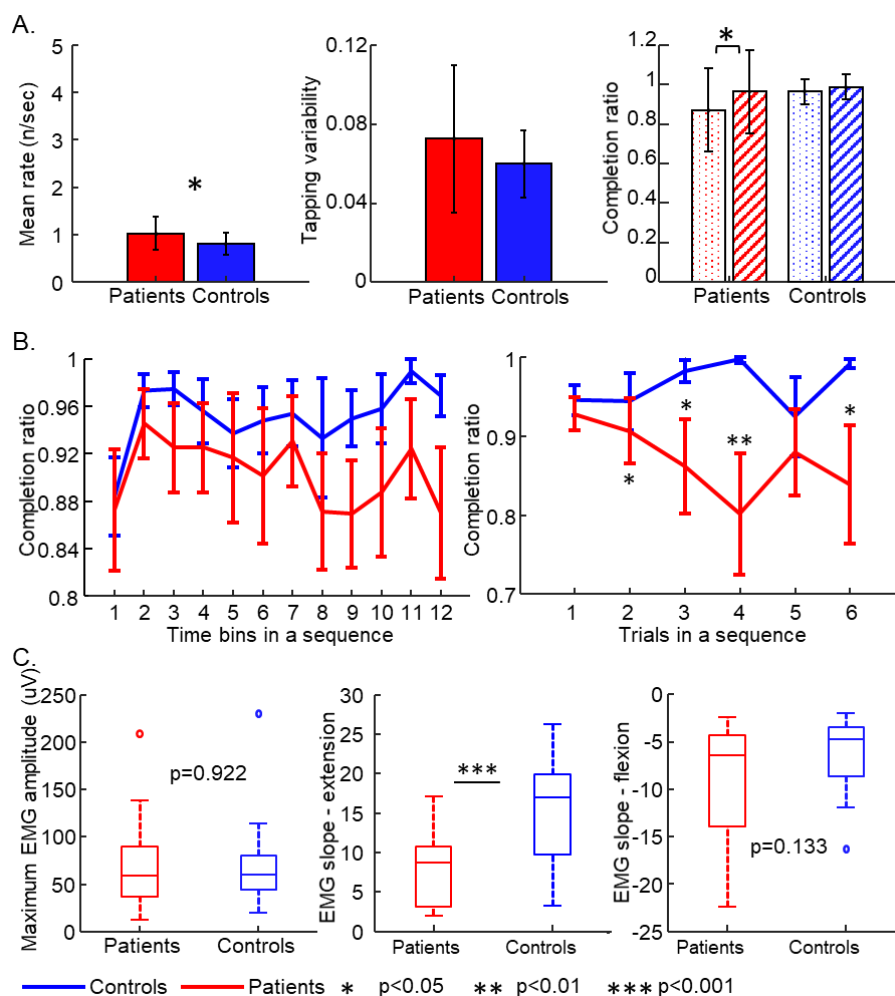


Figure 6.3 Performance estimation in slow tapping tasks. (A) Bar plots showing the tapping rate (left), tapping variability (middle), and completion ratios (right) between patients and controls (dotted – without feedback, hatched - with feedback). (B) Error bar plots showing the decrement of tapping amplitude within a trial as represented by the completion ratios in the sequence of time bins in the first 12 s within a trial (left), and decrement across trials as represented by the completion ratios in the sequence of trials in slow tapping task without feedback (right). (C) Characteristics of EMG signals in slow tapping tasks, showing no significant difference of maximum EMG amplitude between patients and controls (left), a significant difference in the EMG slope regarding index finger extension (middle), and no significant difference of EMG slope regarding index finger flexion (right).

6.3.3 Performance in fast tapping tasks

We also applied the ANOVA analysis to the fast tapping tasks to estimate the effects of Group and Feedback on the subjects' tapping variability, tapping rate, and mean completion ratio. Regarding the test of tapping rate, we found no interaction effects between the Group and Feedback ($F(1,37) = 0.91$, $p = 0.34$). Instead, patients had a lower tapping rate in fast tapping compared with controls (main effect: Group, $F(1,37) = 18.22$, $p < 0.001$, Fig. 6.4A, left). Tapping rate increased with visual feedback (main effect: Feedback, $F(1,37) = 9.46$, $p = 0.004$) for all subjects. Tapping variability was higher during fast tapping in patients compared with

that of controls (main effect: Group, $F(1,37) = 14.33$, $p < 0.001$, Fig. 6.4A, middle), while visual feedback had no effects on the tapping variability (main effect: Feedback, $F(1,37) = 0.68$, $p = 0.416$). Besides, ANOVA analysis on completion ratio showed a significant interaction effect between Group and Feedback ($F(1,37) = 8.65$, $p = 0.006$, Fig. 6.4A, right). Post-hoc tests (Fig. 6.4A, right) revealed that the completion ratio in patients was lower than in controls, both without feedback ($p = 0.021$) and with feedback ($p = 0.013$). Besides, with visual feedback, patients increased the completion ratio to a greater extent than controls (Fig. 6.4A, right).

With respect to the decrement within a trial, the mixed ANOVA analysis on the completion ratio in the sequence of the first 12 s within a trial revealed an interaction between Group and Time Bins in the fast tapping task ($F(11,407) = 3.05$, $p < 0.001$), as shown in the left panel of Fig. 6.4B. In order to evaluate whether there is a decrease of completion ratio over time points, we computed the mixed-effects model 'Completion ratio ~ Time Bin + random(Subjects)' separately for patients and controls. Patients in this case still showed a significant effect of Time Bin on the decrease of the completion ratio in fast tapping ($t(226) = -5.45$, $p < 0.001$, FDR corrected).

Comparing the completion ratios over 10 trials in the task, patients also showed a significantly lower completion ratio compared with controls in the last 4 trials (Fig.6.4B, right). By estimating the decrement across trials using mixed-effects model 'Completion ratio ~ Trial No. + random(Subjects)', we found that the sequence of trials has significant effects on the completion ratio in patients ($t(188) = -5.61$, $p < 0.001$, FDR corrected) but not in controls ($t(198) = 0.25$, $p = 0.804$, FDR corrected). The above findings suggest that, in fast tapping tasks, patients show a marked decrement of tapping amplitude both within a trial and across trials compared with controls.

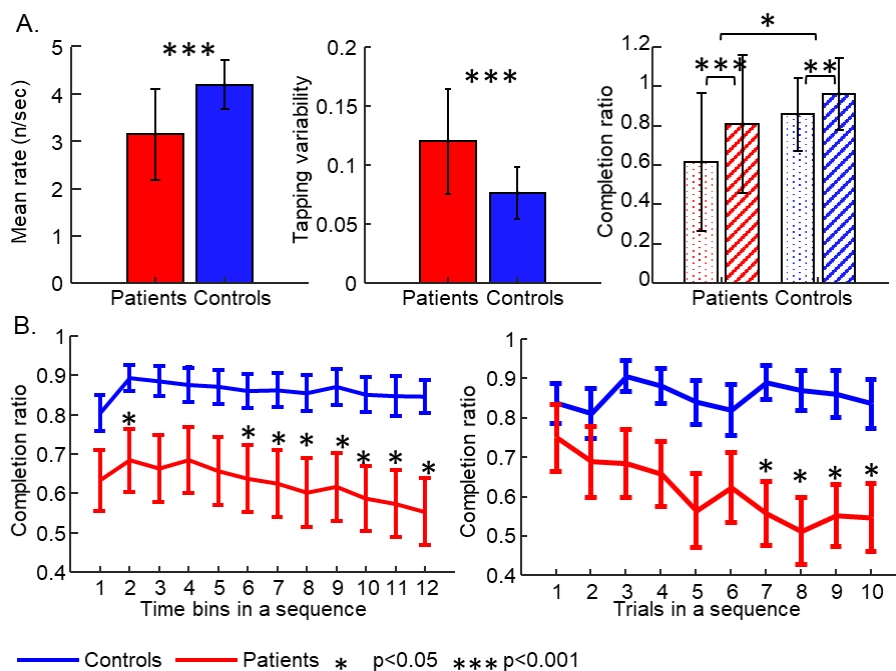


Figure 6.4 Performance estimation in fast tapping tasks. (A) Bar plots showing the tapping rate (left), tapping variability (middle), and completion ratios (right) between patients and controls (dotted – without feedback, hatched - with feedback). (B) Error bar plots showing the decrement of tapping amplitude within a trial as represented by the completion ratios in the sequence of 12 time bins within a trial (left), and decrement across trials as represented by the completion ratios in the sequence of 10 trials in fast tapping task without feedback (right).

6.3.4 The relationship between performance features and clinical severity

We explored the relationship between various abnormal performance metrics in the tapping tasks and the clinical severity of motor impairment in PD patients as indexed by the hemi-body bradykinesia and rigidity scores from MDS–UPDRS III. The EMG slope at tapping onset in slow tapping was significantly correlated with the clinical scores (Fig. 6.5, left, $p=0.015$, $R=-0.55$). There was a tendency of negative correlation between the tapping rate in fast tapping without feedback and the bradykinesia and rigidity hemi-scores (Fig. 6.5, right, $p=0.079$, $R=-0.41$). We did not find any correlation between tapping variabilities and clinical scores. Besides, bradykinesia and rigidity hemi-scores were not correlated with the decrement within a trial (computed as the difference of the completion ratios between the 1st and 12th time bins), neither were they correlated with the decrement across trials.

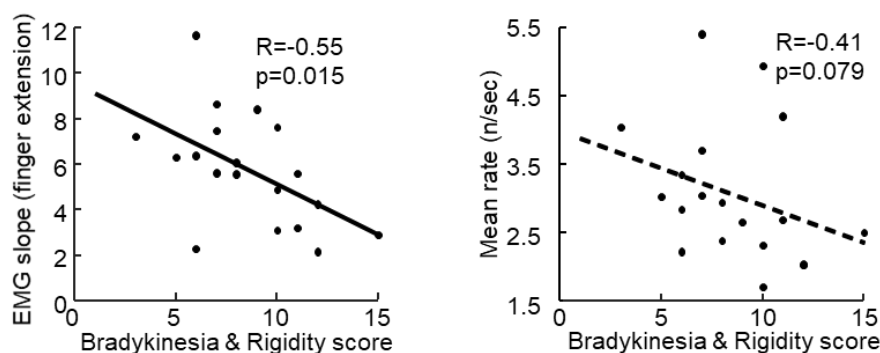


Figure 6.5 Correlation between performance and hemi-body bradykinesia and rigidity scores from MDS-UPDRS III. Left: The scatter plot shows a significant correlation between EMG slope of index finger extension in the slow tapping task and clinical scores. Right: The scatter plot shows a marginally significant correlation between tapping rate in fast tapping without feedback and clinical scores.

6.4 Summary

This chapter comprehensively investigated the behavioural characteristics and the EMG signals in the three forms of self-paced repetitive movements (pressing, slow tapping, and fast tapping) in PD patients compared with healthy controls. In the pressing task, PD patients have the ability to perform press-release actions as normal as healthy persons. By contrast, patients exhibited motor abnormalities in the tapping tasks. In slow tapping, even though the tapping rate was even higher in patients than in controls, evidence for the slowness of the movement was manifested by the reduced EMG slope during finger extension, which indicated that PD patients have difficulties recruiting muscles to initiate finger extension. Regarding the performance in fast tapping, the motor impairment of PD patients did significantly reduce the tapping rate and increased tapping variability. As expected, the slowness of movement execution in patients – kinetically indexed by reduced EMG slope in slow tapping task, and slower tapping rate in fast tapping task – was evident to correlate with clinical scores evaluating bradykinesia and rigidity. Moreover, in contrast to healthy controls, PD patients showed a decrement of tapping amplitude, especially when tapping at their fastest rates. In addition, we also found that the colour feedback could help both patients and controls to improve their tapping performance in meeting the amplitude criterion, even under faster tapping speed. In summary, the motor disabilities of PD patients manifest themselves differently in different types of voluntary repetitive movements. In our study, PD patients presented more behavioural abnormalities in repetitive tapping movements than repetitive pressing movements.

Chapter 7

Phase-amplitude coupling in repetitive movements of patients with Parkinson's disease

Based on:

Cross-frequency phase-amplitude coupling in repetitive movements in patients with Parkinson's disease

Ruxue Gong^{1,2}, Christoph Mühlberg¹, Mirko Wegscheider¹, Christopher Fricke¹, Jost-Julian Rumpf¹, Thomas R. Knösche^{*2}, Joseph Classen^{*1}

(*) co-corresponding authors

1. Department of Neurology, Leipzig University Medical Center, Leipzig, Germany

2. Method and Development Group Brain Networks, Max Planck Institute for Human Cognitive and Brain Sciences, Leipzig, Germany

Posted on medRxiv: <https://medrxiv.org/cgi/content/short/2021.07.26.21261085v1>

Published in Journal of Neurophysiology, Volume 127, Issue 6, June 2022, Pages 1606-1621,

<https://doi.org/10.1152/jn.00541.2021>

7.1 Introduction

Chapter 4 and Chapter 5 have demonstrated the enhanced β -broadband γ phase-amplitude coupling (PAC) in the motor control regions from recordings via scalp electroencephalography (EEG) during the resting state of patients with Parkinson's disease (PD), suggesting that it could be considered as a pathophysiological biomarker of PD. However, even though the exaggerated PAC in the resting state was confirmed to be associated with clinical severity of motor impairment indexed by clinical scores in our study and the previous literature [134], we still lack evidence regarding the direct relationship between PAC and the impaired motor performance of PD patients. Therefore, it is crucial to investigate the features of PAC during movement.

It has been reported that movement-related PAC derived from recordings of local field potentials (LFP) from the subthalamic nucleus (STN) and *globus pallidus externa* (GPe), as well as from electrocorticography (ECoG) recordings in the sensorimotor areas of PD patients was reduced compared with that from the resting state [136, 140, 187, 202]. Furthermore, brain stimulation-induced acceleration of movement during a complex reaching and tracking task was associated with reduced cortical movement-related PAC [140]. These observations appear to provide circumstantial evidence that bradykinesia of PD patients is related to persistently enhanced PAC during movement. However, PAC derived from scalp EEG during a verbally cued intermittent hand opening/closing task did not differ between patients in the off-medication state and healthy subjects [139]. Even in the studies reporting persistent PAC enhancement during movement, the relationship between the strength of PAC and the motor impairment remained unclear since none of the studies reported whether the execution of the movements was actually impaired in PD patients [118, 136]. Because abnormalities of movement-related PAC may not become apparent until kinematic abnormalities occur, the lack of information on kinematics means that it is unknown how PAC is involved in the pathophysiology of movement disorders. On the other hand, there is a possibility that not the overall strength of PAC, but its dynamics during the movement, is related to the production of behavioural abnormalities. Several studies in patients with non-movement disorders [133, 203] and in PD patients [187] suggest that PAC might be involved in the regulation of motor control. However, the question how it is incorporated into the pathophysiology of bradykinesia has not been solved.

In Chapter 6, we have demonstrated that PD patients could perform as normal as healthy subjects in repetitive pressing tasks, while they showed behavioural abnormalities when performing tapping tasks. In this chapter, we aim to investigate the functional role of PAC related to the movement dynamics and the relationship between PAC and various forms of movement behaviour in PD that differ concerning whether or not they are abnormal.

7.2 Methods

7.2.1 EEG signal recording

The characteristics of participants and experimental procedures have been described in Chapter 3, Section 3.1-3.4. In this chapter, we used the recordings of all six conditions conducted in our experiment (i.e., the resting state, pressing task, slow tapping without feedback, slow tapping with feedback, fast tapping without feedback, fast tapping with feedback) from 19 PD patients and 20 healthy controls. The details of experimental settings for movement tasks were

introduced in Chapter 3, Section 3.2.

7.2.2 EEG signal processing

The pre-processing procedures and the procedures for source reconstruction of the EEG signals have been described in Chapter 3 (Section 3.4 & 3.5.2). We applied the standard pre-processing procedures to the EEG sensor signals of all conditions. Regarding the EEG source reconstruction, in brief, we calculated and applied a common linearly constrained minimum variance (LCMV) beamformer filter with the merged data of all conditions, and then applied source-space independent component analysis (ICA) separately to each brain region of each condition. In order to eliminate any interference of high-frequency activities that are not in the range of interest and to optimize the calculation of source-space ICA, before removing the artifacts and merging the raw data for the calculation of the beamformer filter, we applied a 300 Hz low pass filter (EEGLAB default filter) to the EEG sensor signals recorded under all the conditions. The brain regions that we were interested in this study were those motor regions that we found previously to show statistically enhanced PAC in PD patients PD compared with controls (Chapter 4), namely the premotor cortex (PMC), the primary motor cortex (M1), the primary somatosensory cortex (Broadman area 3 [BA3]), and the primary somatosensory complex (Broadman area 1&2 [BA1&2]). The information regarding the average number of components per region for subjects in the six conditions was provided in Table 7.1.

Table 7.1 ICA components derived from ROI source signals

Regions		Resting	Pressing	TappSlow FB-	TappSlow FB+	TappFast FB-	TappFast FB+
PMC	Patients	10.5±0.6	10.2±0.7	10.2±0.9	10.2±0.9	10.0±0.9	10.1±0.9
	Controls	10.7±0.7	10.5±0.5	10.8±0.8	10.6±0.7	10.4±0.8	10.3±0.9
M1	Patients	10.5±0.5	10.5±0.5	10.4±0.8	10.5±0.8	10.4±0.8	10.5±0.9
	Controls	10.7±0.7	10.6±0.8	10.5±0.8	10.5±0.8	10.3±0.9	10.3±0.9
BA3	Patients	10.6±0.7	10.7±0.7	10.6±1.0	10.5±0.9	10.4±1.0	10.5±0.9
	Controls	10.9±0.6	10.8±0.6	10.8±0.7	10.7±0.8	10.7±0.7	10.6±0.7
BA1&2	Patients	10.8±0.7	10.6±0.8	10.7±0.9	10.7±0.9	10.6±0.9	10.7±0.7
	Controls	11.0±0.7	10.9±0.7	10.9±0.8	10.9±0.7	10.7±0.8	10.8±0.8

TappSlow: slow tapping task; TappFast: fast tapping task; FB-: without feedback; FB+: with feedback; PMC: Premotor cortex; M1: Primary motor cortex; BA3: Broadman area 3; BA1&: Broadman area 1&2.

Next, all datasets were segmented in epochs of 3 s duration (-1 s to 2 s relative to the online mechanical onset) to obtain movement-related information. In order to apply the same procedure to the resting dataset, we randomly generated and inserted 150 fake markers into the original raw datasets, and generated the information of epochs based on the fake markers.

Moreover, we only used every second movement onset trigger to minimize the overlapping of movements for the fast tapping task. The number of recorded movement cycles varied among different movement tasks, where the least number of repetitions were performed in the pressing task. To obtain a comparable number of movement cycles across conditions, we selected randomly the number of trials in resting, slow tapping, and fast tapping conditions, such that the number of trials matched that derived from the pressing task. The numbers of epochs of each condition that were entered in the following analysis are provided in Table 7.2.

Table 7.2 Number of epochs in each condition

	Resting	Pressing	TappSlow, FB-	TappSlow, FB+	TappFast, FB-	TappFast, FB+	p-value
Patients	105.6±12.1	104.9±26.3	110.2±26.3	110.8 ±25.5	101.4±15.2	99.4 ±14.8	>0.2
Controls	108.5±5.3	103.6±28.6	101.1±30.6	103.2 ±31.4	103.3±15.7	100.6±18.2	>0.06
p-value	0.36	0.99	0.21	0.39	0.34	0.35	

TappSlow: slow tapping task; TappFast: fast tapping task; FB-: without feedback; FB+: with feedback. p values were estimated by signed-rank tests within group and rank-sum tests between group

7.2.3 Movement-related PAC calculation

The raw data of source signals were first filtered for β (13-30 Hz) activities and γ (50-150 Hz) activities. In subsequent, the Hilbert transform was applied to extract the phase of the β band and the amplitude of the γ band. Then, for each 3 s epoch in a component, we computed PAC in successive windows (300 ms, corresponding to 4-10 cycles for the β activities) shifted by 50ms time steps. We applied the normalized mean vector length (MVL) (for details of the method see Chapter 3, Section 3.6). Since the shifted window was so short that it might result in an inaccurate measurement of the PAC, the z-score of MVL (zMVL) was calculated using the mean and standard deviation of 200 surrogates created by recombining the instantaneous phase and randomized shuffled amplitudes (for details of the method see Chapter 3, Section 3.6). zMVL values not larger than 1.96 (equivalent to 95% confidence interval) were assigned the value 0. Therefore, for each 3 s epoch in a component, we had 55 zMVL values with 50 ms time resolution.

For each subject, we calculated pairwise zMVL values among ICA component pairs within each region as introduced previously (Chapter 4, Section 4.2.3). In brief, we calculated the epochs of the time series of zMVL values among $n \times n$ component pairs in a region. We then computed the single time series by computing the weighted average of zMVL values across epochs and $n \times n$ component. The weights for averaging were defined as the percentage of variance accounted for each component pair per region (also refer to Chapter 4, Section 4.2.3).

7.2.3.1 Fluctuations of movement-related PAC

To estimate the fluctuations of PAC over time in different tasks, we calculated the coefficient of variance (CoV) of the movement-related PAC for each task for each subject. CoV was calculated as the ratio of the standard deviation to the mean across 55 time points of averaged PAC for each subject.

7.2.3.2 State-related PAC

To compare PAC across conditions and groups, we computed the mean PAC value by averaging across the 55 time points of 3 s epochs for each subject in each condition.

7.2.3.3 Dynamic PAC (dynPAC) estimation

To investigate movement-related PAC dynamics, we separated the movement and grouped the respective movement-related PAC values into 5 periods separated by 4 trigger points derived from the digital kinetic (pressing) or kinematic (tapping) signals recorded during the movement for each individual. Trigger points were initially established individually for each movement cycle in each task based on the force threshold for the pressing task and amplitude threshold for the slow tapping task (also refer to Chapter 3, Section 3.2.3). Importantly, to estimate the timing of the transition times at the cortical level with the best possible accuracy, we shifted the mechanical trigger points by considering the influence of the general mechanical delays, the general electromechanical delays (50 ms), and the corticomuscular conduction time (20 ms) across subjects in pressing and slow tapping events relative to the mechanical trigger points. The details for the definition of mechanical trigger points and delays between the mechanical trigger points and the adjusted trigger points at the cortical level were introduced in Chapter 3, Section 3.2.3.

Therefore, for the pressing task, also considering the 50 ms time resolution of the movement-related PAC values, the 4 trigger points at the cortical level were defined as: 1) the movement onset – 150 ms before the real-time mechanical onset; 2) the end of the force build-up – the closest time point to the 70 ms before the mechanical-detected end of the force build-up; 3) the start of releasing – the closest time point to 70 ms before the mechanical-detected start of releasing; and 4) the movement offset – the closest time point to 60 ms before the real-time mechanical offset. Accordingly, the PAC values in movement epochs were grouped into the 5 periods for movements in the pressing task, defined as: P1 (the pre-pressing onset period) – during 200 ms before the movement onset to the movement onset; P2 (the post-pressing onset period) - the period from the movement onset until the end of the force build-up; P3 (the sustained pressing period) – the period from the end of the force build-up to the start of the force release; P4 (the

releasing period) – the period from the start of releasing to the movement offset; and P5 (the post-offset period) – the period from the movement offset to 200 ms after the movement offset.

For the slow tapping task, also considering the time resolution (50 ms) of movement-related PAC time series, the adjusted 4 trigger points on the cortex level were defined based on the lower and upper photoelectric sensors as: 1) movement onset – 150 ms before the real-time mechanical movement onset; 2) the end of finger extension – the time point closest to 70 ms before the mechanical-detected end of finger extension; 3) the start of finger flexion – the time point closest to 70 ms before the mechanical-detected start of finger flexion; and 4) the movement offset – the time point closest to 70 ms before the real-time mechanical movement offset. Accordingly, the 5 periods were defined as: T1 (the pre-extension onset period) – the period from 200 ms before the movement onset to movement onset; T2 (the post-extension onset period) – the period from the movement onset to the end of finger extension; T3 (the extension period) – the period during which the index finger remained extended at or above the upper photoelectric sensor; T4 (the index finger flexion period) – the period from the start of finger flexion to the movement offset of the tap; and T5 (the post-flexion offset period) – the period from the movement offset to 200 ms after the movement offset.

The zMVL values in the single movement cycle were then first grouped in the 5 periods of pressing and slow tapping tasks, respectively. We then averaged the zMVL values in each of the periods across trials for each subject.

7.2.4 Movement-related power spectrum density (PSD)

The movement-related PSD was calculated by the Welch method in MATLAB in time-frequency representation. In order to be comparable with the movement-related PAC, the PSD was calculated in 300 ms shifted windows with 50ms time steps in 3 s epochs (hann window, frequency resolution = 1 Hz) of all conditions. Then, the PSD was transformed to base 10 logarithmic power for group comparison and presenting. The power was normalized by subtracting the mean power across all time points and trials from 4 to 300 Hz (excluding 50 Hz and its harmonics) to account for the inter-subject variability.

7.2.5 Statistical analysis

All analyses were performed in the brain regions contralateral to the hand side on which the subject was asked to perform the movement tasks. We mainly applied non-parametric analysis of variance (ANOVA) tests to examine the main effects and interaction effects of the factors including Group, Tasks and Regions (Please refer to the introduction in Chapter 3, Section 3.7).

For post-hoc tests, we applied a non-parametric Wilcoxon rank-sum test for between-group comparison and Wilcoxon signed-rank test for within-group comparison across conditions. We also applied a paired non-parametric test (Wilcoxon signed-rank test) between PAC values in the movement transients for each task of each group. In addition, we estimated the correlations between the results of PAC and performance parameters by Spearman coefficients. False discovery rate (FDR) correction was applied in multiple tests to avoid type I errors in null hypothesis testing.

7.3 Results

7.3.1 State-related PAC during repetitive movement

We examined whether PAC averaged over the whole movement period of each different condition (“state-related PAC”) was modulated differently by different tasks in patients and controls. To reduce the number of factors, we first established that visual feedback about the upper height criterion did not modulate the strength of state-related PAC by applying 3-way ANOVA with factors of Group (patient, controls), Region (4 levels) and Feedback (FB+, FB-) for the slow tapping and fast tapping tasks. The factor Feedback did not show any interaction effect or main effect in either the slow ($F(1,37) = 0.26$, $p = 0.616$) or the fast tapping tasks ($F(1,37) = 0.04$, $p = 0.840$). Therefore, in the following analysis, we combined the conditions with and without feedback in the slow and fast tapping tasks. A 3-way (Group, Task, Region) mixed ANOVA performed on the zMVL values averaged over the entire 3 s epochs showed that state-related PAC was modulated differently in patients and controls by the tasks (Group \times Task; $F(3,111) = 4.69$, $p = 0.004$; Fig. 7.1). Post-hoc rank-sum testing revealed enhanced PAC in patients compared with controls in the resting state ($p = 0.016$), in agreement with the findings in Chapter 4. PAC was also enhanced in the pressing task ($p = 0.012$), but not in any of the tapping tasks ($p > 0.5$). Post-hoc tests also showed that state-related PAC in patients was reduced during all active movement tasks compared with the resting state (resting vs. pressing, $p = 0.033$; resting vs. slow tapping, $p = 0.010$; resting vs. fast tapping, $p < 0.001$). However, we found no significant reduction of state-related PAC during pressing ($p = 0.296$), during slow tapping ($p = 0.654$) or fast tapping ($p = 0.135$) compared with the resting state. ANOVA revealed that PAC differences among the conditions were affected by the motor control area (Task \times Region; $F(9,333) = 2.64$, $p = 0.006$). However, since we found no interaction effects among the three factors (Task \times Region \times Group; $F(9,333) = 0.40$, $p = 0.933$), the effect of brain regions was unlikely to affect the differences between groups.

The above findings show differences between the resting state and movement-related state-

related PAC, especially in patients. Among the movement tasks, state-related PAC differed between patients and controls only in the pressing task, where motor behaviour was similar between patients and controls. By contrast, state-related PAC was remarkably similar between patients and controls in the tapping tasks, where motor behaviour was different. Because state-related PAC was derived from EEG recorded during active movement, abnormal enhancement of PAC per se is unlikely to be directly connected with the motor impairment.

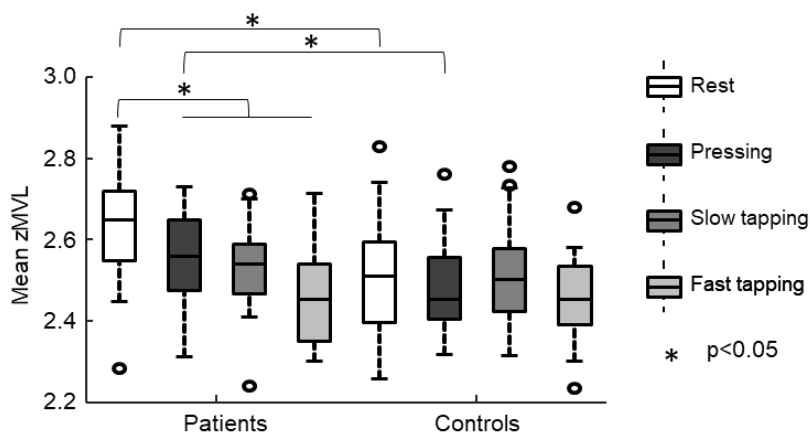


Figure 7.1 State-related PAC derived from movement-related epochs averaged across the 4 regions. Three-way nonparametric ANOVA showed significant interaction effects (designated by an asterisk) between Group and Tasks. Post-hoc tests of the Group*Task interaction effect showed significant differences (designated by an asterisk) between the resting state and all 3 movement tasks in the patients. Note that state-related PAC differed between patients and controls at rest and during pressing.

7.3.2 The fluctuations of movement-related PAC

We then considered the possibility that dynamic modulation of PAC might be more directly related to the underlying pathophysiology of motor impairment than its absolute level. We first visualized dynamic PAC and EMG activity recorded from the first dorsal interosseous (FDI) muscle, aligned with the online mechanical onset of the movement (Fig. 7.2A). Alignment with movement onset confirmed that PAC was generally reduced from rest to all movement tasks in patients, as shown in the previous paragraph. Additionally, it became evident that the PAC values in the pressing and slow tapping tasks appeared to be markedly modulated along the movement cycle in controls. By contrast, this modulation was considerably less pronounced at rest and during fast tapping. For pressing and slow tapping, PAC rapidly and markedly declined from a brief peak before rebounding again around movement onset. Modulation appeared to be less marked in patients.

To statistically assess the degree of fluctuation of movement-related PAC for each task

quantitatively, we computed first the CoV across movement time series. A two-way mixed ANOVA test (CoV \sim Group \times Task) showed significant interaction effects ($F(3,111) = 3.07$, $p = 0.031$, Fig. 7.2B). In pressing, post-hoc tests revealed that the fluctuation was stronger for both patients (signed-rank, $p = 0.005$) and controls ($p = 0.006$) compared with the resting state. In slow tapping, the fluctuation was larger than in the resting state of controls (signed-rank, $p = 0.033$) but not of patients ($p = 0.872$). Since the resolution of PAC calculation does not permit assessment of modulation across very short movement cycles, reductions of fluctuation of PAC across a movement cycle of fast tapping task (signed-rank, controls, $p = 0.044$; patients, $p = 0.084$) must be interpreted with caution.

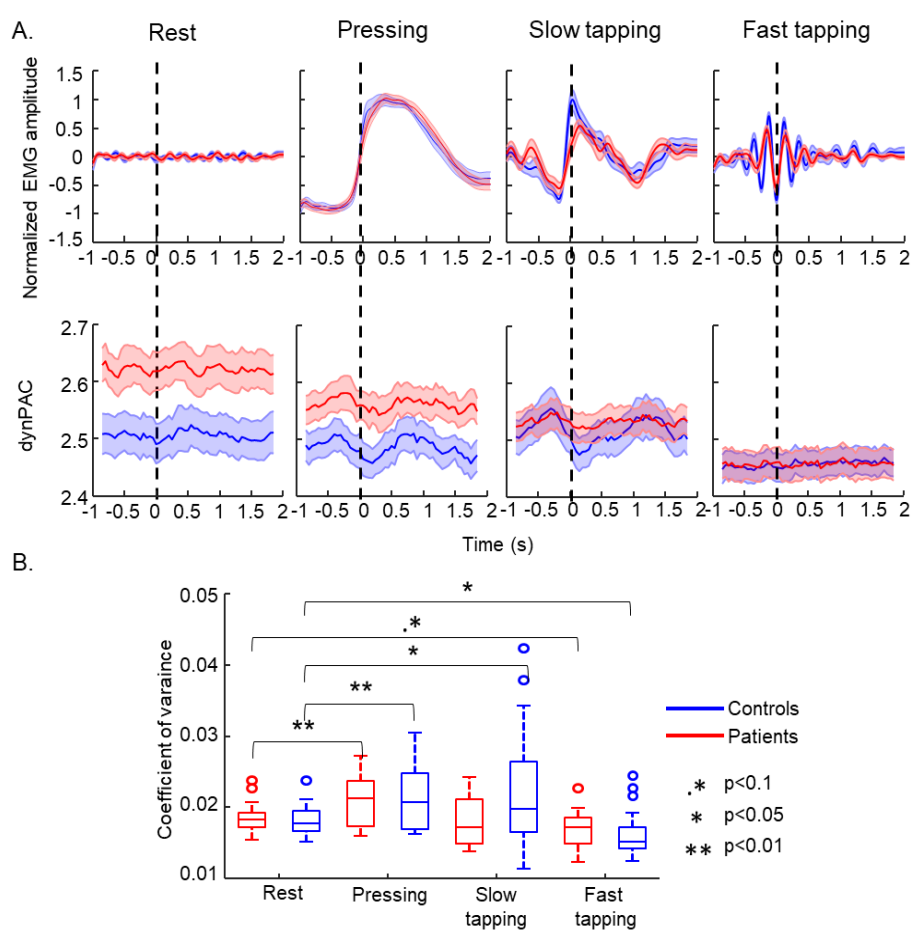


Figure 7.2 The fluctuation of PAC in the 3s time series. (A) Time series (mean \pm standard error [SE]) of rectified EMG recorded from FDI muscle (upper panel) and PAC (lower panel), averaged after alignment with arbitrary time points (rest) or movement onset (pressing, slow and fast tapping). (B) Boxplot showing coefficient of variance across 4 conditions. The two-way ANOVA showed interaction effects between Group and Tasks.

In addition, the post-hoc comparisons of CoV between patients and controls did not reveal differences in the resting state (rank-sum, $p = 0.567$), pressing task ($p = 0.967$), and fast tapping

task ($p = 0.244$), but a marginally significant difference in the slow tapping task ($p = 0.070$). The larger time-series variance of PAC in the pressing and slow tapping tasks compared with rest may indicate a modulation of PAC under particular movement events. Therefore, we subsequently investigated the modulation of movement-related PAC across transitions between different movement states in the pressing and slow tapping tasks (“dynamic PAC”) only.

7.3.3 The dynamics of movement-related PAC

We investigated the dynamics of PAC in more detail by looking at the modulation of PAC between 5 periods separated by 4 measured trigger points. The dynamic trigger points were firstly defined based on the kinetic (pressing) or kinematic (tapping) events along the movement cycle, as shown in Fig. 7.3A. Then, the 4 trigger points from the pressing and tapping mechanical events were further adjusted by considering the general mechanical and electromechanical delays, as well as the corticomuscular conduction time to estimate the timing of the transition times at the cortical level with the best possible accuracy. The details for the definition of the four adjusted trigger points are described in the method section.

In the pressing task, PAC was markedly modulated around movement transitions. Figure 7.3B illustrates the averaged dynamics of PAC across the first 3 periods as resulting from aligning data with the adjusted trigger point #1 (defining the transition between pre-movement onset and force build-up, left panel), and the last 3 periods as resulting from aligning data with the adjusted trigger point #4 (defining the transition between force release and pressing offset, right panel). As shown in Fig. 7.3B, close to the mechanical onset of pressing, PAC appeared to decrease from a brief maximum, reaching a minimum before rising again (also evident in Fig. 7.2). Besides, alignment with the transition at the offset of releasing revealed a PAC motif similar to that at the onset of pressing (Fig. 7.3B, right panel). Two-way mixed ANOVA on Group and Period showed significant main effects for the factors Group ($F(1,37) = 5.51$, $p = 0.024$) and Period ($F(4,148) = 4.90$, $p < 0.001$), whereas there was no interaction effect between the two factors ($F(4,148) = 1.19$, $p = 0.317$). As shown in Fig. 7.3C, post-hoc tests indicated that, across subjects, dynPAC decreased significantly during the build-up of the pressing force compared with the pre-onset period (P1 vs. P2, $p < 0.001$). Then, the PAC value rebounded during maintained pressing (P2 vs. P3, $p = 0.070$) at marginal effects. The dynPAC showed the tendency of decreasing from P3 to P4, which was, however, not significant (P3 vs. P4, $p = 0.118$), while the PAC values significantly decreased from force releasing to post-movement offset period (P4 vs. P5, $p = 0.034$). This finding indicates that dynPAC was modulated across movement transitions before force build-up and releasing actions. Because there was no

interaction effect, PAC was not differently modulated between patients and controls.

We also investigated PAC dynamics in the slow tapping movement cycles in a manner similar to the pressing task. Since the presence or absence of colour feedback had no significant effects on the PAC values in slow tapping, the evaluation of PAC dynamics was based on combining the two conditions. Similar to the pressing task, we found marked modulation of dynPAC in the slow tapping task. As shown in Figure 7.3D, PAC declined from a brief maximum before index finger extension onset to post-extension onset in controls. Then PAC started to rebound after reaching a minimum during the period in which the index finger was above the higher amplitude threshold and continuously increased during the index finger flexion period and post-offset period. Patients showed similar modulation patterns, although PAC changes in patients were flatter than in controls (also evident in Fig. 7.2). A two-way mixed ANOVA of dynPAC values on the factors of Group and Period revealed a significant two-way interaction between Group and Period ($F(4,148) = 3.59, p = 0.008$). This finding indicated that PAC was modulated differently in patients and controls. Post-hoc tests revealed that while dynPAC decreased from T1 to T2 in both patients (signed-rank, $p = 0.016$) and controls (signed-rank, $p = 0.006$), the decrease of PAC associated with index finger extension (T2) was smaller in patients than in controls, as showed in Fig. 7.3E. Then there was a continuous decrease of PAC from T2 to T3 (signed-rank, $p = 0.005$) followed by a rebound from T3 to T4 (signed-rank, $p = 0.021$) in controls, while the modulation was less pronounced in patients (signed-rank, T2-T3: $p = 0.260$, T3-T4: $p = 0.260$). However, from the finger-flexion period to the post-flexion offset period, no significant PAC increase was found in both controls (signed-rank, $p = 0.126$) and patients (signed-rank, $p = 0.520$). Notably, the absolute PAC values did not differ between patients and controls in any of the 5 periods (rank-sum, all $p > 0.2$). This finding showed less PAC modulation in patients during selected periods of the tapping cycle than in controls during slow tapping movement.

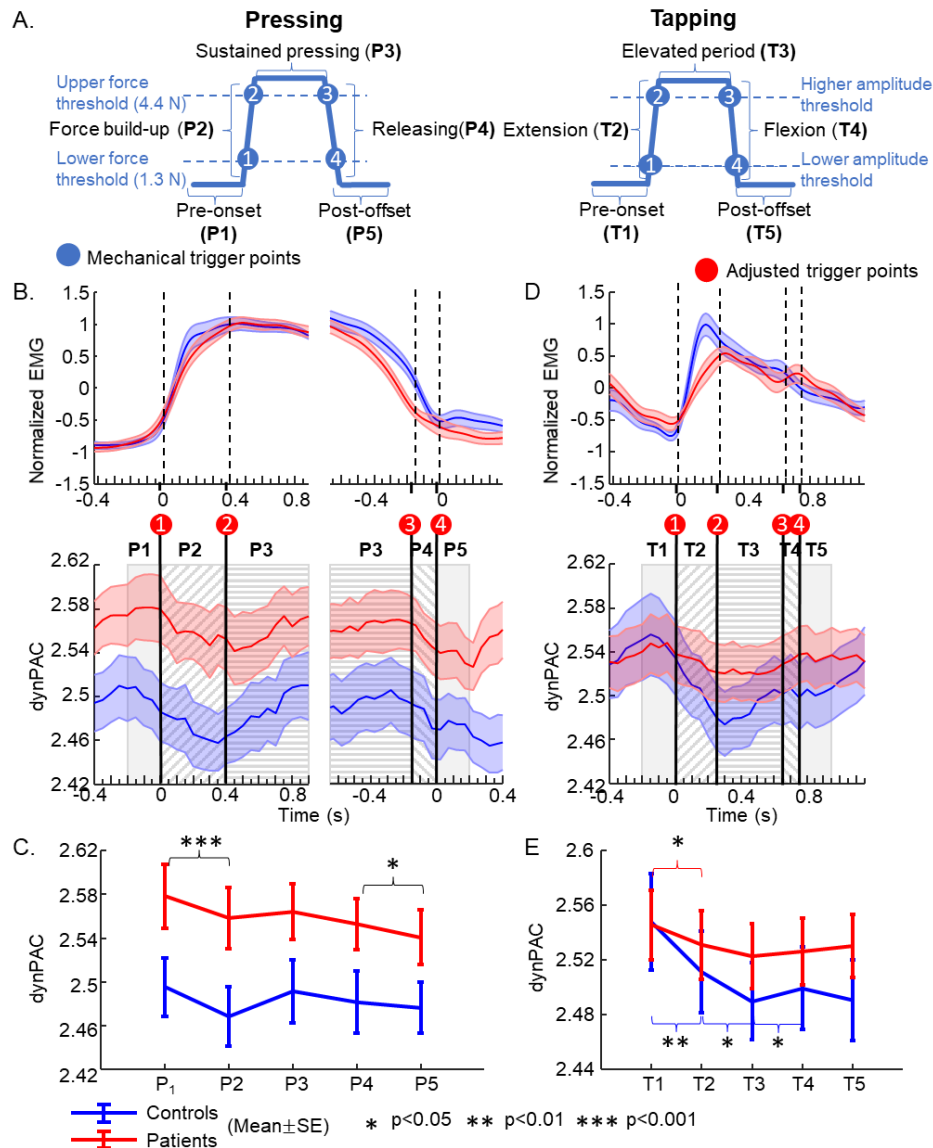


Figure 7.3 PAC dynamics (dynPAC) across movement transitions. (A) Definition of 5 periods of movement transitions based on 4 trigger points in the pressing task (left) and the slow tapping task (right). The trigger points were first established using 4 kinetic (force threshold for pressing) or kinematic (amplitude criterion for tapping) events along the movement cycle. The adjusted trigger points (displayed in B&D) were then determined by further considering the mechanical and electromechanical delays, as well as the corticomuscular conduction time to estimate the transition time points at the cortical level. (B) Pressing task. DynPAC as resulting from averaging after alignment with the adjusted trigger points on the (left) onset (#1) and (right) offset (#4). The timing of the other 2 trigger points #2 and #3) was determined based on the averaged durations of periods across subjects. (C) Error bar plot showing the movement-related dynPAC the 5 periods of the pressing cycle in patients and controls. (D) Slow tapping task. DynPAC resulting from averaging across subjects after alignment with the adjusted trigger point #1. The timing of the other 3 adjusted trigger points was based on the average duration of the following 3 periods across subjects. (E). Error bar plot showing the movement-related dynPAC of the 5 periods in a single tapping cycle in patients and controls. SE: standard error.

We subsequently tested the hypothesis that the magnitude of the PAC change around movement onset determines the ability to recruit FDI muscles engaged in the tapping (EMG slope as introduced in Chapter 6) and thus may contribute to the motor impairment in slow tapping performance in patients. Although the EMG slope was correlated with the PAC change between T1 and T2 in patients ($R = -0.52$, $p = 0.024$). EMG slope and PAC change were not significantly correlated in controls ($R = -0.12$, $p = 0.601$). As expected, the EMG slope was found to be highly correlated with the duration of T2 ($R = -0.61$, $p < 0.001$). Therefore, we considered the possibility that the negative correlation between the EMG slope and change of PAC between T1 and T2 in patients might have arisen because patients with a steeper EMG slope had spent less time reaching the adjusted trigger point #2. This would lead to less modulation of PAC if the PAC change per unit of time were constant across the patients. To test this idea, we computed PAC while fixing the duration of T2 for all subjects to 250 ms (from the adjusted trigger point #1 to 250 ms after that point, as shown in Fig. 7.3D). Using a fixed duration of T2 (250 ms), patients lost the correlation between EMG slope and the PAC change between T1 and T2 ($R = -0.33$, $p = 0.163$). In addition, the two-way mixed ANOVA analysis on the dynPAC values of the first two periods (T1 and fixed T2) revealed a marginally significant interaction effect between Group and Time ($F(1,37) = 4.01$, $p = 0.052$), which still suggests that modulation of PAC is less pronounced in patients than in controls.

7.3.4 Relationship between movement-related PAC dynamics and β power dynamics

It is well established [98, 204, 205] that spectral power in the β frequency band decreases during the initiation and execution of a movement. In the present study, we also found β power to be reduced at movement onset and during movement in both patients and controls (Fig. 7.4 A&B, left panels). Because the strength of β power affects the estimation of phases in the calculation of PAC, we aimed to investigate to which degree modulation of PAC by movement transitions was a consequence of associated changes in β frequency power. We assessed the modulation of β power in the 5 periods of a movement cycle in both the pressing and the slow tapping task (Fig. 7.4 A, B, right panels). A two-way mixed ANOVA with Group and Period factors was applied to the β power in pressing and in slow tapping tasks. The ANOVA in the pressing task revealed only a main effect of Period ($F(4,148) = 13.18$, $p < 0.001$), while the ANOVA in the slow tapping task revealed a significant interaction of Group and Period ($F(4,148) = 3.98$, $p = 0.004$). The modulation pattern of β power appeared to be similar to the modulation pattern of PAC in both tasks as reported above. Although there seems to be a difference between PAC change (Fig. 7.3C) and power change (Fig. 7.4A, left panel) in the

trend from P3 to P4, post-hoc tests did not reveal statistical significance in both PAC modulation and power modulation. This finding raises the question of whether the transient modulation of β power primarily drove PAC modulation during movement. We did not find a significant correlation between the absolute PAC and β power values in any of the periods in either the pressing task or the slow tapping task (p values > 0.3). Two examples of scatter plots between absolute power and PAC in P1 (T1) of pressing (slow tapping) are displayed in Fig. 7.4C. Additionally, we performed a correlation analysis between the PAC differences and the β power differences of each two adjacent periods. At movement onset, the two parameters were not significantly correlated in the pressing task ($R = 0.13$, $p = 0.429$), whereas they were significantly correlated in the slow tapping task ($R = 0.50$, $p = 0.003$). The correlation results for differences between any two adjacent periods are presented in Table 7.3, which showed no consistent relationship between β power change and PAC change during the movement. The above findings suggest that the movement-related dynPAC modulation does not generally reflect movement-related power dynamics. However, the fact that derivatives of the two variables were correlated at slow tapping onset could still have pathophysiological significance.

Table 7.3 Relationship between the change of PAC and β power

Task	P1-P2 // T1-T2	P2-P3 // T2-T3	P3-P4 // T3-T4	P4-P5 // T4-T5
Pressing	R=0.13, p=0.429	R=0.62, p=0.001	R=0.42, p=0.017	R=0.23, p=0.205
Slow tapping	R=0.50, p=0.003	R=0.42, p=0.017	R=-0.09, p=0.568	R=0.18, p=0.362

PAC: Phase-amplitude coupling. p values were FDR corrected for each task, all significant values after correction are marked in bold

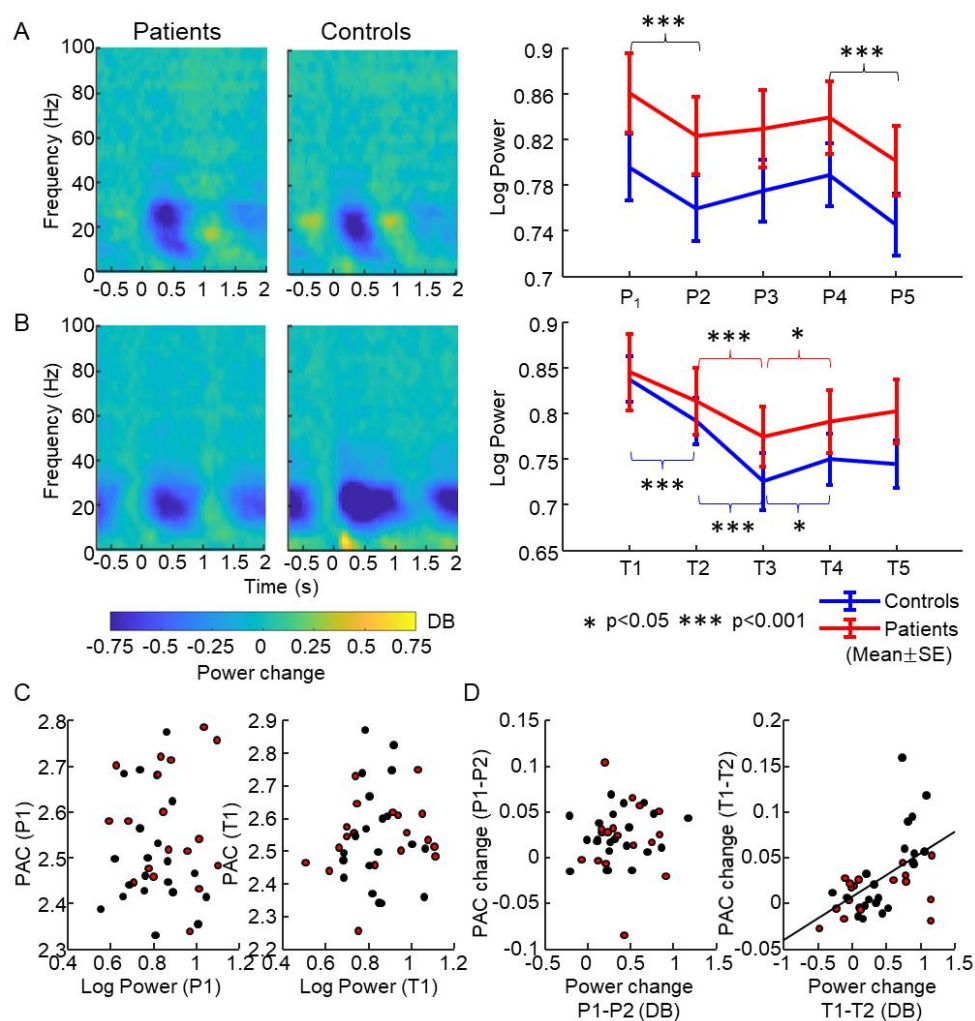


Figure 7.4 Relationship between movement-related dynPAC and β power. (A) Dynamics of β power in the pressing task. Left: time-frequency spectrogram. Right: dynamics of β power across the 5 periods of the pressing movement cycle. (B) Dynamics of β power in the slow tapping task. Left: time-frequency spectrogram. Right: dynamics of β power across the 5 periods of the slow tapping movement cycle. Significant modulations are marked by an asterisk. (C) Scatter plots of the relationship between the absolute strength of PAC and β power in the pre-onset phase of pressing task (left) and slow tapping task (right). (D) Scatter plots of the relationship between PAC change and power change from the first to the second period in the movement cycle of pressing task (left) and slow tapping task (right).

7.4 Summary

In this study, we investigated the characteristics of movement-related PAC corresponding to normal and abnormal behaviour of PD patients under different types of repetitive voluntary movements. We found PAC averaged over motor regions across the entire movement cycle was enhanced in PD patients in the pressing task, while the magnitude of PAC averaged across the whole movement was similar between patients and controls in all tapping tasks. These findings were not aligned with motor performance and EMG data (in Chapter 6), which showed abnormalities in patients for tapping but not for pressing, suggesting that the overall strength

of β - γ PAC during the movement does not directly relate to Parkinsonian bradykinesia. However, we provided evidence to suggest that β - γ PAC may have a physiological role in encoding motor processes during movement transitions. A strikingly similar motif of PAC rise and decay was observed around the onset and offset of pressing and around the onset of slow tapping, suggesting that transient PAC changes may be linked to a change between distinct movement states, and that the increase of PAC may have similarities with the “preparatory state” as defined in dynamical systems theory of motor control [206]. In patients, the dynamical pattern of PAC was similar in pressing (normally executed), where performance did not differ from controls. However, the PAC modulation of PD patients was flattened in slow tapping (abnormally executed) compared with the controls. All the above findings may associate the dynamics of PAC modulation during movements to the pathophysiology of bradykinesia in PD.

Part IV

Discussion

Chapter 8

General summary and discussion

8.1 General summary

Exaggerated β -broadband γ phase-amplitude coupling (PAC) in the motor cortex has been proposed as a promising non-invasive biomarker for Parkinson's disease (PD) [118, 137]. However, there is a lack of information on the characteristics of this abnormal electrophysiological signature, a fact that limits its use in the treatment of PD. This thesis aimed to investigate comprehensively the features of β -broadband γ cortical PAC in the pathophysiology of PD.

We analysed non-invasive electroencephalography (EEG) signals recorded simultaneously at rest and during various motor activities in PD patients and healthy controls. EEG signals were projected onto the individual cortical surfaces using source reconstruction techniques and separated into spatiotemporal components using source-space independent component analysis (ICA). First, we investigated the spatial origin of enhanced β -broadband γ PAC at rest in the cortex of PD patients. Compared with healthy controls, PAC between the phase of β (13-30 Hz) activities and the amplitude of γ (50-150 Hz) activities was significantly enhanced in the dorsolateral prefrontal cortex (DLPFC), the premotor cortex (PMC), the primary motor cortex (M1), and the somatosensory cortex (SS, including the primary somatosensory cortex [Brodmann area 3, BA3] and the primary somatosensory complex [Brodmann area 1&2, BA1&2]) in the hemisphere contralateral to the clinically more affected side.

Second, we investigated the potential mechanisms of the generation of exaggerated PAC by studying its spatiotemporal characteristics at the mesoscopic level. We found that β and γ signals involved in abnormal PAC were not strictly phase-phase coupled, ruling out that it merely reflects a non-sinusoidal activity of a single oscillator in a recurrent network. Moreover, we found that couplings between β and γ signals with different spatial distributions (inter-component couplings) differ in important features from couplings where both β and γ

oscillations have the same spatial distribution (intra-component couplings). While both types of couplings were abnormally enhanced in patients, only the inter-component couplings were correlated with clinical motor severity indexed by part III of Movement Disorder Society Unified Parkinson's Disease Rating Scale (MDS-UPDRS III) in motor control regions. Furthermore, the β - γ topographic similarities of inter-component PAC demonstrated profound differences in PD patients compared with healthy controls, which again highlight the pathophysiological significance of coupling between spatially distinct subnetworks. The above results demonstrate the critical role of abnormal coupling between spatially distinct neural circuits at rest in the pathophysiology of PD.

In the subsequent study, we addressed what is the direct relationship between abnormal PAC and motor impairment in PD patients by investigating the characteristics of movement-related PAC during different types of repetitive movement tasks. We found that patients exhibited slowness of movement in the repetitive tapping tasks (reduced electromyographic [EMG] slope in slow tapping, reduced tapping rate in fast tapping), but not in the pressing task.

We then looked further into movement-state related PAC. During the pressing task, the overall strength of PAC, averaged over the four motor regions (PMC, M1, BA3, and BA1&2) and the entire movement period, was enhanced in PD patients compared with healthy controls, while the performance was similar between the two groups. By contrast, in all tapping tasks, the overall strength of PAC was similar between patients and controls, although patients showed abnormal slowness of movements. This incongruity between the occurrences of abnormal PAC and abnormal movements in PD patients may indicate that the strength of state-related β -broadband γ PAC during movements does not relate directly to impaired motor behaviour in PD patients.

Next, we investigated the dynamic modulation of β - γ PAC during movements. Our results suggest that the modulation of PAC during a movement cycle is linked to transitions between distinct movement states. In patients, the modulation of PAC was similar to controls in pressing (which was normally executed), but flattened in slow tapping (which was abnormally executed). These deviations in PAC around motor action transients may indicate dysfunctional evolution of neuronal population dynamics from the preparatory state to movement generation in PD. These findings may indicate that cross-frequency coupling is involved in the pathophysiology of bradykinesia in PD through its abnormal dynamic modulation.

The above findings help to construct a comprehensive picture of the characteristics of β -

broadband γ PAC at rest and during movements of PD patients. In section 8.2, we discuss the significance of these findings in detail.

8.2 Discussion

8.2.1 Advantages of applying EEG source analysis to abnormal PAC

Previous studies have applied either invasive electrocorticographic (ECoG) or non-invasive EEG recordings to identify enhanced β -broadband γ cortical PAC in PD [118, 137]. Although ECoG has superior spatial resolution and a better signal-to-noise ratio compared with EEG [77], its spatial coverage is limited by the small size of the electrode strips that can be placed through a burr hole. Moreover, it requires surgery, leading to enhanced risk and increased technical effort, and its use raises ethical issues. In particular, it is practically impossible to perform measurements in normal controls. Compared with the ECoG recording technique, EEG is a non-invasive, and therefore a more convenient, safer tool to investigate brain functions with high temporal resolution. However, it suffers from limited spatial resolution because signals are spatially blurred through the effect of volume conduction. In fact, each recording site captures a superposition of signals from multiple origins. While the spatial resolution cannot be improved fundamentally, the mixture problem can be ameliorated using source localization techniques. By taking into account the geometric locations of the electrodes, the anatomy of the head (from magnetic resonance imaging [MRI]), and electric volume conduction physics, it is possible to reconstruct approximately the origins and the distributions of the brain activities in a non-invasive manner. Based on these reconstructions, a finer segregation of spatially distinct networks in each brain region was achieved by applying source-space ICA in our study, an approach that had been suggested by Jonmohamadi et al. [173]. Application of this technique helped us to gain insight into the EEG oscillatory signals at a mesoscopic level.

Importantly, we found abnormal cortical PAC of PD patients in source-localized EEG signals but not in EEG sensor signals. This finding is somewhat in contrast to some previous studies, in which researchers had identified significant PAC differences between PD patients and healthy controls from EEG sensor signals [137, 139]. As we applied commonly used procedures for recording, preprocessing, and PAC calculation, similarly to those employed in previous studies [137, 139], it seems unlikely that these differences would result from methodological details. Instead, we suggest that for PAC to be detectable in sensor signals [139], patients may need to be in more advanced stages of the disease. Our findings that PAC was statistically significantly enhanced only in the clinically more affected hemisphere, which agrees with previous reports [135], may support this suggestion. Besides, in animal models of

PD, PAC did not appear before advanced disease stages [124, 207]. In addition, previous ECoG studies demonstrating PAC [118] has been presented in patients undergoing deep brain stimulation (DBS), so that advanced stages of the disease might be implicated. Moreover, an EEG study demonstrated enhanced PAC at the sensor level excluded the recruitment of patients at early stage (MDS-UPDRS III < 15) [139]. By contrast, the majority of the patients in our present study were at relatively early stages of the disease. Therefore, the PAC effects may have been expressed more weakly in these patients and hence may have been too low to be detected reliably on the EEG sensor level due to the relatively low signal-to-noise ratio and the volume conduction problem. Our results emphasize that the transformation of EEG sensor signals to source signals may be essential to enhance the sensitivity of the biomarker, especially at early stages of the disease. Moreover, a more precise localization of abnormal PAC could help find a more effective neuromodulation target for specific symptoms.

8.2.2 The spatial organization of exaggerated PAC in PD patients at rest

In resting EEG data, we identified abnormal PAC localized in DLPFC, PMC, M1, and SS (including BA3, BA1&2). Such a widespread occurrence of abnormal PAC in PD has not been reported before. Direct ECoG recordings have revealed abnormal PAC in PD patients in signals from subdural electrodes overlying the precentral gyrus, thus probably reflecting activity in PMC/M1 [118]. Enhanced PAC in PD patients has also been observed in signals from EEG electrodes overlying the sensorimotor region [137, 139]. Our evidence that abnormal PAC might also occur in brain regions outside the core motor system like DLPFC and SS may open the door for new interpretations of the role of abnormal PAC in the pathophysiology of PD.

The contribution of SS is noteworthy because recordings were done at rest, which may imply minimal activity of refferent signals from contracting muscles. Furthermore, it has been hypothesized that the ‘hyperdirect’ cortico-subthalamic pathway is essential for generating PAC [118]. SS does not project monosynaptically to the subthalamic nucleus (STN), which receives its excitatory input mainly from neurons located in M1 and the supplementary motor area [26] or the prefrontal regions [208, 209]. Therefore, the presence of PAC in SS indicates that abnormal PAC at rest is unlikely to exclusively involve brain regions connected by the ‘hyperdirect’ tract, but may also involve other basal-ganglia thalamocortical (BGTC) circuits or cortico-cortical connections. A similar conclusion has been reached previously based on recordings from *globus pallidus internus* (GPi) [124, 138]. Although the spatial resolution of scalp EEG is limited even with advanced source localization, our findings strongly suggest that abnormal PAC in PD is present not only in PMC and M1, but in various other cortical regions

involved in motor control even at rest.

The abnormal PAC found in DLPFC of PD patients may suggest that abnormal brain synchronization may also have a role in behavioural domains outside of motor control [210]. It has been demonstrated that DLPFC is involved predominantly in associative BGTC circuits [211], a finding that suggests the abnormal PAC in DLPFC is implicated in executive and other cognitive dysfunctions [212, 213]. This would also explain our finding that the strength of PAC in DLPFC was not correlated with clinical scores indexed by the MDS-UPDRS III, because this instrument exclusively captures motor symptoms of PD. As DLPFC has direct connections to the basal ganglia network and the functional activity in DLPFC can be altered through STN DBS [212, 214], it will be interesting to see whether PAC is correlated with cognitive symptoms in PD and how responsive it is to different clinical interventions.

Our study demonstrated that, at rest, abnormal PAC in the sensorimotor areas of PD patients was correlated with the MDS-UPDRS III hemi-body scores, highlighting the significance of abnormal PAC at rest in the deficits of BGTC motor circuits. Previous reports have already demonstrated correlations between enhanced PAC at rest and the clinical severity of Parkinsonian bradykinesia via invasive recordings, for example, in recordings of local field potentials (LFP) from the human STN [134, 136, 215], the GPi [216], and in ECoG from PMC/M1 [138]. While a previous EEG study also found a correlation between therapy-induced changes in PAC and therapy-induced changes in clinical severity [139], our study is the first to demonstrate a direct relationship between the strength of native PAC computed from scalp EEG and clinical severity scores in the off-medication state. This observation not only enhances the validity of our findings, but may additionally underline the pathophysiological significance of enhanced resting PAC in cortical sources.

8.2.3 Possible mechanisms of abnormal β - γ PAC in PD patients at rest

As the macroscopic distribution of exaggerated PAC in the cortex of PD patients points to BGTC circuits related to motor and non-motor functions, our analyses also provide insight into the potential mechanism of enhanced PAC of PD on a mesoscopic scale. Using waveform analysis, we showed that the PAC-related β and γ activities were not completely phase-phase coupled. This finding specifically renders the possibility unlikely that PAC arises because a recurrent (cortical) network that physiologically oscillates in the γ range [217] is strongly driven by the output of an enhanced (subcortical) β -oscillator [218]. Instead, our findings suggest that PAC arises to a significant extent through the activity of two relatively weakly linked and physiologically distinct oscillators that likely correspond to two spatially distinct

cortical substrates. This conclusion also excludes the possibility that the γ activities involved in the abnormal PAC merely reflect harmonic components in non-sinusoidal β activities as reported based on time-domain analysis of β oscillations in ECoG [141] or scalp EEG recordings [219]. According to this hypothesis, developed by Cole and colleagues, the non-sinusoidal wave shape of the β oscillations is a consequence of over-synchronization of the local firing of action potentials in the cortex [140, 220]. However, they also concluded that the non-sinusoidal waveform of β activity could not wholly explain the enhanced PAC detected in the motor cortex [141]. In principle, PAC could result from excessively synchronized neural activity in the BGTC loop [141] and may still be correlated with clinical motor impairment. Nonetheless, our results suggest that attenuation of PAC by decorrelating excessive synchrony through DBS [220] might fail to break up PAC across spatially separated circuits, which might represent a more relevant pathophysiological target.

Our conclusion, assuming the existence of spatially and physiologically distinct oscillators contributing to PAC, was substantiated by further investigation of ICA components of each of the 5 brain regions mentioned in section 8.2.2. We found enhanced PAC when phase-amplitude pairs were composed of β and γ signals from identical components, but also from distinct components. The coupling within identical components might represent strong coupling in a recurrent network. By contrast, pathological inter-component coupling implies coupling between different cortical columns, because ICA is not suited to distinguish between temporally independent components if they originate from exactly the same cortical patch. Notably, in the present study we found that the correlations between PAC and clinical motor severity were only statistically significant in inter-component couplings in motor control regions (PMC, M1, BA3 and BA1&2). These findings emphasize the importance of abnormal PAC generation by spatially distinct subnetworks. However, despite the fact that the electric activity was generated in the cortex, our findings do not contradict the notion that one or both cortical oscillators might be driven by activity from subcortical nuclei. The nature of the coupling could even be routed entirely in distinct subcortical projections driving independent cortical oscillations [45, 221, 222].

The estimation of the contributions of components brought a deeper insight into the mechanisms of abnormal inter-subnetwork couplings. We applied the Gini coefficient to estimate the degree of equality among contributions of subnetworks in a local region to the abnormal enhanced PAC. We found that Gini coefficients were higher in patients than in controls; this finding indicates that the enhanced PAC in PD relies on a relatively small number

of components. This result provides additional support for the assertion that synchronization between the activities of spatially distinct neuronal circuits is of greater pathophysiological relevance than that between the activities of the same topographical origin. This conclusion was further corroborated when the spatial organization of the ICA components was tested explicitly. In M1 and BA1&2, where the spatial similarities between β and γ topographies of each individual were generally high, this similarity was reduced in patients. Moreover, we found that the higher the Gini coefficients, the greater the spatial discrepancy between the source distributions of β and γ activities involved in PAC. This implies that the abnormal enhancement of PAC in PD reflects the abnormal dominance of a relatively small number of coupled sub-networks. Animal experiments have shown that the loss of dopamine impairs the directionality and hierarchical organization of normal β and γ propagation through different BGTC pathways [223]. Against this background, we suggest that in the Parkinsonian state, dopamine depletion may disrupt the regular operation of the BGTC loops by reinforcing and altering the connectivity between sub-networks so that the physiological segregation of certain feedback loops in BGTC circuits is lost. This phenomenon may then lead to more widespread coupling between diverse circuits. Coupling of circuits with similar intrinsic frequencies will be evident as abnormal synchronization and reduction of dimensionality in the EEG signals, whereas coupling of circuits with different frequencies will manifest as enhanced PAC.

However, PAC-weighted topographies in patients did not display a uniform Parkinsonian pattern; rather, they differed considerably among individuals. This finding indicates a pathophysiological heterogeneity that may reflect different clinical motor phenotypes and the variability of the disease stage. It further implies that pathophysiologically based future treatment of PD by non-invasive brain stimulation (NIBS) may need to be highly individualized and adjusted dynamically. For this purpose, advanced biomarkers such as the source localized and decomposed β - γ PAC described in this work might be of great help.

8.2.4 The magnitude of movement-related PAC in multiple types of repetitive movement

Our study on the exaggerated β - γ PAC in the resting state of PD patients extended the current knowledge of the characteristics of this electrophysiological biomarker and its relevance to the pathophysiology of PD. However, the possibility exists that PAC merely represents an epiphenomenon or a surrogate parameter of a remote pathophysiological mechanism and, hence, it is not causally linked to impaired performance. This question can be addressed by studying PAC at the time of the occurrence of motor impairment in PD patients. However, in

previous reports researchers have provided inconsistent findings of PAC differences during movement between PD patients and controls [136, 139, 140]. This may be due to the variations among sample cohorts and differences between the movement tasks designed by different research groups. Moreover, it remained unclear in these studies whether movement-related PAC was derived from signals recorded during the execution of kinematically normal or abnormal movements [136, 139, 140].

Our study contributed to clarifying this issue by comparing different types of movements in the same cohort of patients. Normal performance was found in patients when performing repetitive pressing and releasing actions (pressing task). In addition, during tapping at patients' own comfortable rate (slow tapping task), important performance parameters, such as mean movement rate and tapping variability, appeared normal. However, during that task, we observed markedly reduced EMG slopes in patients, which correlated with their bradykinesia and rigidity scores, suggesting that PD patients recruited muscles needed for finger extension with impaired efficiency [224]. Moreover, in the fast tapping task in which the subjects were asked to tap as fast as possible, patients exhibited slower tapping rates, larger tapping variability, and a decrement of the tapping amplitude (also present during the longer duration of slow tapping task), findings that are consistent with previous reports [199, 225]. Therefore, the repetitive tapping movements conducted in our study reflected bradykinesia, the cardinal manifestations of motor impairment in PD patients [146]. These results demonstrate that different types of movements with distinct demands regarding movement vigor (such as movement rate, frequency, and amplitude) differ in their potential to manifest Parkinsonian motor impairment.

While in the pressing task, there was no manifest motor impairment but significantly enhanced PAC in patients, the opposite occurred in the tapping tasks – no exaggerated PAC but clear signs of Parkinsonian motor impairment. Moreover, although the feedback on the tapping amplitude could improve the movements during tapping tasks, the movement-related PAC did not show differences between conditions with and without feedback. These findings demonstrate that the PAC difference between patients and controls varies among multiple types of repetitive movements, a phenomenon that may explain the controversial findings from previous studies [136, 139, 140]. It also suggests that the strength of state-related PAC during movements is not directly related to the motor impairment in PD. This eventuality implies that the general level of PAC during movements might not be a simple index for the severity of the disease. Hence, we subsequently investigated the PAC dynamics during movement transitions.

8.2.5 The dynamics of β - γ PAC during movements

We found that β -broadband γ PAC decreased around movement onsets in both PD patients and healthy controls. This PAC reduction during movements is in line with studies where PAC was derived from oscillatory signals recorded from the STN, *globus pallidus*, and M1 of PD patients [136, 139, 140, 187]. Besides, previous studies have also demonstrated modulation of PAC during movement in patients with a non-movement disorder (epilepsy), suggesting an important role of PAC in the dynamics of motor control [133, 203]. We obtained further insight into the role of β - γ PAC in motor control from our detailed analysis of its dynamic modulation across a movement cycle (dynPAC). When controls performed the pressing task, PAC exhibited a brief peak followed by a decline during the initial pressing phase and a subsequent rebound while the index finger still maintained a constant press. Of note, during the initial releasing phase, dynPAC showed a similar pattern (decrease following a brief peak). Moreover, in the slow tapping task, a similar pattern with a brief peak followed by a decrease in PAC was present around the onset of the finger extension, followed by a rebound. These findings in healthy controls suggest that the PAC decrease is not merely associated with initiating a movement. Rather, there appears to be a characteristic PAC motif (brief peak – decrease – rebound) that signals a change in movement states. This phenomenon resembles the preparatory neuronal activity in the dynamical systems theory of motor control [206]. According to this theory, preparatory activity brings the dynamical state of the neuronal population through state-space rotations to an initial value. This process, characterized by brief cortical oscillatory activity [226], ensures that muscle activity can be generated efficiently for all types of movements [206, 226]. If dynPAC reflects normal preparatory activity, then it is perhaps not surprising that movement-related PAC was found to be similar in patients with PD and with essential tremor [187], especially in the absence of kinematic differences between both patient groups.

In addition, it has long been known that voluntary motor activity is also accompanied by event-related β -power desynchronization in the cortex [204, 227, 228]. However, we found that the magnitude of PAC was not related to the absolute β power in either the resting state or in the movement states of our study, a finding supported by previous studies [137, 140]. Likewise, during movement, the dynamics of PAC were not consistently associated with the β power change shown in our study and the previous literature [187]. Therefore, this finding excludes the possibility that the dynamic modulation of β - γ PAC during repetitive voluntary movements merely reflects general β -power dynamics. The couplings encode an essential component of the motor command that is different from the mechanism underlying event-related β -power

desynchronization. Because β activities in the motor cortex are considered to reflect intracortical inhibition [229, 230], the incomplete correlations between β activities and the couplings may also support the implication that β - γ dynPAC reflects a population dynamic characteristic rather than a defective single cellular physiological mechanism such as neuronal inhibition [231], as mentioned in the previous paragraph.

8.2.6 Abnormal dynamics of cortical β - γ PAC in PD

Interestingly, we found that dynPAC was abnormal in slow tapping in PD patients. While PAC values attained similar levels before initiating the tapping movements, the subsequent decrease was smaller, and the later rebound less marked than in controls. By contrast, during pressing, dynPAC modulation was similar in patients and controls. Our findings appear to be the first to report that abnormal PAC during movement is associated with concurrent abnormal motor performance in PD. If our hypothesis on dynPAC as a marker for a preparatory movement state is accepted (see section 8.2.5), PD patients may be subjected to a defective evolution of neuronal population dynamics from the preparatory state to overt movement generation. While PAC would be a necessary physiological phenomenon during movement preparation, its persistence into the unfolding movement would interfere with the proper execution of that movement. Although abnormal dynPAC modulation was associated with slowed muscle recruitment during the onset of slow tapping, the finding that PAC change did not correlate with the magnitude of the EMG slope suggests a complex and non-linear relationship between dynPAC and the build-up process of corticospinal neuronal activity. Interestingly, studies probing cortical physiology in the preparatory phase of voluntary movements have provided similar evidence to suggest that bradykinesia does not result from a single deficient physiological mechanism such as the ability to release from ongoing inhibition [232, 233], but rather reflects a more complex circuit abnormality [234]. Notably, preparatory activity in the dynamical systems theory of motor control is sensitive to timing events supporting motor transitions [235] but does not reflect specific movement features (e.g., direction, force, velocity), nor does it simply represent the release from inhibition of a motor program [236].

We also showed that the PAC change was significantly correlated with spectral power change at the β frequency band around tapping movement onset, characterized by the abnormal EMG recruitment. Although this correlation was not specific to slow tapping onset, this finding suggests that β activity could at certain critical times have pathophysiological significance for dynPAC. One could speculate that higher frequency or duration of β bursts in STN [237] around the onset of bradykinetic movements allows more time to stabilize PAC abnormally.

However, as there was no relationship with the absolute β power, the significance of this finding is still uncertain.

8.2.7 Functional role of abnormal PAC in the pathophysiology of PD

Because the above-mentioned results showed the absence of a relationship between motor impairment of PD and state-related PAC during movement, but were associated with abnormal PAC dynamics during movement execution of slow tapping tasks, two following questions may arise. 1) What is the explanation of the exaggerated PAC at rest and its association with Parkinsonian motor impairment reported in previous literature [139, 140] and also demonstrated in our study? 2) What could be the possible mechanisms underlying the functional role of the two abnormal signatures? We provide two hypotheses in this thesis. One possibility would be that PAC at rest, or any state-related PAC, is not mechanistically related to the dynPAC abnormality found during slow tapping. It has been reported that levodopa treatment for PD patients suppressed the magnitude of abnormal PAC at rest and attenuated bradykinesia evaluated by MDS-UPDRS scores, suggesting that PAC at rest may reflect the background dopamine level [139]. The background dopamine level is often considered the sum of tonic and phasic dopamine activities. It is generally accepted that voluntary movements are controlled by both tonic dopamine that releases and activates relatively slowly from seconds to minutes as well as phasic dopamine modulation that varies on a sub-second time scale [238]. Therefore, it is possible that the state-related PAC modulation and PAC dynamics during movement transitions could map onto tonic and phasic dopamine activities [231, 239], respectively, a mechanism that may be tied to deficits in motivation and the invigoration of movements [94, 231]. This hypothesis linking dopamine activities and cortical PAC should be tested in future animal experiments.

Although we cannot rule out the former hypothesis, we could think of an alternative hypothesis based on the findings from abnormal PAC dynamics. If both PAC phenomena are based on a common mechanism, they could reflect processes of movement preparation. In this scenario, on the one hand, the increase in dynPAC would indicate a preparatory state during movement dynamics, and its reduced attenuation at movement transitions would indicate a spillover of the preparatory state into the unfolding movement. On the other hand, enhancement of PAC at rest could reflect the abnormal generation of brief cortical states resembling preparatory population activity in the absence of an intention to move. Researchers have suggested that β activity is composed of physiologically short-lived phasic bursts in the brain [240], implying that β - γ PAC could be formed as spontaneous brief couplings in continuous recordings. Thus, the

abnormal preparatory activities could be related to an increased frequency of occurrence of spontaneous brief stretches of coupling. In this way, both the enhanced resting PAC and the reduced dynPAC modulation could be caused by the dysfunction of a single (subcortical) mechanism that controls or regulates the generation of cross-frequency couplings in cortical microcircuits. However, in the absence of direct evidence, the nature of the link between abnormally enhanced PAC at rest and abnormal modulation of dynPAC remains a topic for future investigations.

8.3 Limitations and outlook

This thesis reports the results of a detailed investigation on the characteristics of cortical PAC via non-invasive recording techniques, accumulating evidence on the role of β - γ PAC on the pathophysiology of PD. However, our investigation has also brought up several concerns and questions that need to be answered in future studies.

First, the participants had to be able to complete multiple types of movements in this study. Therefore, recordings were done in patients with early to moderate stages of PD. Moreover, to avoid the interference of muscle activities in the resting state recordings, patients with marked resting tremor were excluded from recruitment. Therefore, it remains unclear how generalizable our findings are to tremulous or more severe PD phenotypes. Greater variability of clinical severity and a larger sample of PD patients may allow for even more robust assessments of the nature of the correlation between pathological synchronization and individual items of the clinical phenotype. Besides, while the current thesis has focused on the role of PAC in the motor symptoms of PD, we also found the enhancement of PAC in DLPFC of PD patients, suggesting that abnormal PAC may also be relevant to cognitive dysfunctions outside of the motor domain. In future experimental designs, data from clinical cognitive assessments will also need to be collected to allow for a more complete evaluation of the role of PAC in PD.

Second, we still lack information regarding the effects of treatment interventions, such as dopamine replacement therapy and DBS, on the abnormal magnitude of PAC or the abnormal PAC modulation. This information is essential because a reliable biomarker should not only distinguish PD from the normal state and monitor the disease progression, but also measure the success of therapeutic intervention. Investigating the effects of different treatments on the symptoms of PD and the alteration of the abnormal oscillatory activities could, in turn, reveal the association between abnormal PAC with other diverse subcortical or cortical manifestations

of PD pathology. This information may lead to a more comprehensive understanding of the mechanism of PD pathophysiology. It has been reported that levodopa reduced exaggerated PAC at rest in PD patients, a finding that indicates the level of dopamine in the brain is associated with the magnitude of PAC at rest [139]. Similar results have also been obtained by applying STN DBS, suggesting that cortical PAC could be altered by changing activities in the STN through BGTC circuits [140]. Moreover, NIBS treatments could also be used to address the role of oscillatory activities in motor symptoms of PD by entraining or intervening the cortical rhythms directly [241]. However, it is still unknown whether the spatial organization of the abnormal PAC would also change due to different treatment strategies. In future studies, we will continue to investigate the spatiotemporal characteristics of PAC with different treatment therapies.

Besides, there are some limitations in the experimental design. Although self-paced repetitive movements may be considered relatively elementary movements, and although they reflected the motor impairment of PD in our study, they represent only a small subset of the daily movement repertoire which also includes cued and goal-directed behaviour, proximal movements, and locomotion. Different mechanisms may underlie performance impairment in other types of movement. Therefore, future studies need to explore abnormal cross-frequency coupling more comprehensively during more variable motor behaviours. The resolution of the analysis of PAC dynamics across the movement cycle is constrained by the minimum number of oscillatory cycles required to compute PAC, a factor that, in turn, depends on the involved oscillation frequencies, especially on the phase frequencies. Therefore, the current methods computing the time-resolved PAC cannot address the dynamic modulation of PAC during fast repetitive movements, which needs further investigation by using the new algorithms for computing PAC. Moreover, although we compared the state-related PAC under different conditions, the settings of the movement tasks limited the possibility to investigate the continuous recordings from the resting state to the peri-movement state in each movement cycle, which is also an essential question because transitions between different active states are equally important parts of voluntary movement behaviour. In addition, separation of the movement cycles into discrete periods may not apply to everyday behaviour, which in many instances is more appropriately conceived of as a continuous action with no discrete transitions. It remains to be studied whether concepts derived from analysing movement periods translate into the control of continuous movements.

Moreover, as also introduced in section 8.2.7, in future studies researchers could help to link

the abnormally enhanced PAC at rest and abnormal modulation of dynPAC by developing a method to estimate the frequency of occurrence of brief periods of cross-frequency coupling in a given period. This issue remains unresolved because the criteria for determining the presence of the brief couplings are unclear. One possible direction would be to set a magnitude threshold to decide whether the computed value should be considered a valid coupling, as introduced by estimating the frequencies of β bursts [106]. However, the validity of this method is compromised by the fact that the results are strongly dependent on the definition of the threshold; hence, changing the threshold may yield different occurrence frequency values. Therefore, future efforts should be made to develop a robust measurement method that allows the evaluation of brief coupled features.

Last but not least, although PAC was derived from EEG signals that reflect cortical neural activities, the present findings do not allow us to distinguish between a cortical or a subcortical origin of abnormal cross-frequency coupling in cortical microcircuits. The issue is likely to be solved by conducting experiments with simultaneous recordings from scalp EEG and LFP in sub-cortical regions. For example, researchers could record simultaneously EEG signals and LFP activities in the STN of PD patients who have been implanted with an appropriate DBS device [118]. Besides, modelling work could also help provide in-depth evidence about the origin of cortical activities by simulating the characteristics and connectivity of neural populations of the BGTC network [242].

8.4 Conclusion

In this thesis, we have investigated comprehensively the spatiotemporal characteristics of β -broadband γ PAC derived from non-invasive EEG recordings. Source localization of PAC elucidated the spatial origins of exaggerated PAC of PD patients, which not only include PMC and M1, as previously known, but also DLPFC and SS. The existence of enhanced PAC in more extended areas suggests that the generation of abnormal coupling does not merely come about through the cortical-subthalamic ‘hyperdirect’ pathway, but might also include other BGTC circuits and cortical-cortical connections. The study of abnormal PAC at the mesoscopic level further revealed its potential generation mechanisms, suggesting that β and γ activities involved in the abnormal PAC originate from distinct oscillators. The results highlight the crucial role of abnormal PAC generated from spatially separated sub-networks in motor control regions, implying that breaking up the lateral coupling between neural circuits may be a more promising treatment target of PD than approaches that attenuate abnormally synchronized neuronal oscillations. Furthermore, the investigation of PAC during movement provides a

novel insight into the functional role of PAC in the pathophysiology of PD. The findings regarding the dynamics of PAC during movement transitions present evidence that PAC may serve a role in normal motor behaviour, where it appears to indicate a preparatory state of the motor system. The association of abnormal PAC dynamics with bradykinesia is compatible with the hypothesis that deficient regulation of PAC is involved causally in the pathophysiology of Parkinsonian motor impairment. Taken together, the findings from the work in this thesis have helped us understand the relationship between an EEG oscillatory signature and the pathophysiology of PD, indicating that β -broadband γ PAC in the cortex is not a simple phenotype of PD, but rather is involved in pathological alterations of the BGTC functional system. These results could support further the development of guidelines for selecting targets and parameters for brain stimulation through the utility of cortical PAC via non-invasive recording techniques, laying a foundation for future research on the treatment of PD.

Summary of the dissertation

Dissertation for the award of the academic degree of Dr. rer. nat.

Title: β - γ phase-amplitude coupling derived from non-invasive electroencephalogram – insight into the pathophysiology of Parkinson’s disease

submitted by: Ruxue Gong

prepared at/in: Dept. Neurology, Leipzig University Medical Center
Max-Planck Institute of Human Cognitive and Brain Sciences

supervised by: Prof. Dr. Joseph Classen, Prof. Dr. Thomas Knösche

09.2021, Leipzig

Introduction

Parkinson’s disease (PD) is a neurodegenerative disorder whose pathological hallmark is the loss of dopamine neurons in the *substantia nigra pars compacta* [1]. Physiologically, the loss of nigral dopaminergic neurons is associated with disrupted signals of the basal ganglia-thalamocortical (BGTC) circuits [211]. To better understand the pathophysiology of PD and to develop more efficient brain state-dependent therapies of Parkinsonian symptoms by interfering with the BGTC circuits, researchers have undertaken considerable work to identify reliable electrophysiological biomarkers for PD.

Exaggerated coupling between the phase of β (13-30 Hz) activities and the amplitude of γ (50-150 Hz) activities is now widely recognized as a pathophysiological biomarker of PD. This abnormal phase-amplitude coupling (PAC) has been detected from recordings in the subthalamic nucleus (STN) and the motor cortex [118, 134]. It has also been shown that the enhanced PAC can be suppressed by deep brain stimulation of the STN or by dopamine replacement therapy, which ameliorates motor impairment of PD patients [139, 140].

Importantly, enhanced cortical PAC in PD patients can even be detected via non-invasive electroencephalography (EEG) recordings [137, 139], suggesting that it might potentially be a non-invasive biomarker for diagnosing and treating PD.

In order to establish β - γ PAC as a reliable surface biomarker of PD, we need to understand its role in the pathophysiology of PD and its relationship to motor symptoms. Therefore, in this thesis we aim to investigate comprehensively the spatiotemporal characteristics of β - γ cortical PAC in the resting state and its dynamics during voluntary movements associated with the motor symptoms of PD patients.

Experiments and results

To address the research questions, we conducted an experiment by using a high-resolution 64-channel EEG system to record signals from 19 PD patients and 20 age- and sex-matched healthy subjects during a 5-min resting state and several types of repetitive voluntary finger movements. The motor tasks consisted of repetitive index finger pressing as well as repetitive index finger tapping performed at the participants' comfortable pace ('slow tapping') or their fastest pace ('fast tapping'). We then applied advanced source analysis to localize more precisely the signals in distinct regions of individual brains. To differentiate further the fine spatial structure of the involved oscillators within each region, we employed source-space independent component analysis (ICA) [173]. ICA provides a unique spatial signature for each separated sub-network. These techniques helped us investigate the spatiotemporal properties of regional PAC in the resting state and during movements.

We found that β - γ PAC abnormalities of PD patients could be extracted from source-located EEG signals, although they were not detectable in EEG sensor signals in this study. More interestingly, the EEG source signals provided information about the spatial location of enhanced PAC in the cortex of patients, compared with healthy controls. We demonstrated that cortical PAC at rest of PD patients was enhanced in more regions than previously known [118], namely in the dorsolateral prefrontal cortex (DLPFC), the premotor cortex (PMC), the primary motor cortex (M1), the primary somatosensory cortex (Brodmann area 3 [BA3]), and primary somatosensory complex (Brodmann area 1&2 [BA1&2]). The PAC difference between patients and controls was more pronounced in the hemisphere contralateral to the clinically more affected side.

Next, we were interested in the potential generation mechanisms of exaggerated cortical PAC at rest. We found that β and γ signals involved in generating abnormal PAC were not strictly

phase-phase coupled, ruling out that it merely reflects the abnormal activity of a single non-sinusoidal oscillator in a recurrent network. The findings further demonstrated that the PAC differences between patients and controls were detected from couplings between β and γ activities from both identical ICA components and different ICA components (originating from distinct spatial locations). More importantly, only the latter were correlated with clinical motor severity as indexed by scores of the Movement Disorders Society Unified Parkinson's Disease Rating Scale III (MDS-UPDRS III). We found correlations between clinical scores of Parkinsonian motor symptoms and such inter-component couplings in PMC, M1, and somatosensory areas (SS, including BA3 and BA1&2), but not in DLPFC, indicating the pathophysiological importance of inter-subnetwork coupling specifically in the motor domain. Furthermore, when looking more deeply into the inter-subnetwork couplings, we found more inequivalent contributions of ICA components to PAC in patients than in controls. Interestingly, this inequivalent contribution of components was associated with a reduced similarity between the spatial distribution of sources generating PAC-involved β activities and γ activities. Our findings suggest that PAC abnormalities in PD at rest may not only reflect hyper-synchronous activity; they may also be associated with the abnormal coupling between spatially separated neural networks.

The findings from the resting-state data suggested that the enhanced β - γ cortical PAC at rest plays an essential role in the pathophysiology of PD. However, PAC abnormalities at rest cannot reveal direct relationships with motor impairment, because patients do not manifest movement-related symptoms at rest. Therefore, in the subsequent study, we investigated the characteristics of movement-related PAC during different types of repetitive movement tasks. Some of these tasks were chosen to specifically reflect the cardinal motor signs as revealed by clinical examination.

Behaviourally, PD patients performed as healthy controls when performing repetitive pressing-releasing actions, but they showed abnormal behaviour during repetitive tapping. Specifically, compared with healthy controls, the abnormal behaviour of PD patients was mainly reflected by deficits in recruiting the first dorsal interosseus muscle for finger extension (reduced electromyographic slope) during slow tapping, and by a slower tapping rate when subjects tapped at their fastest speed, reflecting the general slowing of movement ('bradykinesia') in PD patients. In addition, when tapping at their fastest speed, PD patients also presented a decrement in tapping amplitude.

We then evaluated the movement-related PAC in the four motor regions (PMC, M1, BA3, and

BA1&2), all of which have shown enhanced PAC at rest. First, we compared the state-related PAC between patients and controls by averaging the PAC values across the time series. In addition to the enhancement of PAC at rest, we found that patients also showed enhanced PAC in the pressing task, in which patients performed normally compared to controls. On the other hand, during slow and fast tapping, when the patients did show performance deficits, there were no differences in state-related PAC between patients and controls. These findings suggest that the magnitude of state-related PAC during the movement has no direct relationship with the motor impairment severity of PD. Subsequently, we examined the transient dynamics of PAC during movement. In the movement cycle of repetitive pressing, dynamic PAC decreased during the pressing after a brief peak in the pre-onset period. A strikingly similar modulation pattern of PAC rise and decay was observed around the offset of pressing and around the onset of finger extension in the slow tapping task, suggesting that the modulation of PAC is associated with the transitions between different movement states. Moreover, statistical tests showed that patients presented a similar modulation pattern with controls in the pressing task, but a reduced PAC modulation across movement transients in the slow tapping task (abnormal movement execution).

Discussion

The findings presented in the thesis have revealed comprehensively the characteristics of PAC derived from source localized non-invasive EEG recordings in PD patients. The exaggerated PAC at rest was localized not only in the motor cortex, but also in DLPFC and SS, suggesting that abnormal PAC at rest is not exclusively generated by the ‘hyperdirect’ tract of the BGTC circuit, but also involves other BGTC or cortical-cortical connections. Besides, we have provided evidence that β and γ activities involved in the generation of exaggerated PAC originate from spatially distinct sub-networks. The correlation between enhanced inter-subnetwork coupling and motor impairment severity implies that breaking up the lateral coupling between neural circuits may be a promising treatment target for PD. Furthermore, the findings of the dynamics of movement-related PAC suggest a physiological role in encoding motor commands, in that the increase in PAC might be related to preparatory activities before the change of movement states. With this hypothesis, which is inspired by the dynamical systems theory of motor control [206], we suggest that enhanced PAC at rest indicates abnormal preparatory activities in the absence of an intention to move. In addition, the flattened PAC modulation during abnormally executed repetitive slow tapping might indicate dysfunctional evolution of neuronal population dynamics from the preparatory state to movement generation in PD. In summary, in this thesis we have demonstrated 1) the spatial

origins of exaggerated β -broadband γ PAC in the cortex of PD patients at rest; 2) the possible mechanisms of the exaggerated PAC in the cortex of PD patients; 3) the physiological significance of movement-related PAC dynamics and its relationship with motor impairment of PD. This work has advanced our understanding of the functional relationship between this non-invasive electrophysiological marker and the pathophysiology of PD, and these findings could guide the development of future brain state-dependent neurostimulation therapies for PD.

Zusammenfassung der Arbeit

Dissertation zur Erlangung des akademischen Grades Dr. rer. nat.

Titel: β - γ Phasen-Amplituden Kopplung im nicht-invasiv abgeleiteten Elektroenzephalogramm – Einblick in die Pathophysiologie der Idiopathischen Parkinson-Syndroms

eingereicht von: Ruxue Gong

angefertigt an / in: Klinik und Poliklinik für Neurologie, Universitätsklinikum Leipzig
Max - Planck - Institut für Kognitions- und Neurowissenschaften

betreut von: Prof. Dr. Joseph Claßen, Prof. Dr. Thomas Knösche

09.2021, Leipzig

Einführung

Das idiopathische Parkinsonsyndrom (IPS, engl., Parkinson's disease, PD) ist eine neurodegenerative Erkrankung, deren pathologisches Merkmal der Verlust von dopaminergen Neuronen in der *substantia nigra pars compacta* ist [1]. Physiologisch gesehen ist der Verlust nigraler dopaminergener Neuronen mit einer Unterbrechung der gesamten Basalganglien-thalamo-kortikalen (engl., basal ganglia-thalamocortical, BGTC) Schleifen verbunden [211]. Um die Pathophysiologie des IPS besser zu verstehen und wirksamere hirnzustandsabhängige Therapien für die Parkinson-Symptome durch Eingriffe in die BGTC-Schleifen zu entwickeln, haben Forscher erhebliche Anstrengungen unternommen, um zuverlässige elektrophysiologische Biomarker für das IPS zu identifizieren.

Die gesteigerte Kopplung zwischen der Phase der β (13-30 Hz)-Aktivitäten und der Amplitude der γ (50-150 Hz)-Aktivitäten ist inzwischen als pathophysiologischer Biomarker für das IPS anerkannt. Diese pathologische Phasen-Amplituden Kopplung (engl., phase-amplitude

coupling, PAC) wurde bei Ableitungen der elektrischen Aktivität des Gehirns im Ncl. subthalamicus (STN) und im motorischen Kortex festgestellt [118, 134]. Eine erhöhte PAC kann durch eine tiefe Hirnstimulation des STN oder die Gabe von dopaminergem Medikation unterdrückt werden, was mit einer Verbesserung der motorischen Symptome bei Parkinsonpatienten einhergeht [139, 140]. Eine erhöhte kortikale PAC bei Parkinsonpatienten kann sogar durch nicht-invasive Elektroenzephalographie (EEG) nachgewiesen werden [137, 139], was darauf hindeutet, dass man sie möglicherweise als einen nicht-invasiven Biomarker für die Diagnose und Behandlung des IPS betrachten könnte.

Um die β - γ PAC als zuverlässigen nicht-invasiven Biomarker für das IPS zu etablieren, müssen wir ihre Rolle in der Pathophysiologie des IPS und ihren Bezug zu motorischen Symptomen verstehen. Daher zielt diese Arbeit darauf ab, die raum-zeitlichen Charakteristika der kortikalen β - γ PAC in Ruhe und ihre Dynamik während der Ausführung von willkürlichen Bewegungen in Verbindung mit motorischen Symptomen bei Parkinsonpatienten umfassend zu untersuchen.

Experimente und Ergebnisse

Wir führten ein Experiment durch, bei dem wir mit Hilfe von einem hochauflösenden 64-Kanal EEG-System die Signale von 19 Patienten mit IPS und 20 alters- und geschlechtsgleichen gesunden Probanden während eines 5-minütigen Ruhezustands und verschiedener Arten von Fingerbewegungen aufzeichneten. Die Bewegungsaufgaben bestanden aus wiederholtem Drücken mit dem Zeigefinger und wiederholtem Tippen mit dem Zeigefinger mit entweder einer für die Versuchsteilnehmer angenehmen Geschwindigkeit („langsam tippen“) oder mit der jeweils schnellstmöglichen Geschwindigkeit („schnelles tippen“). Anschließend haben wir eine Quellenanalyse durchgeführt, um die Signale in den einzelnen Hirnregionen genauer zu lokalisieren. Um die feine räumliche Struktur der beteiligten Oszillatoren innerhalb jeder Region weiter zu differenzieren, verwendeten wir die unabhängige Komponentenanalyse (engl., independent component analysis, ICA) im Quellenabstand [173]. Die ICA ermöglicht eine eindeutige räumliche Signatur für jedes getrennte Subnetz zu ermitteln. Mit Hilfe dieser Techniken konnten wir die raum-zeitlichen Eigenschaften der regionalen PAC in Ruhe und bei Bewegungen untersuchen.

Wir konnten zeigen, dass bei Parkinsonpatienten β - γ PAC Abweichungen aus quellenlokalisierten EEG-Signalen extrahiert werden konnten, wobei sie in dieser Studie nicht in EEG-Sensorsignalen nachweisbar waren. Die EEG-Quellensignale lieferten Informationen über die räumliche Lage der gesteigerten PAC im Kortex der Patienten im Vergleich zu den gesunden Kontrollpersonen. Die kortikale PAC war bei den Parkinsonpatienten in Ruhe in

mehr Hirnregionen erhöht als bisher bekannt war [118], nämlich im dorsolateralen präfrontalen Kortex (DLPFC), im prämotorischen Kortex (PMC), im primären motorischen Kortex (M1), im primären somatosensorischen Kortex (Broadman Area 3 [BA3]) und im primären somatosensorischen Komplex (Broadman Area 1&2 [BA1&2]). Der PAC-Unterschied zwischen Patienten und Kontrollpersonen war in der zur klinisch stärker betroffenen Seite kontralateralen Hemisphäre stärker ausgeprägt.

Als Nächstes interessierten wir uns für die möglichen Entstehungsmechanismen der gesteigerten kortikalen PAC in Ruhe. Wir fanden heraus, dass die β - und γ -Signale, die an der Erzeugung der abnormalen PAC beteiligt sind, nicht streng Phase-Phase-gekoppelt sind, was die Möglichkeit ausschließt, dass sie lediglich die pathologische Aktivität eines einzelnen nicht-sinusförmigen Oszillators in einem rekurrenten Netzwerk widerspiegeln. Die Ergebnisse zeigten auch, dass die PAC-Unterschiede zwischen Patienten und Kontrollen durch Kopplungen zwischen β - und γ -Aktivitäten sowohl von identischen ICA-Komponenten als auch von unterschiedlichen ICA-Komponenten (die von verschiedenen räumlichen Orten stammen) nachgewiesen werden konnten. Wichtig ist, dass nur die Letzteren mit dem klinischen motorischen Schweregrad korrelierten, der durch den Score der Movement Disorders Society Unified Parkinson's Disease Rating Scale III (MDS-UPDRS III) festgestellt wurde. Wir fanden Korrelationen zwischen klinischen Scores von motorischen Parkinson-Symptomen und solchen Inter-Komponenten-Kopplungen im PMC, im M1 und im somatosensorischen Regionen (SS, einschließlich BA3 und BA1&2), aber nicht im DLPFC, was auf die pathophysiologische Bedeutung der Kopplung zwischen Teil-Netzwerken speziell im motorischen Bereich hinweist. Bei einer genaueren Betrachtung der Kopplungen zwischen den Teil-Netzwerken fanden wir außerdem ungleichartige Beiträge der ICA-Komponenten zur PAC bei Patienten im Vergleich zu den Kontrollpersonen. Interessanterweise war die Ungleichartigkeit des Beitrags der ICA-Komponenten mit einer geringeren Ähnlichkeit zwischen der räumlichen Verteilung der Quellen verbunden, die die an der PAC beteiligten β -Aktivitäten und γ -Aktivitäten erzeugen. Unsere Ergebnisse deuten darauf hin, dass die PAC-Abweichungen beim IPS in Ruhe nicht nur eine hypersynchrone Aktivität widerspiegeln, sondern auch mit einer abnormalen Kopplung zwischen räumlich getrennten neuronalen Netzwerken verbunden sind.

Die in Ruhe vorhandene Veränderung der PAC bei Parkinsonpatienten muss nicht notwendigerweise einen direkten Zusammenhang mit motorischen Beeinträchtigungen aufweisen, da in Ruhe definitionsgemäß keine bewegungsbezogenen Störungen vorliegen.

Daher untersuchten wir anschließend die Eigenschaften der bewegungsbezogenen PAC bei verschiedenen Arten von sich wiederholenden Bewegungsaufgaben. Einige dieser Aufgaben wurden so ausgewählt, dass sie speziell die motorischen Kardinalsymptome widerspiegeln, die bei der klinischen Untersuchung festgestellt wurden.

Verhaltensmäßig zeigten Parkinsonpatienten die gleichen Leistungen wie gesunde Kontrollpersonen, wenn sie wiederholte Druck- und Loslass-Aktionen durchführten, aber sie zeigten ein anderes Verhalten beim wiederholten Tippen. Im Vergleich zu gesunden Kontrollpersonen zeigten die Parkinsonpatienten während des langsamen Tippens Defizite bei der Rekrutierung des M. interosseus dorsalis I für die Fingerextension (reduzierter elektromyografischer Anstieg), und eine langsamere Bewegungsgeschwindigkeit, die erreicht wurde, wenn die Parkinsonpatienten mit ihrer schnellsten Geschwindigkeit tippten, was für eine allgemeine Verlangsamung der Bewegung („Bradykinesie“) bei Parkinsonpatienten charakteristisch ist. Darüber hinaus zeigten Parkinsonpatienten eine Abnahme der Amplitude der Fingerbewegung, wenn sie mit ihrer schnellsten Geschwindigkeit tippten.

Anschließend untersuchten wir die bewegungsbezogene PAC in den vier motorische Regionen (PMC, M1, BA3, und BA1&2), die in Ruhe eine erhöhte PAC aufwiesen. Zunächst verglichen wir die PAC zwischen Patienten und Kontrollpersonen, indem wir die PAC-Werte über die Zeitreihen hinweg gemittelt haben. Zusätzlich zur Verstärkung der PAC in Ruhe zeigten die Patienten auch eine erhöhte PAC während der Pressaufgabe, in welcher keine Verhaltensunterschiede vorhanden waren. Andererseits gab es beim langsamen und schnellen Tippen, trotz vorhandener Leistungsunterschiede, keine Abweichungen in der zustandsbezogenen PAC zwischen Parkinsonpatienten und Kontrollpersonen. Diese Ergebnisse legen nahe, dass die Amplitude der zustandsbezogenen PAC während der Bewegung nicht direkt mit dem Schweregrad der motorischen Beeinträchtigung bei Parkinsonpatienten zusammenhängt. Anschließend untersuchten wir die Dynamik von PAC während der Bewegung. Im Bewegungszyklus des wiederholten Drückens nahm die dynamische PAC während des Drückens nach einem kurzen Anstieg in der pre-onset Periode ab. Ein auffallend ähnliches Modulationsmuster des PAC-Anstiegs und -Rückgangs wurde um das Offset des Drückens und um den Beginn der Fingerstreckung bei der langsamen Tippaufgabe beobachtet, was darauf hindeutet, dass die Modulation der PAC mit Übergängen zwischen verschiedenen Bewegungszuständen verbunden ist. Darüber hinaus zeigten die Parkinsonpatienten bei der Drückaufgabe ein ähnliches Modulationsmuster wie die Kontrollpersonen, aber eine reduzierte PAC Modulation über die Bewegungstransienten bei

der langsamen Tippaufgabe (pathologische Bewegungsausführung).

Diskussion

In dieser Arbeit werden die Eigenschaften von PAC, die aus dem nicht-invasiven EEG bei Patienten mit idiopathischen Parkinsonsyndrom abgeleitet wurden, umfassend dargestellt. Die erhöhte PAC in Ruhe war nicht nur im motorischen Kortex, sondern auch im DLPFC und SS lokalisiert, was darauf hindeutet, dass die veränderte PAC in Ruhe nicht ausschließlich durch den ‚hyperdirekten‘ Trakt der BGTC-Schleife erzeugt wird, sondern auch andere BGTC- oder kortikale Verbindungen involviert sind. Darüber hinaus haben wir gezeigt, dass die β - und γ -Aktivitäten, die an der erhöhten PAC beteiligt sind, aus räumlich getrennten Teil-Netzen stammen. Die Korrelation zwischen der verstärkten Kopplung zwischen Teil-Netzen und dem Schweregrad der motorischen Störung legt nahe, dass die Unterbrechung der lateralen Kopplung zwischen neuronalen Schaltkreisen ein vielversprechendes Target für die Behandlung der Parkinsonerkrankung sein könnte. Darüber hinaus deuteten die Ergebnisse der bewegungsbezogenen PAC-Dynamik auf eine physiologische Rolle bei der Kodierung motorischer Befehle hin, da der Anstieg der PAC mit vorbereitenden Aktivitäten vor dem Wechsel der Bewegungszustände zusammenhängen könnte. Nach dieser Hypothese, die von der Theorie dynamischer Systeme der motorischen Kontrolle inspiriert ist [206], nehmen wir an, dass die erhöhte PAC in Ruhe auf die krankhafte Vorbereitung von Aktivitäten hinweisen könnte, wenn keine Absicht zur Bewegung besteht. Darüber hinaus könnte die abgeflachte PAC-Modulation während des langsamer ausgeführten repetitiven Tippens auf eine dysfunktionale Entwicklung der neuronalen Populationsdynamik vom Vorbereitungs- zum Bewegungszustand bei Parkinsonpatienten hinweisen. Zusammenfassend zeigte diese Arbeit 1) die räumlichen Ursprünge der gesteigerten β -Breitband γ PAC im Kortex von Parkinsonpatienten in Ruhe; 2) die möglichen Mechanismen der gesteigerten PAC im Kortex von Parkinsonpatienten; 3) die physiologische Bedeutung der bewegungsbezogenen PAC-Dynamik und ihre Beziehung zu motorischen Symptomen bei Patienten mit idiopathischen Parkinsonsyndrom. Diese Arbeit trägt zu unserem Verständnis der funktionellen Beziehung zwischen diesem nicht-invasiven elektrophysiologischen Marker und der Pathophysiologie von Parkinsonpatienten bei und könnte für die Entwicklung von künftigen hirnzustandsabhängigen Neurostimulationstherapien Bedeutung haben.

Bibliography

- [1]. Balestrino, R. and A.H. Schapira, Parkinson disease. *European journal of neurology*, 2020. **27**(1): p. 27-42.
- [2]. Poewe, W., et al., Parkinson disease. *Nature reviews Disease primers*, 2017. **3**(1): p. 1-21.
- [3]. Van Den Eeden, S.K., et al., Incidence of Parkinson's disease: variation by age, gender, and race/ethnicity. *American journal of epidemiology*, 2003. **157**(11): p. 1015-1022.
- [4]. Gillies, G.E., et al., Sex differences in Parkinson's disease. *Frontiers in neuroendocrinology*, 2014. **35**(3): p. 370-384.
- [5]. Klein, C. and A. Westenberger, Genetics of Parkinson's disease. *Cold Spring Harbor perspectives in medicine*, 2012. **2**(1): p. a008888.
- [6]. Di Monte, D.A., M. Lavasani, and A.B. Manning-Bog, Environmental factors in Parkinson's disease. *Neurotoxicology*, 2002. **23**(4-5): p. 487-502.
- [7]. Ruiz, P.J.G., M. Catalan, and J.F. Carril, Initial motor symptoms of Parkinson disease. *The neurologist*, 2011. **17**: p. S18-S20.
- [8]. Moustafa, A.A., et al., Motor symptoms in Parkinson's disease: A unified framework. *Neuroscience & Biobehavioral Reviews*, 2016. **68**: p. 727-740.
- [9]. Sveinbjornsdottir, S., The clinical symptoms of Parkinson's disease. *Journal of neurochemistry*, 2016. **139**: p. 318-324.
- [10]. Xia, R. and Z.-H. Mao, Progression of motor symptoms in Parkinson's disease. *Neuroscience bulletin*, 2012. **28**(1): p. 39-48.
- [11]. Chaudhuri, K.R., L. Yates, and P. Martinez-Martin, The non-motor symptom complex of Parkinson's disease: a comprehensive assessment is essential. *Current neurology and neuroscience reports*, 2005. **5**(4): p. 275-283.
- [12]. Schapira, A.H., K.R. Chaudhuri, and P. Jenner, Non-motor features of Parkinson disease. *Nature Reviews Neuroscience*, 2017. **18**(7): p. 435.
- [13]. Postuma, R.B., et al., Identifying prodromal Parkinson's disease: pre-motor disorders in Parkinson's disease. *Movement Disorders*, 2012. **27**(5): p. 617-626.
- [14]. Goetz, C.G., et al., Movement Disorder Society-sponsored revision of the Unified Parkinson's Disease Rating Scale (MDS-UPDRS): scale presentation and clinimetric testing results. *Movement disorders: official journal of the Movement Disorder Society*, 2008. **23**(15): p. 2129-2170.
- [15]. Tolosa, E., G. Wenning, and W. Poewe, The diagnosis of Parkinson's disease. *The Lancet Neurology*, 2006. **5**(1): p. 75-86.
- [16]. Graybiel, A.M., The basal ganglia. *Current biology*, 2000. **10**(14): p. R509-R511.
- [17]. Lanciego, J.L., N. Luquin, and J.A. Obeso, Functional neuroanatomy of the basal ganglia. *Cold Spring Harbor perspectives in medicine*, 2012. **2**(12): p. a009621.
- [18]. Blandini, F., et al., Functional changes of the basal ganglia circuitry in Parkinson's disease. *Progress in neurobiology*, 2000. **62**(1): p. 63-88.
- [19]. Obeso, J.A., et al., The expanding universe of disorders of the basal ganglia. *The Lancet*, 2014. **384**(9942): p. 523-531.
- [20]. Mink, J.W., The basal ganglia: focused selection and inhibition of competing motor programs. *Progress in neurobiology*, 1996. **50**(4): p. 381-425.
- [21]. Surmeier, D.J., et al., D1 and D2 dopamine-receptor modulation of striatal glutamatergic signaling in striatal medium spiny neurons. *Trends in neurosciences*, 2007. **30**(5): p. 228-235.
- [22]. Obeso, J.A., et al., Functional organization of the basal ganglia: therapeutic implications for

- Parkinson's disease. *Movement disorders: official journal of the Movement Disorder Society*, 2008. **23**(S3): p. S548-S559.
- [23]. Smith, Y., et al., Microcircuitry of the direct and indirect pathways of the basal ganglia. *Neuroscience*, 1998. **86**(2): p. 353-387.
- [24]. Freeze, B.S., et al., Control of basal ganglia output by direct and indirect pathway projection neurons. *Journal of Neuroscience*, 2013. **33**(47): p. 18531-18539.
- [25]. Kravitz, A.V., L.D. Tye, and A.C. Kreitzer, Distinct roles for direct and indirect pathway striatal neurons in reinforcement. *Nature neuroscience*, 2012. **15**(6): p. 816-818.
- [26]. Nambu, A., et al., Dual somatotopic representations in the primate subthalamic nucleus: evidence for ordered but reversed body-map transformations from the primary motor cortex and the supplementary motor area. *Journal of Neuroscience*, 1996. **16**(8): p. 2671-2683.
- [27]. Nambu, A., H. Tokuno, and M. Takada, Functional significance of the cortico-subthalamo-pallidal 'hyperdirect' pathway. *Neuroscience research*, 2002. **43**(2): p. 111-117.
- [28]. Nambu, A., A new approach to understand the pathophysiology of Parkinson's disease. *Journal of Neurology*, 2005. **252**(4): p. iv1-iv4.
- [29]. Wilson, C.J. and M.D. Bevan, Intrinsic dynamics and synaptic inputs control the activity patterns of subthalamic nucleus neurons in health and in Parkinson's disease. *Neuroscience*, 2011. **198**: p. 54-68.
- [30]. Degos, B., et al., Evidence for a direct subthalamo-cortical loop circuit in the rat. *European Journal of Neuroscience*, 2008. **27**(10): p. 2599-2610.
- [31]. Gerfen, C.R., et al., D1 and D2 dopamine receptor-regulated gene expression of striatonigral and striatopallidal neurons. *Science*, 1990. **250**(4986): p. 1429-1432.
- [32]. Wichmann, T. and M.R. DeLONG, Pathophysiology of Parkinson's disease: the MPTP primate model of the human disorder. *Annals of the New York Academy of Sciences*, 2003. **991**: p. 199-213.
- [33]. Pan, H.S. and J.R. Walters, Unilateral lesion of the nigrostriatal pathway decreases the firing rate and alters the firing pattern of globus pallidus neurons in the rat. *Synapse*, 1988. **2**(6): p. 650-656.
- [34]. Bergman, H., et al., The primate subthalamic nucleus. II. Neuronal activity in the MPTP model of parkinsonism. *Journal of neurophysiology*, 1994. **72**(2): p. 507-520.
- [35]. Mallet, N., et al., Cortical inputs and GABA interneurons imbalance projection neurons in the striatum of parkinsonian rats. *Journal of Neuroscience*, 2006. **26**(14): p. 3875-3884.
- [36]. Bar-Gad, I. and H. Bergman, Stepping out of the box: information processing in the neural networks of the basal ganglia. *Current opinion in neurobiology*, 2001. **11**(6): p. 689-695.
- [37]. Chu, H.-Y., et al., Loss of hyperdirect pathway cortico-subthalamic inputs following degeneration of midbrain dopamine neurons. *Neuron*, 2017. **95**(6): p. 1306-1318. e5.
- [38]. Benazzouz, A., et al., Involvement of dopamine loss in extrastriatal basal ganglia nuclei in the pathophysiology of Parkinson's disease. *Frontiers in aging neuroscience*, 2014. **6**: p. 87.
- [39]. Klaus, A., et al., The spatiotemporal organization of the striatum encodes action space. *Neuron*, 2017. **95**(5): p. 1171-1180. e7.
- [40]. Tecuapetla, F., et al., Complementary contributions of striatal projection pathways to action initiation and execution. *Cell*, 2016. **166**(3): p. 703-715.
- [41]. Wichmann, T., Changing views of the pathophysiology of Parkinsonism. *Movement Disorders*, 2019. **34**(8): p. 1130-1143.
- [42]. Lindenbach, D. and C. Bishop, Critical involvement of the motor cortex in the pathophysiology and treatment of Parkinson's disease. *Neuroscience & Biobehavioral Reviews*, 2013. **37**(10): p. 2737-2750.
- [43]. Bateup, H.S., et al., Distinct subclasses of medium spiny neurons differentially regulate striatal motor behaviors. *Proceedings of the National Academy of Sciences*, 2010. **107**(33): p. 14845-14850.
- [44]. Kravitz, A.V., et al., Regulation of parkinsonian motor behaviours by optogenetic control of basal ganglia circuitry. *Nature*, 2010. **466**(7306): p. 622-626.
- [45]. Pasquereau, B. and R.S. Turner, Primary motor cortex of the parkinsonian monkey: differential effects on the spontaneous activity of pyramidal tract-type neurons. *Cerebral cortex*, 2011. **21**(6): p. 1362-1378.

- [46]. Parr-Brownlie, L.C. and B.I. Hyland, Bradykinesia induced by dopamine D2 receptor blockade is associated with reduced motor cortex activity in the rat. *Journal of Neuroscience*, 2005. **25**(24): p. 5700-5709.
- [47]. Guo, H., J.B. Callaway, and J.P. Ting, Inflammasomes: mechanism of action, role in disease, and therapeutics. *Nature medicine*, 2015. **21**(7): p. 677-687.
- [48]. Berardelli, A., et al., Pathophysiology of bradykinesia in Parkinson's disease. *Brain*, 2001. **124**(11): p. 2131-2146.
- [49]. Wu, T., M. Hallett, and P. Chan, Motor automaticity in Parkinson's disease. *Neurobiology of disease*, 2015. **82**: p. 226-234.
- [50]. Oertel, W. and J.B. Schulz, Current and experimental treatments of Parkinson disease: a guide for neuroscientists. *Journal of neurochemistry*, 2016. **139**: p. 325-337.
- [51]. Haddad, F., et al., Dopamine and levodopa prodrugs for the treatment of Parkinson's disease. *Molecules*, 2018. **23**(1): p. 40.
- [52]. Coelho, M. and J.J. Ferreira, Late-stage Parkinson disease. *Nature Reviews Neurology*, 2012. **8**(8): p. 435-442.
- [53]. Connolly, B.S. and A.E. Lang, Pharmacological treatment of Parkinson disease: a review. *Jama*, 2014. **311**(16): p. 1670-1683.
- [54]. Pandey, S. and P. Srivannithapoom, Levodopa-induced dyskinesia: clinical features, pathophysiology, and medical management. *Annals of Indian Academy of Neurology*, 2017. **20**(3): p. 190.
- [55]. Benabid, A.-L., et al., Combined (thalamotomy and stimulation) stereotactic surgery of the VIM thalamic nucleus for bilateral Parkinson disease. *Stereotactic and functional neurosurgery*, 1987. **50**(1-6): p. 344-346.
- [56]. Martinez-Ramirez, D., et al., Update on deep brain stimulation in Parkinson's disease. *Translational Neurodegeneration*, 2015. **4**(1): p. 12.
- [57]. Pollak, P., Deep brain stimulation for Parkinson's disease—patient selection, in *Handbook of clinical neurology*. 2013, Elsevier. p. 97-105.
- [58]. Volkmann, J., Deep brain stimulation for the treatment of Parkinson's disease. *Journal of clinical neurophysiology*, 2004. **21**(1): p. 6-17.
- [59]. Limousin, P. and I. Martinez-Torres, Deep brain stimulation for Parkinson's disease. *Neurotherapeutics*, 2008. **5**(2): p. 309-319.
- [60]. Habets, J.G., et al., An update on adaptive deep brain stimulation in Parkinson's disease. *Movement Disorders*, 2018. **33**(12): p. 1834-1843.
- [61]. Priori, A., et al., Adaptive deep brain stimulation (aDBS) controlled by local field potential oscillations. *Experimental neurology*, 2013. **245**: p. 77-86.
- [62]. Swann, N.C., et al., Adaptive deep brain stimulation for Parkinson's disease using motor cortex sensing. *Journal of neural engineering*, 2018. **15**(4): p. 046006.
- [63]. Oh, M.Y., et al., Long-term hardware-related complications of deep brain stimulation. *Neurosurgery*, 2002. **50**(6): p. 1268-1276.
- [64]. Biagioni, M.C., et al., Non-Invasive Neuromodulation Therapies for Parkinson's Disease, in *Parkinson's Disease-Understanding Pathophysiology and Developing Therapeutic Strategies*. 2018, IntechOpen. p. 51-75.
- [65]. Strafella, A.P., et al., Striatal dopamine release induced by repetitive transcranial magnetic stimulation of the human motor cortex. *Brain*, 2003. **126**(12): p. 2609-2615.
- [66]. Fonteneau, C., et al., Frontal transcranial direct current stimulation induces dopamine release in the ventral striatum in human. *Cerebral Cortex*, 2018. **28**(7): p. 2636-2646.
- [67]. Loo, C.K. and P.B. Mitchell, A review of the efficacy of transcranial magnetic stimulation (TMS) treatment for depression, and current and future strategies to optimize efficacy. *Journal of affective disorders*, 2005. **88**(3): p. 255-267.
- [68]. Schlaug, G., V. Renga, and D. Nair, Transcranial direct current stimulation in stroke recovery. *Archives of neurology*, 2008. **65**(12): p. 1571-1576.
- [69]. Kim, Y.W., et al., Effects of non-invasive brain stimulation on freezing of gait in parkinsonism: a systematic review with meta-analysis. *Parkinsonism & related disorders*, 2019. **64**: p. 82-89.
- [70]. Benninger, D.H., et al., Transcranial direct current stimulation for the treatment of Parkinson's disease. *Journal of Neurology, Neurosurgery & Psychiatry*, 2010. **81**(10): p. 1105-1111.

- [71]. Dinkelbach, L., et al., Non-invasive brain stimulation in Parkinson's disease: exploiting crossroads of cognition and mood. *Neuroscience & Biobehavioral Reviews*, 2017. **75**: p. 407-418.
- [72]. Filipović, S.R., et al., Repetitive transcranial magnetic stimulation for levodopa-induced dyskinesias in Parkinson's disease. *Movement disorders: official journal of the Movement Disorder Society*, 2009. **24**(2): p. 246-253.
- [73]. Brys, M., et al., Multifocal repetitive TMS for motor and mood symptoms of Parkinson disease: a randomized trial. *Neurology*, 2016. **87**(18): p. 1907-1915.
- [74]. Haken, H., Principles of brain functioning: a synergetic approach to brain activity, behavior and cognition. Vol. 67. 2013: Springer Science & Business Media.
- [75]. Wang, X.J., Neural oscillations. *Encyclopedia of cognitive science*, 2006.
- [76]. Jensen, O., E. Spaak, and J.M. Zumer, Human brain oscillations: from physiological mechanisms to analysis and cognition. *Magnetoencephalography: From signals to dynamic cortical networks*, 2019: p. 471-517.
- [77]. Buzsáki, G., C.A. Anastassiou, and C. Koch, The origin of extracellular fields and currents—EEG, ECoG, LFP and spikes. *Nature reviews neuroscience*, 2012. **13**(6): p. 407-420.
- [78]. David, O., J.M. Kilner, and K.J. Friston, Mechanisms of evoked and induced responses in MEG/EEG. *Neuroimage*, 2006. **31**(4): p. 1580-1591.
- [79]. Cebolla, A.-M. and G. Cheron, Understanding Neural Oscillations in the Human Brain: From movement to consciousness and vice & versa. *Frontiers in psychology*, 2019. **10**: p. 1930.
- [80]. Başar, E., et al., Brain oscillations in perception and memory. *International journal of psychophysiology*, 2000. **35**(2-3): p. 95-124.
- [81]. Abel, T., et al., Sleep, plasticity and memory from molecules to whole-brain networks. *Current biology*, 2013. **23**(17): p. R774-R788.
- [82]. Levy, R., et al., Synchronized neuronal discharge in the basal ganglia of parkinsonian patients is limited to oscillatory activity. *Journal of Neuroscience*, 2002. **22**(7): p. 2855-2861.
- [83]. Brown, P., Oscillatory nature of human basal ganglia activity: relationship to the pathophysiology of Parkinson's disease. *Movement disorders: official journal of the Movement Disorder Society*, 2003. **18**(4): p. 357-363.
- [84]. Guehl, D., et al., Tremor-related activity of neurons in the 'motor' thalamus: changes in firing rate and pattern in the MPTP vervet model of parkinsonism. *European Journal of Neuroscience*, 2003. **17**(11): p. 2388-2400.
- [85]. Hurtado, J.M., et al., Dynamics of tremor-related oscillations in the human globus pallidus: a single case study. *Proceedings of the National Academy of Sciences*, 1999. **96**(4): p. 1674-1679.
- [86]. Tass, P., et al., The causal relationship between subcortical local field potential oscillations and Parkinsonian resting tremor. *Journal of neural engineering*, 2010. **7**(1): p. 016009.
- [87]. Helmich, R.C., et al., Cerebral causes and consequences of parkinsonian resting tremor: a tale of two circuits? *Brain*, 2012. **135**(11): p. 3206-3226.
- [88]. Klockgether, T., Parkinson's disease: clinical aspects. *Cell and tissue research*, 2004. **318**(1): p. 115-120.
- [89]. Bergman, H. and G. Deuschl, Pathophysiology of Parkinson's disease: from clinical neurology to basic neuroscience and back. *Movement disorders: official journal of the Movement Disorder Society*, 2002. **17**(S3): p. S28-S40.
- [90]. Ni, Z., et al., Involvement of the cerebellothalamocortical pathway in Parkinson disease. *Annals of neurology*, 2010. **68**(6): p. 816-824.
- [91]. Davis, N.J., S.P. Tomlinson, and H.M. Morgan, The role of beta-frequency neural oscillations in motor control. *Journal of Neuroscience*, 2012. **32**(2): p. 403-404.
- [92]. Engel, A.K. and P. Fries, Beta-band oscillations—signalling the status quo? *Current opinion in neurobiology*, 2010. **20**(2): p. 156-165.
- [93]. Armstrong, S., M.V. Sale, and R. Cunnington, Neural oscillations and the initiation of voluntary movement. *Frontiers in psychology*, 2018. **9**: p. 2509.
- [94]. Jenkinson, N. and P. Brown, New insights into the relationship between dopamine, beta oscillations and motor function. *Trends in neurosciences*, 2011. **34**(12): p. 611-618.
- [95]. Deffains, M. and H. Bergman, Parkinsonism-related β oscillations in the primate basal ganglia networks—recent advances and clinical implications. *Parkinsonism & related disorders*, 2019.

- 59**: p. 2-8.
- [96]. Avila, I., et al., Beta frequency synchronization in basal ganglia output during rest and walk in a hemiparkinsonian rat. *Experimental neurology*, 2010. **221**(2): p. 307-319.
- [97]. Levy, R., et al., Dependence of subthalamic nucleus oscillations on movement and dopamine in Parkinson's disease. *Brain*, 2002. **125**(6): p. 1196-1209.
- [98]. Little, S. and P. Brown, The functional role of beta oscillations in Parkinson's disease. *Parkinsonism & related disorders*, 2014. **20**: p. S44-S48.
- [99]. Kühn, A.A., et al., Reduction in subthalamic 8–35 Hz oscillatory activity correlates with clinical improvement in Parkinson's disease. *European Journal of Neuroscience*, 2006. **23**(7): p. 1956-1960.
- [100]. Giannicola, G., et al., The effects of levodopa and ongoing deep brain stimulation on subthalamic beta oscillations in Parkinson's disease. *Experimental neurology*, 2010. **226**(1): p. 120-127.
- [101]. McCarthy, M., et al., Striatal origin of the pathologic beta oscillations in Parkinson's disease. *Proceedings of the National Academy of Sciences*, 2011. **108**(28): p. 11620-11625.
- [102]. Damodaran, S., et al., Desynchronization of fast-spiking interneurons reduces β -band oscillations and imbalance in firing in the dopamine-depleted striatum. *Journal of Neuroscience*, 2015. **35**(3): p. 1149-1159.
- [103]. Sharott, A., et al., Dopamine depletion increases the power and coherence of β -oscillations in the cerebral cortex and subthalamic nucleus of the awake rat. *European Journal of Neuroscience*, 2005. **21**(5): p. 1413-1422.
- [104]. Litvak, V., et al., Resting oscillatory cortico-subthalamic connectivity in patients with Parkinson's disease. *Brain*, 2011. **134**(2): p. 359-374.
- [105]. Alavi, M., et al., Spatial extent of beta oscillatory activity in and between the subthalamic nucleus and substantia nigra pars reticulata of Parkinson's disease patients. *Experimental neurology*, 2013. **245**: p. 60-71.
- [106]. Tinkhauser, G., et al., Beta burst dynamics in Parkinson's disease OFF and ON dopaminergic medication. *Brain*, 2017. **140**(11): p. 2968-2981.
- [107]. Meidahl, A.C., et al., Synchronised spiking activity underlies phase amplitude coupling in the subthalamic nucleus of Parkinson's disease patients. *Neurobiology of disease*, 2019. **127**: p. 101-113.
- [108]. Bouthour, W., et al., Biomarkers for closed-loop deep brain stimulation in Parkinson disease and beyond. *Nature Reviews Neurology*, 2019. **15**(6): p. 343-352.
- [109]. McNamara, C.G., M. Rothwell, and A. Sharott, Phase-dependent closed-loop modulation of neural oscillations in vivo. *BioRxiv*, 2020.
- [110]. Hirschmann, J., et al., Distinct oscillatory STN-cortical loops revealed by simultaneous MEG and local field potential recordings in patients with Parkinson's disease. *Neuroimage*, 2011. **55**(3): p. 1159-1168.
- [111]. Lalo, E., et al., Patterns of bidirectional communication between cortex and basal ganglia during movement in patients with Parkinson disease. *Journal of Neuroscience*, 2008. **28**(12): p. 3008-3016.
- [112]. Jávora-Duray, B.N., et al., Early-onset cortico-cortical synchronization in the hemiparkinsonian rat model. *Journal of neurophysiology*, 2015. **113**(3): p. 925-936.
- [113]. Brazhnik, E., et al., State-dependent spike and local field synchronization between motor cortex and substantia nigra in hemiparkinsonian rats. *Journal of Neuroscience*, 2012. **32**(23): p. 7869-7880.
- [114]. Pollok, B., et al., Motor-cortical oscillations in early stages of Parkinson's disease. *The Journal of physiology*, 2012. **590**(13): p. 3203-3212.
- [115]. O'Keefe, A.B., et al., Synchrony Drives Motor Cortex Beta Bursting, Waveform Dynamics, and Phase-Amplitude Coupling in Parkinson's Disease. *Journal of Neuroscience*, 2020. **40**(30): p. 5833-5846.
- [116]. Cao, C.-Y., et al., Modulations on cortical oscillations by subthalamic deep brain stimulation in patients with Parkinson disease: a MEG study. *Neuroscience letters*, 2017. **636**: p. 95-100.
- [117]. Crowell, A.L., et al., Oscillations in sensorimotor cortex in movement disorders: an electrocorticography study. *Brain*, 2012. **135**(2): p. 615-630.

- [118]. De Hemptinne, C., et al., Exaggerated phase–amplitude coupling in the primary motor cortex in Parkinson disease. *Proceedings of the National Academy of Sciences*, 2013. **110**(12): p. 4780-4785.
- [119]. Kempf, F., et al., Gamma activity and reactivity in human thalamic local field potentials. *European Journal of Neuroscience*, 2009. **29**(5): p. 943-953.
- [120]. Jenkinson, N., A.A. Kühn, and P. Brown, Gamma oscillations in the human basal ganglia. *Experimental neurology*, 2013. **245**: p. 72-76.
- [121]. Litvak, V., et al., Movement-related changes in local and long-range synchronization in Parkinson's disease revealed by simultaneous magnetoencephalography and intracranial recordings. *Journal of Neuroscience*, 2012. **32**(31): p. 10541-10553.
- [122]. Chen, C., et al., Oscillatory pallidal local field potential activity correlates with involuntary EMG in dystonia. *Neurology*, 2006. **66**(3): p. 418-420.
- [123]. Ahn, S., et al., Interaction of synchronized dynamics in cortex and basal ganglia in Parkinson's disease. *European Journal of Neuroscience*, 2015. **42**(5): p. 2164-2171.
- [124]. Connolly, A.T., et al., Modulations in oscillatory frequency and coupling in globus pallidus with increasing parkinsonian severity. *Journal of Neuroscience*, 2015. **35**(15): p. 6231-6240.
- [125]. Jensen, O. and L.L. Colgin, Cross-frequency coupling between neuronal oscillations. *Trends in cognitive sciences*, 2007. **11**(7): p. 267-269.
- [126]. Hyafil, A., et al., Neural cross-frequency coupling: connecting architectures, mechanisms, and functions. *Trends in neurosciences*, 2015. **38**(11): p. 725-740.
- [127]. Cai, L., et al., Reconstruction of functional brain network in Alzheimer's disease via cross-frequency phase synchronization. *Neurocomputing*, 2018. **314**: p. 490-500.
- [128]. Allen, E.A., et al., Components of cross-frequency modulation in health and disease. *Frontiers in systems neuroscience*, 2011. **5**: p. 59.
- [129]. Salimpour, Y. and W.S. Anderson, Cross-frequency coupling based neuromodulation for treating neurological disorders. *Frontiers in neuroscience*, 2019. **13**: p. 125.
- [130]. Canolty, R.T. and R.T. Knight, The functional role of cross-frequency coupling. *Trends in cognitive sciences*, 2010. **14**(11): p. 506-515.
- [131]. Schroeder, C.E. and P. Lakatos, Low-frequency neuronal oscillations as instruments of sensory selection. *Trends in neurosciences*, 2009. **32**(1): p. 9-18.
- [132]. Bergmann, T.O. and J. Born, Phase-amplitude coupling: a general mechanism for memory processing and synaptic plasticity? *Neuron*, 2018. **97**(1): p. 10-13.
- [133]. Combrisson, E., et al., From intentions to actions: Neural oscillations encode motor processes through phase, amplitude and phase-amplitude coupling. *Neuroimage*, 2017. **147**: p. 473-487.
- [134]. van Wijk, B.C., et al., Subthalamic nucleus phase–amplitude coupling correlates with motor impairment in Parkinson's disease. *Clinical Neurophysiology*, 2016. **127**(4): p. 2010-2019.
- [135]. Shreve, L.A., et al., Subthalamic oscillations and phase amplitude coupling are greater in the more affected hemisphere in Parkinson's disease. *Clinical Neurophysiology*, 2017. **128**(1): p. 128-137.
- [136]. López-Azcárate, J., et al., Coupling between beta and high-frequency activity in the human subthalamic nucleus may be a pathophysiological mechanism in Parkinson's disease. *Journal of Neuroscience*, 2010. **30**(19): p. 6667-6677.
- [137]. Swann, N.C., et al., Elevated synchrony in Parkinson disease detected with electroencephalography. *Annals of neurology*, 2015. **78**(5): p. 742-750.
- [138]. Malekmohammadi, M., et al., Pallidal deep brain stimulation modulates excessive cortical high β phase amplitude coupling in Parkinson disease. *Brain stimulation*, 2018. **11**(3): p. 607-617.
- [139]. Miller, A.M., et al., Effect of levodopa on electroencephalographic biomarkers of the parkinsonian state. *Journal of neurophysiology*, 2019. **122**(1): p. 290-299.
- [140]. De Hemptinne, C., et al., Therapeutic deep brain stimulation reduces cortical phase-amplitude coupling in Parkinson's disease. *Nature neuroscience*, 2015. **18**(5): p. 779-786.
- [141]. Cole, S.R., et al., Nonsinusoidal beta oscillations reflect cortical pathophysiology in Parkinson's disease. *Journal of Neuroscience*, 2017. **37**(18): p. 4830-4840.
- [142]. Vaz, A.P., et al., Dual origins of measured phase-amplitude coupling reveal distinct neural mechanisms underlying episodic memory in the human cortex. *Neuroimage*, 2017. **148**: p. 148-159.

- [143]. Sharma, S., et al., Biomarkers in Parkinson's disease (recent update). *Neurochemistry international*, 2013. **63**(3): p. 201-229.
- [144]. Hwang, B.Y., et al., Perspective: Phase Amplitude Coupling–Based Phase–Dependent Neuromodulation in Parkinson's Disease. *Frontiers in Neuroscience*, 2020. **14**: p. 558967.
- [145]. Holt, A.B., et al., Phase-dependent suppression of beta oscillations in Parkinson's disease patients. *Journal of Neuroscience*, 2019. **39**(6): p. 1119-1134.
- [146]. Bologna, M., et al., Evolving concepts on bradykinesia. *Brain*, 2020. **143**(3): p. 727-750.
- [147]. Oldfield, R.C., The assessment and analysis of handedness: the Edinburgh inventory. *Neuropsychologia*, 1971. **9**: p. 97-113.
- [148]. Postuma, R.B., et al., MDS clinical diagnostic criteria for Parkinson's disease. *Movement Disorders*, 2015. **30**: p. 1591-1601.
- [149]. Goetz, C.G., et al., Movement Disorder Society-sponsored revision of the Unified Parkinson's Disease Rating Scale (MDS-UPDRS): scale presentation and clinimetric testing results. *Movement disorders: official journal of the Movement Disorder Society*, 2008. **23**: p. 2129-2170.
- [150]. Cavanagh, P.R. and P.V. Komi, Electromechanical delay in human skeletal muscle under concentric and eccentric contractions. *European journal of applied physiology and occupational physiology*, 1979. **42**(3): p. 159-163.
- [151]. Samii, A., et al., Central motor conduction time: reproducibility and discomfort of different methods. *Muscle & Nerve: Official Journal of the American Association of Electrodiagnostic Medicine*, 1998. **21**(11): p. 1445-1450.
- [152]. Delorme, A. and S. Makeig, EEGLAB: an open source toolbox for analysis of single-trial EEG dynamics including independent component analysis. *Journal of neuroscience methods*, 2004. **134**: p. 9-21.
- [153]. Miller, K.J., et al., Power-law scaling in the brain surface electric potential. *PLoS computational biology*, 2009. **5**: p. e1000609.
- [154]. Cohen, M.X., Analyzing neural time series data: theory and practice. 2014: MIT press.
- [155]. Perrin, F., et al., Spherical splines for scalp potential and current density mapping. *Electroencephalography and clinical neurophysiology*, 1989. **72**(2): p. 184-187.
- [156]. Fischl, B., FreeSurfer. *Neuroimage*, 2012. **62**: p. 774-781.
- [157]. Oostenveld, R., et al., FieldTrip: open source software for advanced analysis of MEG, EEG, and invasive electrophysiological data. *Computational intelligence and neuroscience*, 2011. **2011**: p. 156869.
- [158]. Liu, A.K., A.M. Dale, and J.W. Belliveau, Monte Carlo simulation studies of EEG and MEG localization accuracy. *Human brain mapping*, 2002. **16**(1): p. 47-62.
- [159]. Fuchs, M., et al., A standardized boundary element method volume conductor model. *Clinical neurophysiology*, 2002. **113**(5): p. 702-712.
- [160]. Adde, G., et al. Symmetric BEM formulation for the M/EEG forward problem. in *Biennial International Conference on Information Processing in Medical Imaging*. 2003: Springer: p. 524-535.
- [161]. Oostendorp, T.F. and A. Van Oosterom, Source parameter estimation in inhomogeneous volume conductors of arbitrary shape. *IEEE Transactions on Biomedical Engineering*, 1989. **36**: p. 382-391.
- [162]. Dannhauer, M., et al., Modeling of the human skull in EEG source analysis. *Human brain mapping*, 2011. **32**: p. 1383-1399.
- [163]. Hallez, H., et al., Review on solving the forward problem in EEG source analysis. *Journal of neuroengineering and rehabilitation*, 2007. **4**: p. 46.
- [164]. Michel, C.M., et al., EEG source imaging. *Clinical neurophysiology*, 2004. **115**(10): p. 2195-2222.
- [165]. Van Veen, B.D. and K.M. Buckley, Beamforming: A versatile approach to spatial filtering. *IEEE assp magazine*, 1988. **5**(2): p. 4-24.
- [166]. Samadzadehaghdam, N., et al., A new linearly constrained minimum variance beamformer for reconstructing EEG sparse sources. *International Journal of Imaging Systems and Technology*, 2019. **29**(4): p. 686-700.
- [167]. Jonmohamadi, Y., et al., Comparison of beamformers for EEG source signal reconstruction.

- Biomedical Signal Processing and Control*, 2014. **14**: p. 175-188.
- [168]. Chen, J.C., K. Yao, and R.E. Hudson, Source localization and beamforming. *IEEE Signal Processing Magazine*, 2002. **19**(2): p. 30-39.
- [169]. Van Veen, B.D., et al., Localization of brain electrical activity via linearly constrained minimum variance spatial filtering. *IEEE Transactions on biomedical engineering*, 1997. **44**(9): p. 867-880.
- [170]. Glasser, M.F., et al., A multi-modal parcellation of human cerebral cortex. *Nature*, 2016. **536**(7615): p. 171-178.
- [171]. Glasser, M.F., et al., A multi-modal parcellation of human cerebral cortex (Supplementary Neuroanatomical Results). *Nature*, 2016. **536**(7615): p. S1-97.
- [172]. Makeig, S., et al., Independent component analysis of electroencephalographic data. *Advances in neural information processing systems*, 1996: p. 145-151.
- [173]. Jonmohamadi, Y., et al., Source-space ICA for EEG source separation, localization, and time-course reconstruction. *NeuroImage*, 2014. **101**: p. 720-737.
- [174]. Bruns, A., Fourier-, Hilbert-and wavelet-based signal analysis: are they really different approaches? *Journal of neuroscience methods*, 2004. **137**(2): p. 321-332.
- [175]. Vanhatalo, S., et al., Infralow oscillations modulate excitability and interictal epileptic activity in the human cortex during sleep. *Proceedings of the National Academy of Sciences*, 2004. **101**(14): p. 5053-5057.
- [176]. Canolty, R.T., et al., High gamma power is phase-locked to theta oscillations in human neocortex. *science*, 2006. **313**(5793): p. 1626-1628.
- [177]. Tort, A.B., et al., Dynamic cross-frequency couplings of local field potential oscillations in rat striatum and hippocampus during performance of a T-maze task. *Proceedings of the National Academy of Sciences*, 2008. **105**(51): p. 20517-20522.
- [178]. Samiee, S. and S. Baillet, Time-resolved phase-amplitude coupling in neural oscillations. *NeuroImage*, 2017. **159**: p. 270-279.
- [179]. Tort, A.B., et al., Measuring phase-amplitude coupling between neuronal oscillations of different frequencies. *Journal of neurophysiology*, 2010. **104**(2): p. 1195-1210.
- [180]. Penny, W., et al., Testing for nested oscillation. *Journal of neuroscience methods*, 2008. **174**(1): p. 50-61.
- [181]. Seymour, R.A., G. Rippon, and K. Kessler, The detection of phase amplitude coupling during sensory processing. *Frontiers in neuroscience*, 2017. **11**: p. 487.
- [182]. van Driel, J., R. Cox, and M.X. Cohen, Phase-clustering bias in phase-amplitude cross-frequency coupling and its removal. *Journal of Neuroscience Methods*, 2015. **254**: p. 60-72.
- [183]. Hülsemann, M.J., E. Naumann, and B. Rasch, Quantification of phase-amplitude coupling in neuronal oscillations: comparison of phase-locking value, mean vector length, modulation index, and generalized-linear-modeling-cross-frequency-coupling. *Frontiers in neuroscience*, 2019. **13**: p. 573.
- [184]. Munia, T.T. and S. Aviyente, Time-frequency based phase-amplitude coupling measure for neuronal oscillations. *Scientific reports*, 2019. **9**(1): p. 1-15.
- [185]. Gohel, B., et al., Evaluation of phase-amplitude coupling in resting state magnetoencephalographic signals: effect of surrogates and evaluation approach. *Frontiers in computational neuroscience*, 2016. **10**: p. 120.
- [186]. Wobbrock, J.O., et al. The aligned rank transform for nonparametric factorial analyses using only anova procedures. in *Proceedings of the SIGCHI conference on human factors in computing systems*. 2011: p. 143-146.
- [187]. Kondylis, E.D., et al., Movement-related dynamics of cortical oscillations in Parkinson's disease and essential tremor. *Brain*, 2016. **139**(8): p. 2211-2223.
- [188]. DeLong, M. and T. Wichmann, Changing views of basal ganglia circuits and circuit disorders. *Clinical EEG and neuroscience*, 2010. **41**: p. 61-67.
- [189]. Berman, J.I., et al., Variable bandwidth filtering for improved sensitivity of cross-frequency coupling metrics. *Brain connectivity*, 2012. **2**: p. 155-163.
- [190]. Welch, P., The use of fast Fourier transform for the estimation of power spectra: a method based on time averaging over short, modified periodograms. *IEEE Transactions on audio and electroacoustics*, 1967. **15**(2): p. 70-73.

- [191]. Swann, N.C., et al., Elevated synchrony in Parkinson disease detected with electroencephalography. *Annals of neurology*, 2015. **78**: p. 742-750.
- [192]. Lozano-Soldevilla, D., N. Ter Huurne, and R. Oostenveld, Neuronal oscillations with non-sinusoidal morphology produce spurious phase-to-amplitude coupling and directionality. *Frontiers in computational neuroscience*, 2016. **10**: p. 87.
- [193]. Gast, R., H. Schmidt, and T.R. Knösche, A mean-field description of bursting dynamics in spiking neural networks with short-term adaptation. *Neural Computation*, 2020. **32**(9): p. 1615-1634.
- [194]. Ermentrout, G.B., n: m Phase-locking of weakly coupled oscillators. *Journal of Mathematical Biology*, 1981. **12**(3): p. 327-342.
- [195]. Langdon, A.J., T.W. Boonstra, and M. Breakspear, Multi-frequency phase locking in human somatosensory cortex. *Progress in biophysics and molecular biology*, 2011. **105**(1-2): p. 58-66.
- [196]. Farris, F.A., The Gini index and measures of inequality. *The American Mathematical Monthly*, 2010. **117**(10): p. 851-864.
- [197]. Chen, J.L., T. Ros, and J.H. Gruzelier, Dynamic changes of ICA-derived EEG functional connectivity in the resting state. *Human brain mapping*, 2013. **34**(4): p. 852-868.
- [198]. Pascual-Leone, A., et al., Akinesia in Parkinson's disease. I. Shortening of simple reaction time with focal, single-pulse transcranial magnetic stimulation. *Neurology*, 1994. **44**(5): p. 884-884.
- [199]. Yahalom, G., et al., Hand rhythmic tapping and timing in Parkinson's disease. *Parkinsonism & related disorders*, 2004. **10**(3): p. 143-148.
- [200]. Klockgether, T., et al., A defect of kinesthesia in Parkinson's disease. *Movement disorders: official journal of the Movement Disorder Society*, 1995. **10**(4): p. 460-465.
- [201]. Levy-Tzedek, S., et al., Rhythmic movement in Parkinson's disease: effects of visual feedback and medication state. *Experimental brain research*, 2011. **211**(2): p. 277.
- [202]. AuYong, N., et al., Movement-modulation of local power and phase amplitude coupling in bilateral globus pallidus interna in Parkinson disease. *Frontiers in human neuroscience*, 2018. **12**: p. 270.
- [203]. Yanagisawa, T., et al., Regulation of motor representation by phase–amplitude coupling in the sensorimotor cortex. *Journal of Neuroscience*, 2012. **32**(44): p. 15467-15475.
- [204]. Pfurtscheller, G., EEG event-related desynchronization (ERD) and synchronization (ERS). *Electroencephalography and Clinical Neurophysiology*, 1997. **1**(103): p. 26.
- [205]. Zaepffel, M., et al., Modulations of EEG beta power during planning and execution of grasping movements. *PloS one*, 2013. **8**(3): p. e60060.
- [206]. Shenoy, K.V., M. Sahani, and M.M. Churchland, Cortical control of arm movements: a dynamical systems perspective. *Annual review of neuroscience*, 2013. **36**: p. 337-359.
- [207]. Devergnas, A., et al., Cortical phase–amplitude coupling in a progressive model of parkinsonism in nonhuman primates. *Cerebral Cortex*, 2019. **29**(1): p. 167-177.
- [208]. Haynes, W.I. and S.N. Haber, The organization of prefrontal-subthalamic inputs in primates provides an anatomical substrate for both functional specificity and integration: implications for Basal Ganglia models and deep brain stimulation. *Journal of Neuroscience*, 2013. **33**(11): p. 4804-4814.
- [209]. Bruni, S., et al., Cortical and subcortical connections of parietal and premotor nodes of the monkey hand mirror neuron network. *Brain Structure and Function*, 2018. **223**(4): p. 1713-1729.
- [210]. Oswal, A., P. Brown, and V. Litvak, Synchronized neural oscillations and the pathophysiology of Parkinson's disease. *Current opinion in neurology*, 2013. **26**(6): p. 662-670.
- [211]. DeLong, M. and T. Wichmann, Changing views of basal ganglia circuits and circuit disorders. *Clinical EEG and neuroscience*, 2010. **41**(2): p. 61-67.
- [212]. DeLong, M.R. and T. Wichmann, Basal ganglia circuits as targets for neuromodulation in Parkinson disease. *JAMA neurology*, 2015. **72**(11): p. 1354-1360.
- [213]. Magrinelli, F., et al., Pathophysiology of motor dysfunction in Parkinson's disease as the rationale for drug treatment and rehabilitation. *Parkinson's disease*, 2016. **2016**.
- [214]. Boertien, T., et al., Functional imaging of subthalamic nucleus deep brain stimulation in Parkinson's disease. *Movement Disorders*, 2011. **26**(10): p. 1835-1843.
- [215]. Ozturk, M., et al., Distinct subthalamic coupling in the ON state describes motor performance

- in Parkinson's disease. *Movement Disorders*, 2020. **35**(1): p. 91-100.
- [216]. Tsiokos, C., et al., Pallidal low β -low γ phase-amplitude coupling inversely correlates with Parkinson disease symptoms. *Clinical Neurophysiology*, 2017. **128**(11): p. 2165-2178.
- [217]. Ray, S., et al., Neural correlates of high-gamma oscillations (60–200 Hz) in macaque local field potentials and their potential implications in electrocorticography. *Journal of Neuroscience*, 2008. **28**(45): p. 11526-11536.
- [218]. Spiegler, A., et al., Modeling brain resonance phenomena using a neural mass model. *PLoS computational biology*, 2011. **7**(12): p. e1002298.
- [219]. Jackson, N., et al., Characteristics of waveform shape in Parkinson's disease detected with scalp electroencephalography. *eneuro*, 2019. **6**(3): p. 1-11.
- [220]. Voytek, B. and R.T. Knight, Dynamic network communication as a unifying neural basis for cognition, development, aging, and disease. *Biological psychiatry*, 2015. **77**(12): p. 1089-1097.
- [221]. Shimamoto, S.A., et al., Subthalamic nucleus neurons are synchronized to primary motor cortex local field potentials in Parkinson's disease. *Journal of Neuroscience*, 2013. **33**(17): p. 7220-7233.
- [222]. Belluscio, M.A., et al., Oscillations in the basal ganglia in Parkinson's disease: role of the striatum. *Basal Ganglia*, 2014. **3**(4): p. 203-212.
- [223]. West, T.O., et al., Propagation of beta/gamma rhythms in the cortico-basal ganglia circuits of the parkinsonian rat. *Journal of Neurophysiology*, 2018. **119**(5): p. 1608-1628.
- [224]. deVries, H.A., "Efficiency of electrical activity" as a physiological measure of the functional state of muscle tissue. *American Journal of Physical Medicine & Rehabilitation*, 1968. **47**(1): p. 10-22.
- [225]. Bologna, M., et al., Bradykinesia in early and advanced Parkinson's disease. *Journal of the neurological sciences*, 2016. **369**: p. 286-291.
- [226]. Churchland, M.M., et al., Neural population dynamics during reaching. *Nature*, 2012. **487**(7405): p. 51-56.
- [227]. Stancák Jr, A. and G. Pfurtscheller, Desynchronization and recovery of β rhythms during brisk and slow self-paced finger movements in man. *Neuroscience letters*, 1995. **196**(1-2): p. 21-24.
- [228]. Crone, N.E., et al., Functional mapping of human sensorimotor cortex with electrocorticographic spectral analysis. II. Event-related synchronization in the gamma band. *Brain: a journal of neurology*, 1998. **121**(12): p. 2301-2315.
- [229]. Takemi, M., et al., Event-related desynchronization reflects downregulation of intracortical inhibition in human primary motor cortex. *Journal of neurophysiology*, 2013. **110**(5): p. 1158-1166.
- [230]. Stanford, I.M., et al., The role of GABAergic modulation in motor function related neuronal network activity. *Neuroimage*, 2011. **56**(3): p. 1506-1510.
- [231]. Klaus, A., J. Alves da Silva, and R.M. Costa, What, if, and when to move: basal ganglia circuits and self-paced action initiation. *Annual review of neuroscience*, 2019. **42**: p. 459-483.
- [232]. Duque, J. and R.B. Ivry, Role of corticospinal suppression during motor preparation. *Cerebral cortex*, 2009. **19**(9): p. 2013-2024.
- [233]. Ibáñez, J., et al., Premovement suppression of corticospinal excitability may be a necessary part of movement preparation. *Cerebral Cortex*, 2020. **30**(5): p. 2910-2923.
- [234]. Hannah, R., et al., Selective suppression of local interneuron circuits in human motor cortex contributes to movement preparation. *Journal of Neuroscience*, 2018. **38**(5): p. 1264-1276.
- [235]. Kaufman, M.T., et al., The largest response component in the motor cortex reflects movement timing but not movement type. *eneuro*, 2016. **3**(4): p. 1-25.
- [236]. Churchland, M.M., et al., Cortical preparatory activity: representation of movement or first cog in a dynamical machine? *Neuron*, 2010. **68**(3): p. 387-400.
- [237]. Torrecillos, F., et al., Modulation of beta bursts in the subthalamic nucleus predicts motor performance. *Journal of neuroscience*, 2018. **38**(41): p. 8905-8917.
- [238]. Schultz, W., Multiple dopamine functions at different time courses. *Annu. Rev. Neurosci.*, 2007. **30**: p. 259-288.
- [239]. Panigrahi, B., et al., Dopamine is required for the neural representation and control of movement vigor. *Cell*, 2015. **162**(6): p. 1418-1430.
- [240]. Feingold, J., et al., Bursts of beta oscillation differentiate postperformance activity in the

- striatum and motor cortex of monkeys performing movement tasks. *Proceedings of the National Academy of Sciences*, 2015. **112**(44): p. 13687-13692.
- [241]. Guerra, A., et al., Driving motor cortex oscillations modulates bradykinesia in Parkinson's disease. *Brain*, 2021(Accepted).
- [242]. Gast, R., et al., On the Role of Arkypallidal and Prototypical Neurons for Phase Transitions in the External Pallidum. *The Journal of Neuroscience*, 2021. **41**(31): p. 6673-6683.

Erklärung über die eigenständige Abfassung der Arbeit

Hiermit erkläre ich, dass ich die vorliegende Arbeit selbstständig und ohne unzulässige Hilfe oder Benutzung anderer als der angegebenen Hilfsmittel angefertigt habe. Ich versichere, dass Dritte von mir weder unmittelbar noch mittelbar eine Vergütung oder geldwerte Leistungen für Arbeiten erhalten haben, die im Zusammenhang mit dem Inhalt der vorgelegten Dissertation stehen, und dass die vorgelegte Arbeit weder im Inland noch im Ausland in gleicher oder ähnlicher Form einer anderen Prüfungsbehörde zum Zweck einer Promotion oder eines anderen Prüfungsverfahrens vorgelegt wurde. Alles aus anderen Quellen und von anderen Personen übernommene Material, das in der Arbeit verwendet wurde oder auf das direkt Bezug genommen wird, wurde als solches kenntlich gemacht. Insbesondere wurden alle Personen genannt, die direkt an der Entstehung der vorliegenden Arbeit beteiligt waren. Die aktuellen gesetzlichen Vorgaben in Bezug auf die Zulassung der klinischen Studien, die Bestimmungen des Tierschutzgesetzes, die Bestimmungen des Gentechnikgesetzes und die allgemeinen Datenschutzbestimmungen wurden eingehalten. Ich versichere, dass ich die Regelungen der Satzung der Universität Leipzig zur Sicherung guter wissenschaftlicher Praxis kenne und eingehalten habe.

07.2022

Ruxue Gong

Publications

Paper:

Ruxue Gong, Christoph Mühlberg, Mirko Wegscheider, Christopher Fricke, Jost-Julian Rumpf, Thomas R. Knösche, and Joseph Classen. Cross-frequency phase-amplitude coupling in repetitive movements in patients with Parkinson's disease. *Journal of Neurophysiology*. 2022. 127(6), 1606-1621.

Richard Gast, **Ruxue Gong**, Helmut Schmidt, Hil G.E. Meijer, Thomas R. Knösche. On the Role of Arkyallidal and Prototypical Neurons for Phase Transitions in the External Pallidum. *Journal of Neuroscience*. 2021. **41** (31): 6673-6683

Ruxue Gong, Mirko Wegscheider, Christoph Mühlberg, Richard Gast, Christopher Fricke, Jost-Julian Rumpf, Vadim V. Nikulin, Thomas R. Knösche, and Joseph Classen. Spatiotemporal features of β - γ phase-amplitude coupling in Parkinson's disease derived from scalp EEG. *Brain*. 2021. **144**(2): 487-503.

Abstract:

Ruxue Gong, Christoph Mühlberg, Mirko Wegscheider, Thomas R. Knösche, and Joseph Classen. P 40. β - γ phase-amplitude coupling during movements in Parkinson's disease. *Clinical Neurophysiology*. 2021. **132**(8): e18.

Ruxue Gong, Christoph Mühlberg, Mirko Wegscheider, Vadim V. Nikulin, Thomas R. Knösche, and Joseph Classen. P58 Increased phase-amplitude coupling in Parkinson's disease: Evidence from source localized electroencephalography. *Clinical Neurophysiology*. 2020. **131**(4): e44.

Poster (International conferences):

Ruxue Gong, Christoph Mühlberg, Mirko Wegscheider, Vadim V. Nikulin, Thomas R. Knösche, and Joseph Classen. Increased Phase-Amplitude Coupling in Parkinson's Disease: Evidence from Source Localized Electroencephalography. *6th International Conference on non-invasive Brain Stimulaion*. 12 November 2020, online conference

Ruxue Gong, Mirko Wegscheider, Christoph Mühlberg, Richard Gast, Christopher Fricke, Jost-Julian Rumpf, Vadim V. Nikulin, Thomas R. Knösche, and Joseph Classen. Spatially specific increase of abnormal phase-amplitude coupling in M1 of Parkinson patients – an EEG study. *FENS*. 11-15 July 2020, online conference.

Acknowledgement

This thesis is dedicated to all those who have helped me in my project and my life during the last four years.

First and foremost, I would like to express my most tremendous gratitude to my supervisors: Prof. Joseph Classen and Prof. Thomas Knösche. You gave me the opportunity to carry out this exciting project and support me throughout my whole doctoral study. This thesis would not have been possible without your supervision, revision, suggestions, and encouragement. And I also would like to thank my advisor Dr. Vadim Nikulin who gave me valuable advice and feedback on my research projects.

I consider it an honor to work with all my colleagues in Group “Brain Networks”, MPI CBS, and the neurology department, University of Leipzig. Great thanks to Christoph Mühlberg, Mirko Wegscheider for your support from the experimental side, helping me collect data and obtain clinical measurements. Great thanks to Vincent Chien and Peng Wang for your countless help for either scientific or just daily non-scientific issues. And also, many thanks to Richard Gast, Anastasiia Zlotnyk, Fricke Christopher, Rumpf Jost-Julian for your scientific discussion, help, and support to my manuscripts and thesis. Of course, I would like to thank the subjects who participated my study. Without your willingness, I would never make progress on my project. Besides, I would like to thank Veronika Krieghoff and Susann Glasewald for your generous help with my personal affairs and IMPRS program affairs.

I am really thankful to my friends in and out of office, even in and out of Germany, who have always shared the ups and downs, supported me, and always believed in me. Xuehu, Ying, Peiju, Ting, Jie, Vincent, I’m glad to meet you here in Leipzig.

Last but not least, I am incredibly grateful to my boyfriend, Xiaolong. Even thousands of miles apart, I can feel you always be my side, sharing my happiness and sorrow, giving me love and courage. Moreover, I owe my deepest gratitude to my parents, who always gave me their unconditional support and understanding.